MECHANISM AND ACTIVATION ENERGY FOR DIFFUSION THROUGH SINGLE CRYSTAL AND POLYCRYSTALLINE HIGH TEMPERATURE MATERIALS

2 5

no trim top

12-X

By

WILLIS E. MOODY

Progress Report 1-3

Final Report

Project B-146

Engineering Experiment Station
Georgia Institute of Technology
Atlanta, Georgia
1959-61

CONTENTS

PROGRESS REPORT NO. 1

PROJECT NO. B-146

MECHANISM AND ACTIVATION ENERGY FOR DIFFUSION THROUGH SINGLE CRYSTAL AND POLYCRYSTALLINE HIGH TEMPERATURE MATERIALS

By

WILLIS E. MOODY

- o - o - o - o - o -

CONTRACT NO. AT (40-1)-2420

ATOMIC ENERGY COMMISSION

- o - o - o - o - o -

1 FEBRUARY 1959

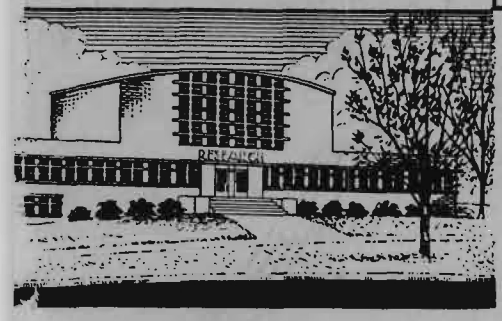

Engineering Experiment Station
Georgia Institute of Technology
Atlanta, Georgia

GEORGIA INSTITUTE OF TECHNOLOGY
ENGINEERING EXPERIMENT STATION
ATLANTA, GEORGIA

PROGRESS REPORT NO. 1

PROJECT NO. B-146

MECHANISM AND ACTIVATION ENERGY FOR DIFFUSION THROUGH SINGLE CRYSTAL AND POLYCRYSTALLINE HIGH TEMPERATURE MATERIALS

By

WILLIS E. MOODY

- o - o - o - o - o -

CONTRACT NO. AT (40-1)-2420

ATOMIC ENERGY COMMISSION

- o - o - o - o - o -

1 FEBRUARY 1959

I. INTRODUCTION

The objective of this program is to advance in a systematic manner the basic scientific knowledge of imperfections and mass-transport phenomena in metallic-oxide materials. Because of the almost infinite number of combinations, this investigation is being confined to UO_2 and Al_2O_3 as the metallic-oxides and the inert gas series of elements, Xe, Kr, A, Ne and He. The inert gas series of elements will give information concerning diffusion as a function of size and eliminate the complications of valence.

II. SUMMARY OF RESULTS

A considerable amount of time has been devoted to the procurement and assembly of equipment. The fabrication of the UO_2 tubes has become a problem, as the Ceramic Laboratory, ORNL, Oak Ridge has not had furnaces available because of other projects of higher priority. The Ceramic Laboratory has been fabricating the Gas Cycle Reactor fuel elements. Therefore, the planned procedure has been changed to some extent in that an attempt is being made to fabricate these at Georgia Tech. An atmospheric furnace with a molybdenum heating element, Fig. 1, has been constructed for the UO_2 tube fabrication problem. Coors Porcelain Co., Golden, Colorado, is fabricating the Al_2O_3 single crystal and polycrystalline tubes which should be delivered soon. They have made, Fig. 2, some polycrystalline Al_2O_3 tubes, 95% Al_2O_3, for the purpose of sealing a UO_2 barrier between them to make the UO_2 tube at Georgia Tech. Coors Porcelain is fabricating the Al_2O_3 tubes in a similar manner. A high density UO_2 single crystal and polycrystalline material produced by Norton Company, Worcester, Massachusetts, is being investigated as a diffusion barrier. A paper, Appendix, concerning this material has been submitted for publication in the Journal of the American Ceramic Society.

UO_2 and Al_2O_3 has some similar and dissimilar characteristics which must be given consideration for bond development. It has been reported by some investi-

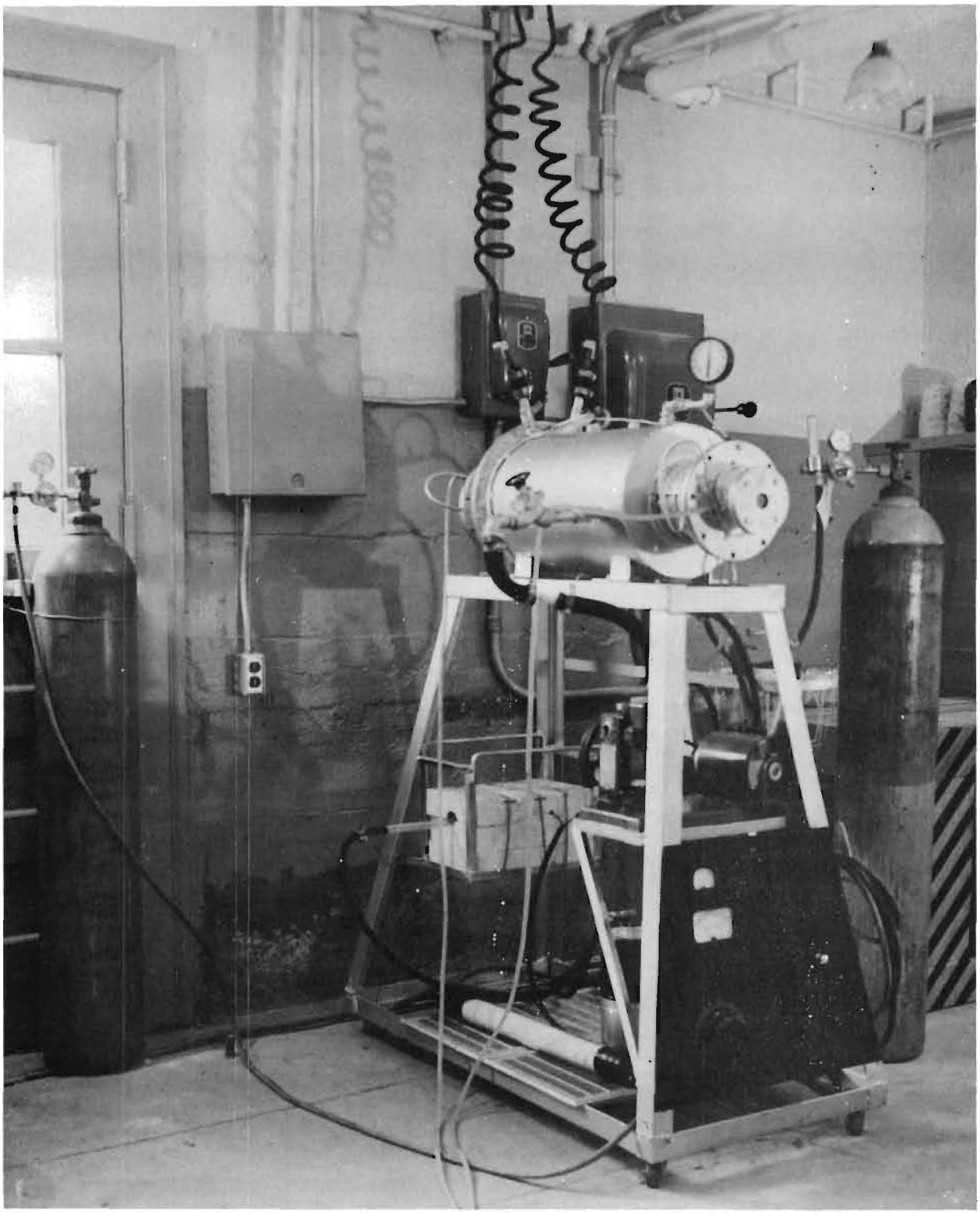

Figure 1. High Temperature Atmospheric Furnace.

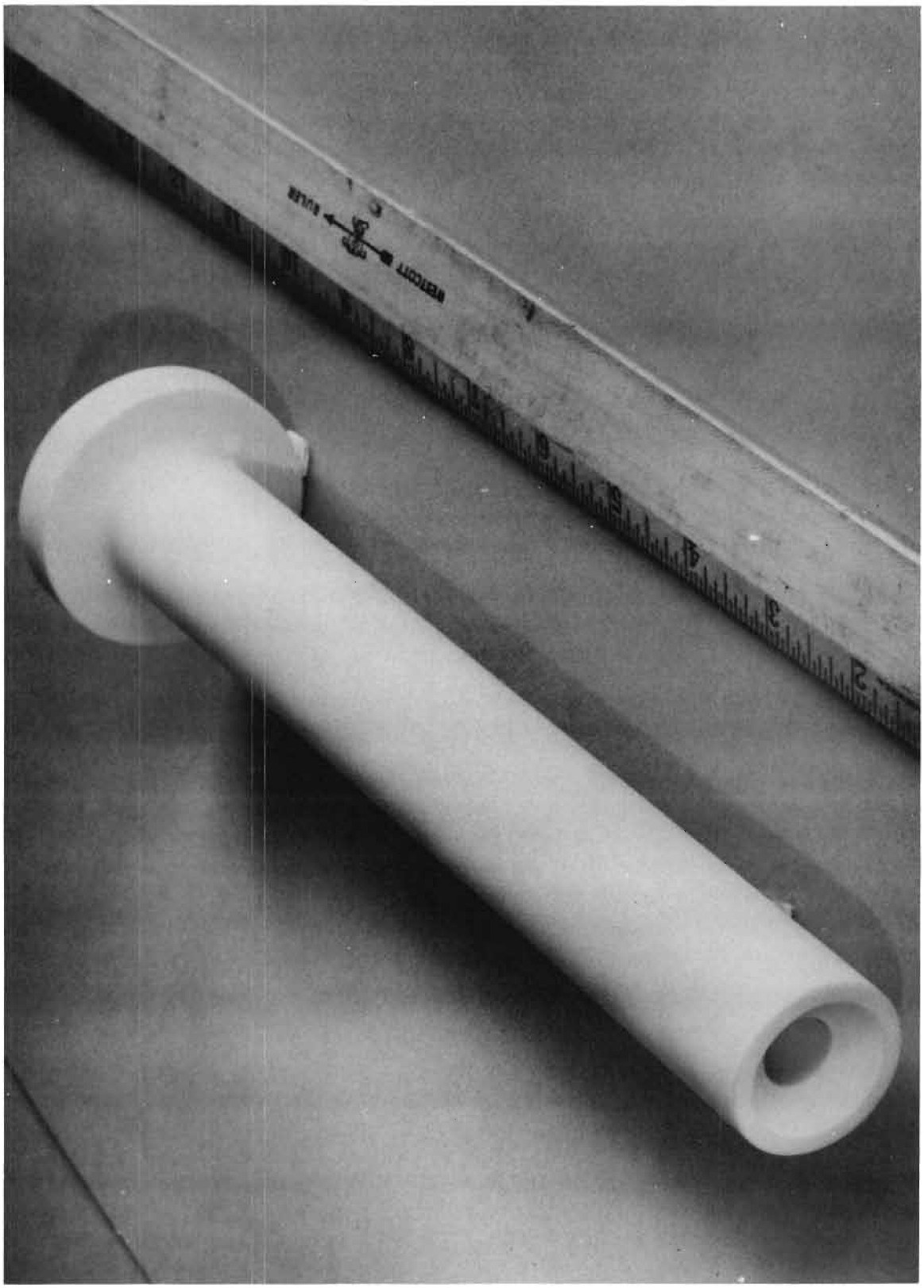

Figure 2. Polycrystalline Al_2O_3 Tube Section.

gations[1] that they do not react with each other to form compounds or solid solutions and that there are regions of liquid immiscibility as shown in Fig. 3[1].

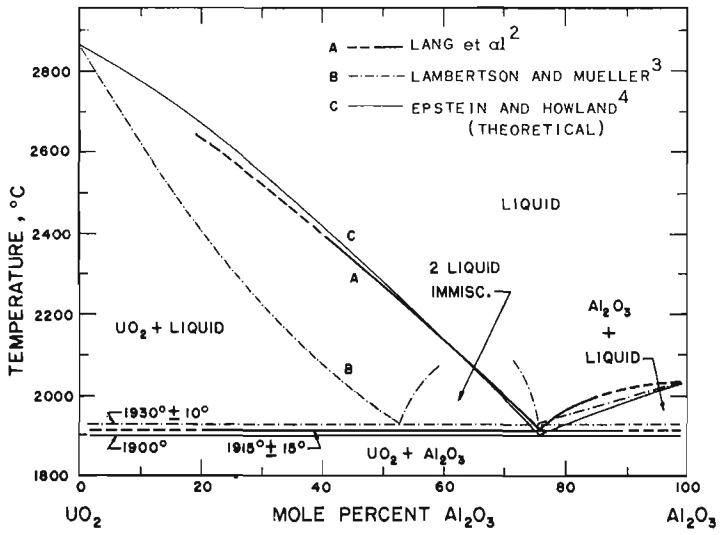

FIGURE 3. THE SYSTEM UO_2 - Al_2O_3

There are many constituents which will react with UO_2 such as ThO_2, SiO_2, Y_2O_3, TiO_2, etc. and also react with Al_2O_3. The usual glaze coating for Al_2O_3 polycrystalline electrical insulators is feldspar, $KNaO \cdot Al_2O_3 \cdot 6SiO_2$. As this is a high temperature glass, approximately 1550° C melting point, it may be suitable as a bonding material or the low temperature component of a mixture with Al_2O_3.

---

[1] "High Temperature Reactions of Uranium Dioxide with Various Metal Oxides," NBS Circular 568, 1956.

[2] Lang, S. M. "An Annotated Bibliography of Selected References on the Solid-state Reactions of the Uranium Oxides", NBS Cir. 535 (Jan. 9, 1953).

[3] Lambertson, W. A. and Mueller, M. H., "Uranium Oxide Phase Equilibrium Systems: I, UO_2-Al_2O_3," J. Am. Ceram. Soc. 36, 329 (1953).

[4] Epstein, L. F. and Howland, W. H., "Binary Mixtures of UO_2 and other Oxides," J. Am. Ceram. Soc. 36, 334 (1953).

and UO_2. Another requirement of the bonding material is that it have a high coefficient of thermal expansion as UO_2 and Al_2O_3 have thermal expansion coefficient of[5] 11 x 10^{-6} /°C and 10 x 10^{-6} /° C.

The first attempt to make such a bond was not successful in that the bond did not react to any appreciable extent with the UO_2, Fig. 4. The bond consisted of components which will form solid solutions or eutectics with both UO_2 and Al_2O_3. The specimens, Fig. 4, were fired to 1700° C in a hydrogen atmosphere. The composition of the bond was as follows:

Material	% wt
UO_2	40
Ti_2O_2	5
ThO_2	10
†Al_2O_3	40
	100

†Composition same as Coors Composition of tube:
94% Al_2O_3
2% MgO and CaO
4% SiO_2

From Figure 4, it can be observed that the UO_2 cracked away from the original flat surface as obtained by cutting slabs with a diamond saw. This may have been caused by a too rapid cooling rate or occluded gases as these were a polycrystalline material. However, a more complete examination is being made now. If this UO_2 appears unsatisfactory, diffusion barriers will be made by the ordinary pressing and firing techniques for bond development studies.

---

[5]Warde, J. M., "Refractories For Nuclear Energy", Bull. 94, The Refractories Inst., 1956.

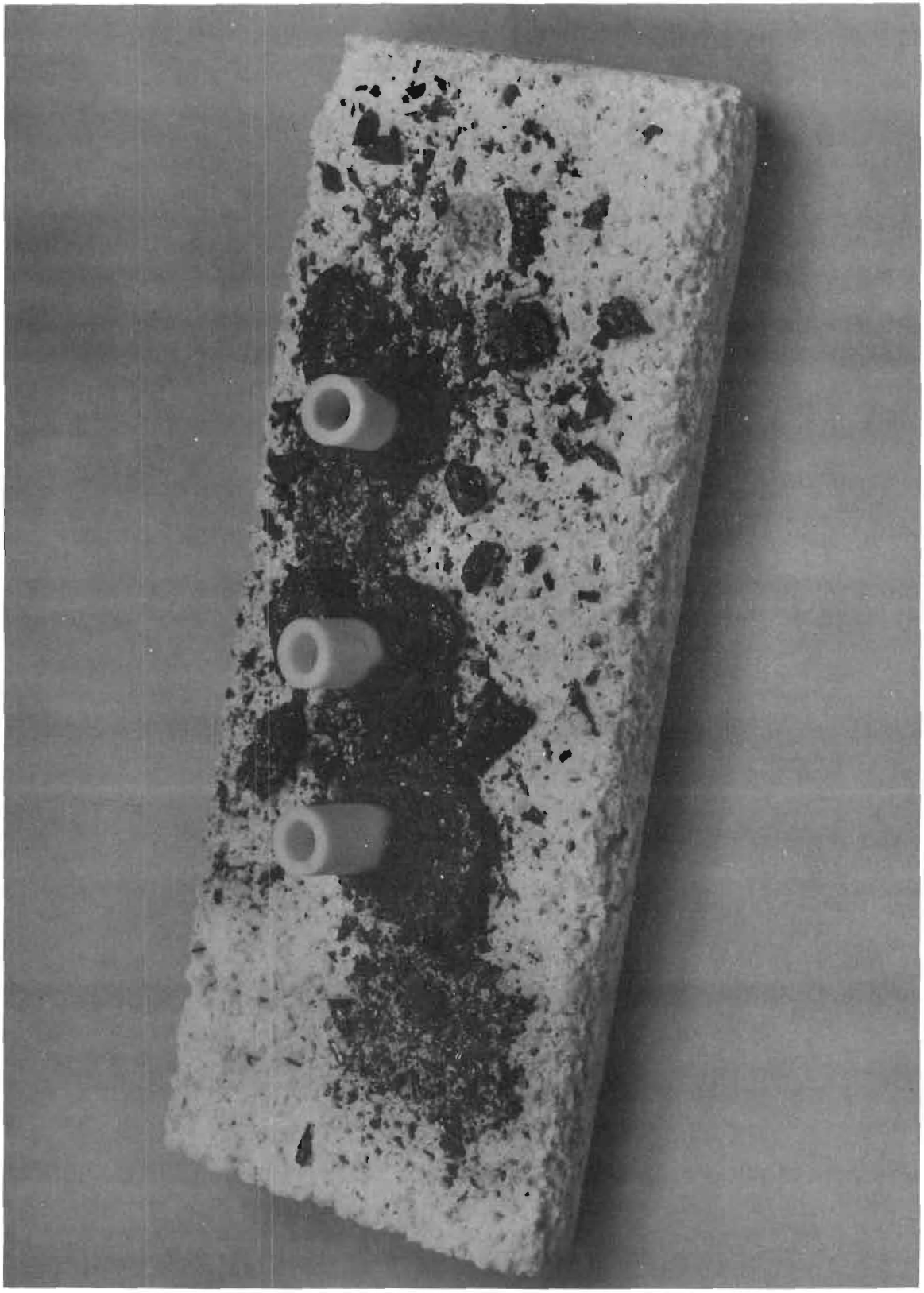

Figure 4. Al_2O_3 Bonding to UO_2.

Other bond composition that are more reactive with UO_2, will be selected from phase diagram studies. The selection of bonding materials is complicated to some extent because of the high coefficient of thermal expansion of both UO_2 and Al_2O_3. In general, the more promising combinations for bonding will be investigated in a systematic manner such as to minimize the number of trials. By termination of the contract period, June 1, 1959, the feasibility of developing a bond should be known to a great extent.

A schematic diagram of the diffusion cell is shown in Figure 5. The temperature controller and electronic circuit for vacuum measurements have been constructed and are shown in Fig. 6 and 7. All the equipment for the diffusion cell has been procured and sub-assembly completed. Final assembly will be made as tubes are fitted into it.

Consideration is being given to the feasibility of generating some of the inert gases in UO_2 by irradiation in a nuclear reactor. It may be possible to accomplish this by surrounding enriched UO_2 with depleted UO_2 of the proper geometrical configuration. The solution of the diffusion equation may require such approximations as to give results which may not be adequate. Additional study will be necessary before a better understanding of this problem can be ascertained.

It is anticipated that diffusion studies for Argon and possibly one or two of the other inert gases through the single crystal and polycrystalline Al_2O_3 will be completed by the end of the contract year, June 1, 1959. It is planned to continue studies on bonding Al_2O_3 to UO_2. However, should tube fabrication become possible with a bond or solid UO_2 tube, the tubes will be produced and diffusion studies completed as rapidly as possible.

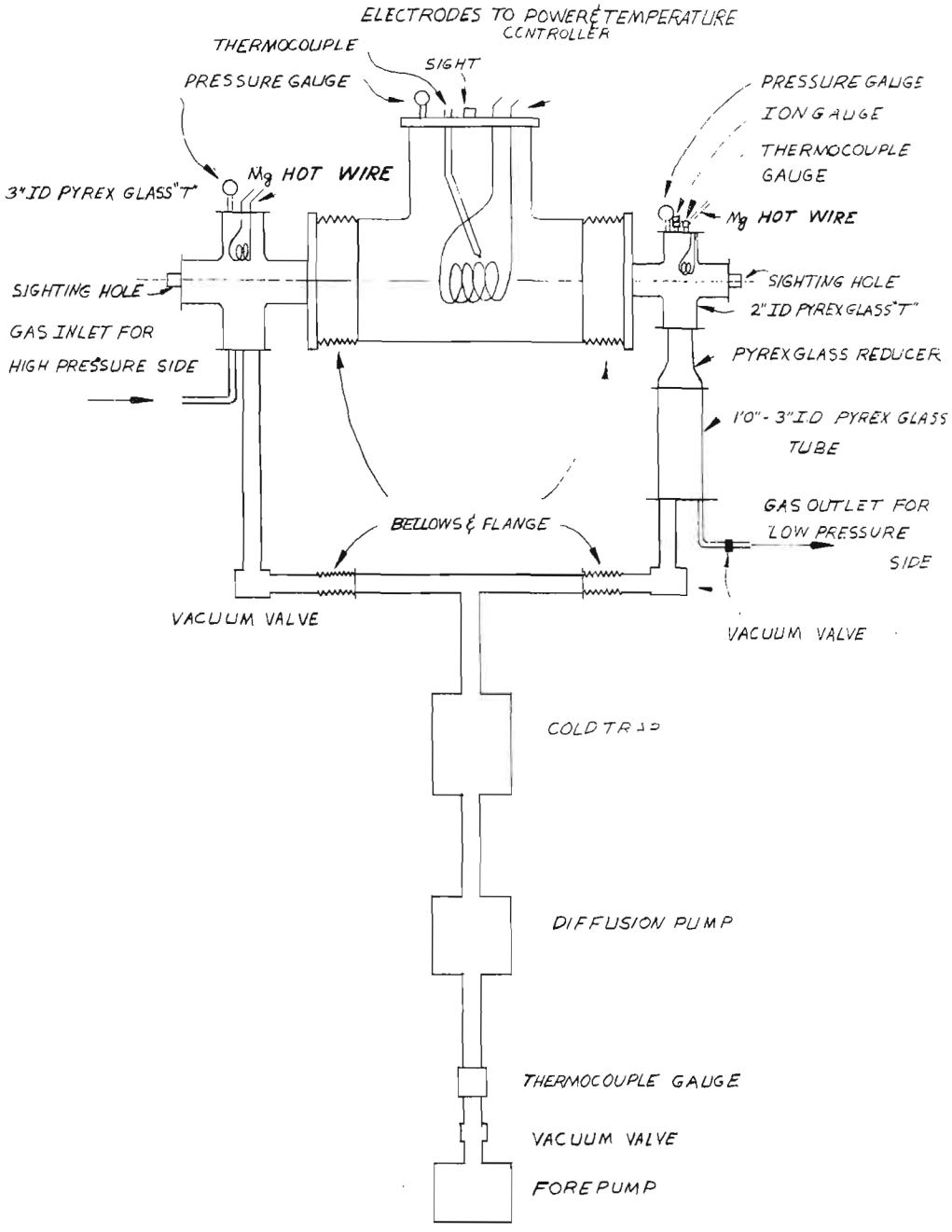

Figure 5. Schematic Diagram of Diffusion Cell.

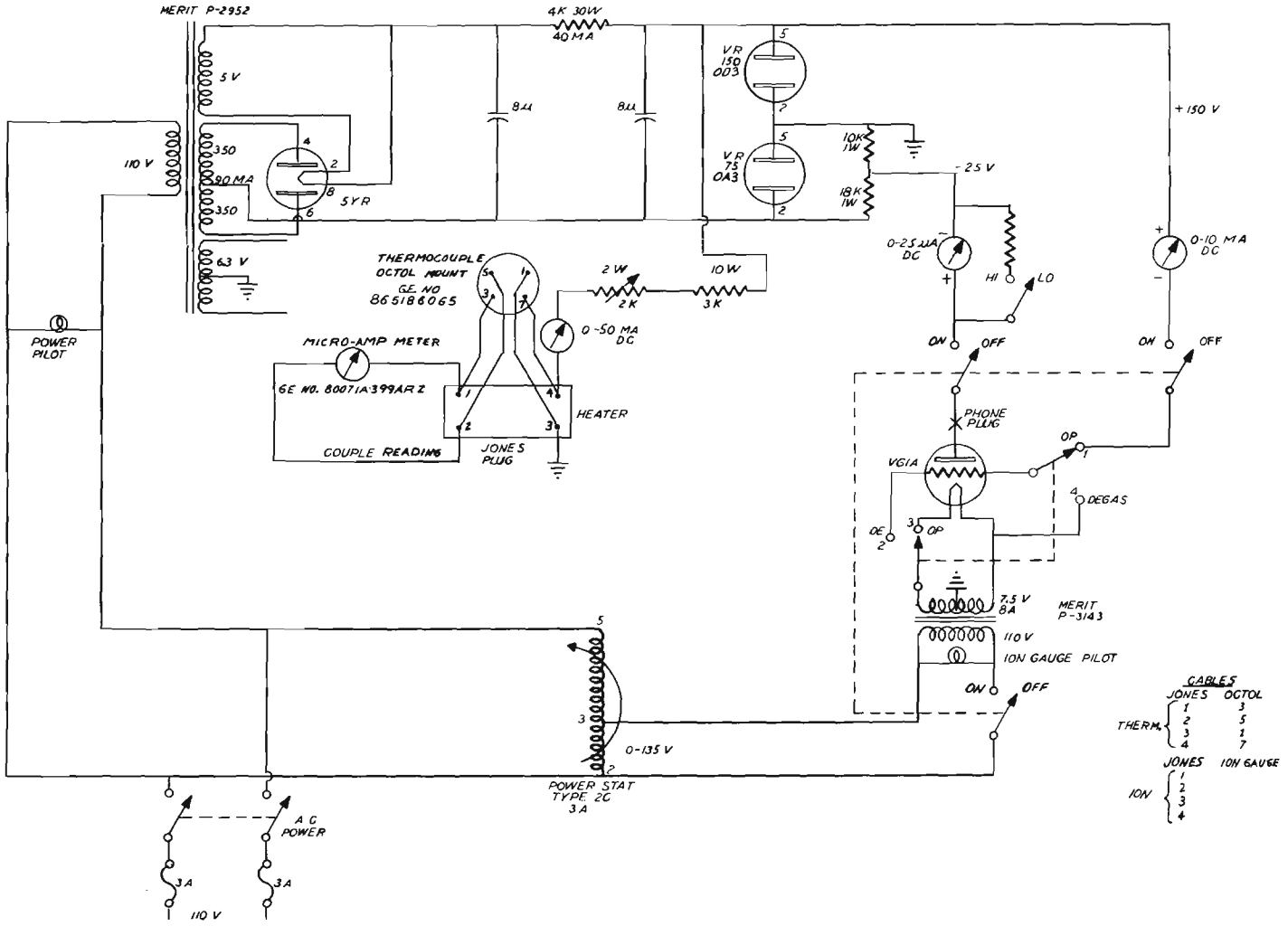

Figure 6. Ion Gauge and Thermocouple Gauge Electronic Circuit.

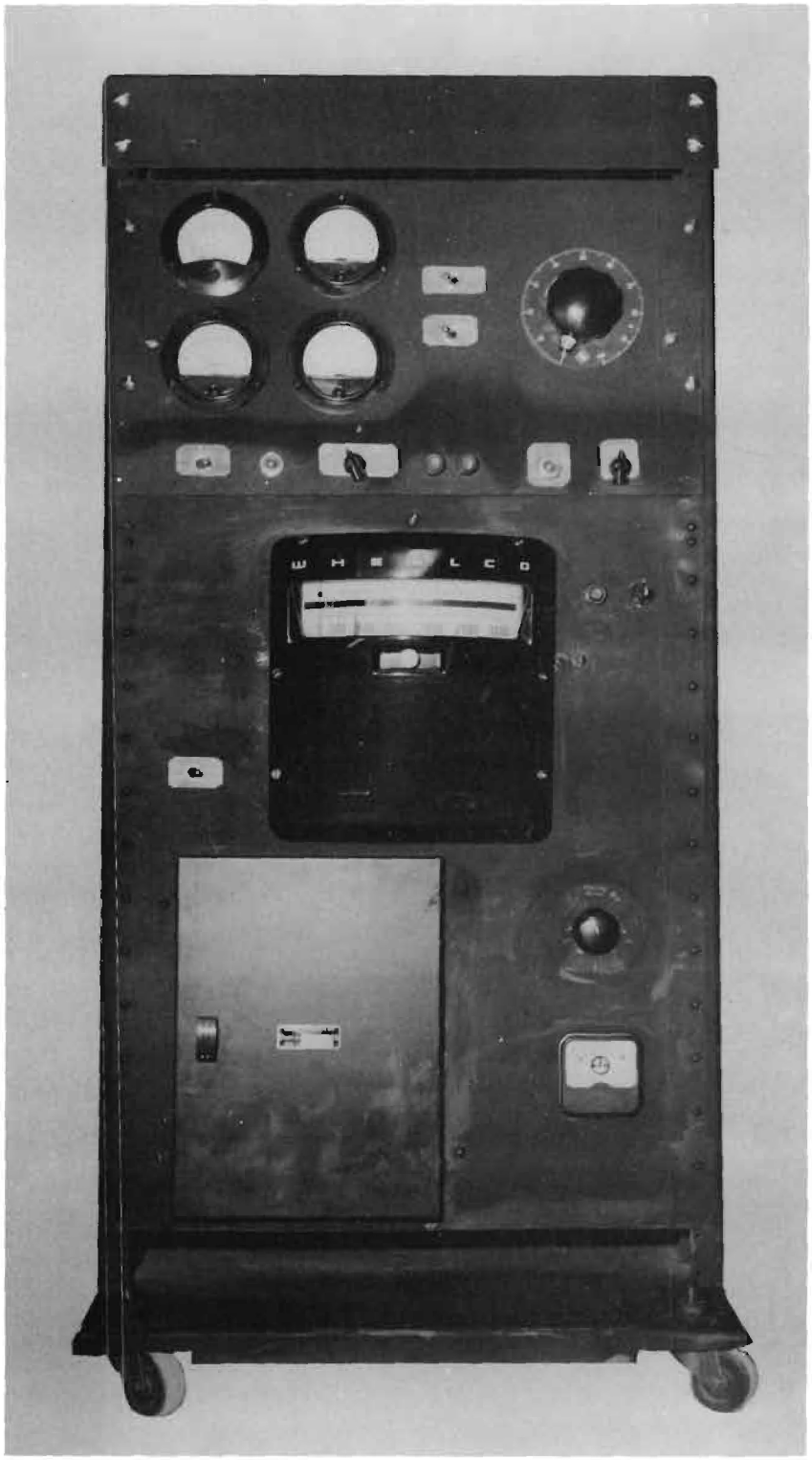

Figure 7. Temperature Controller and Vacuum Measurement Equipment.

III. APPENDIX

Thorium Oxide and Uranium Oxide Cleavage

William B. Campbell, Vernon J. Hurst, and Willis E. Moody

The crystallographic properties of most natural crystals have been determined. However, some of the crystals in use today do not occur in nature. These synthetic crystals are in limited distribution and have not been studied extensively. Apparatus involving these synthesized crystals necessitates a knowledge of specific crystal properties such as cleavage planes and their associated imperfections. A search of the literature disclosed no information pertaining to the cleavage of ThO_2 or UO_2.

A thorium oxide crystal obtained from the electric furnace process by Norton Company, Worcester, Mass., was examined[6] with a two-circle optical goniometer, and the cleavage poles plotted on a stereographic net. An oriented fragment of the same crystal was mounted on a Buerger precession camera and a plot of the axes obtained. This plot was superimposed on the stereographic net. Although the uncertainty in translating the crystallographic orientation of the x-rayed fragment back to the parent crystal might easily be as much as 5°; the correspondence of the axes and cleavage poles clearly shows that the cleavage is cubic, i.e., parallel to the (100), (010) and (001) planes.

The cleavage of the specimen was good but not perfect. All three cleavage surfaces gave streaky and multiple reflections on the optical goniometer. On a stereographic plot the cleavage poles were grouped about the crystallographic axes as shown in Fig. 1. One cleavage reflection was offset 6-10° from $\underline{a}$; another 12° from $\underline{b}$; and the third cleavage gave a streaky reflection which ranged from $\underline{\bar{c}}$ to 24° away from $\underline{c}$. This was attributed to internal strain in the synthesized crystal.

---

[6] This investigation was conducted under a Georgia Institute of Technology Engineering Experiment Station Project sponsored by the Atomic Energy Commission.

A synthesized Urania (UO_2) crystal obtained from the same source was subjected to a similar investigation and was found to have no cleavage. Its fracture was conchoidal and, in a few cases, planer. The single crystal specimens are shown in Fig. 2.

About the Authors:

1) William B. Campbell, Research Assistant, Engineering Experiment Station, Georgia Institute of Technology

2) Vernon J. Hurst, Geologist, Department of Mines, Mining and Geology, State of Georgia

3) Willis E. Moody, Associate Professor, School of Ceramic Engineering, Georgia Institute of Technology.

Respectfully submitted,

Willis E. Moody
Project Director

Approved:

Frederick Bellinger, Chief
Material Sciences Division

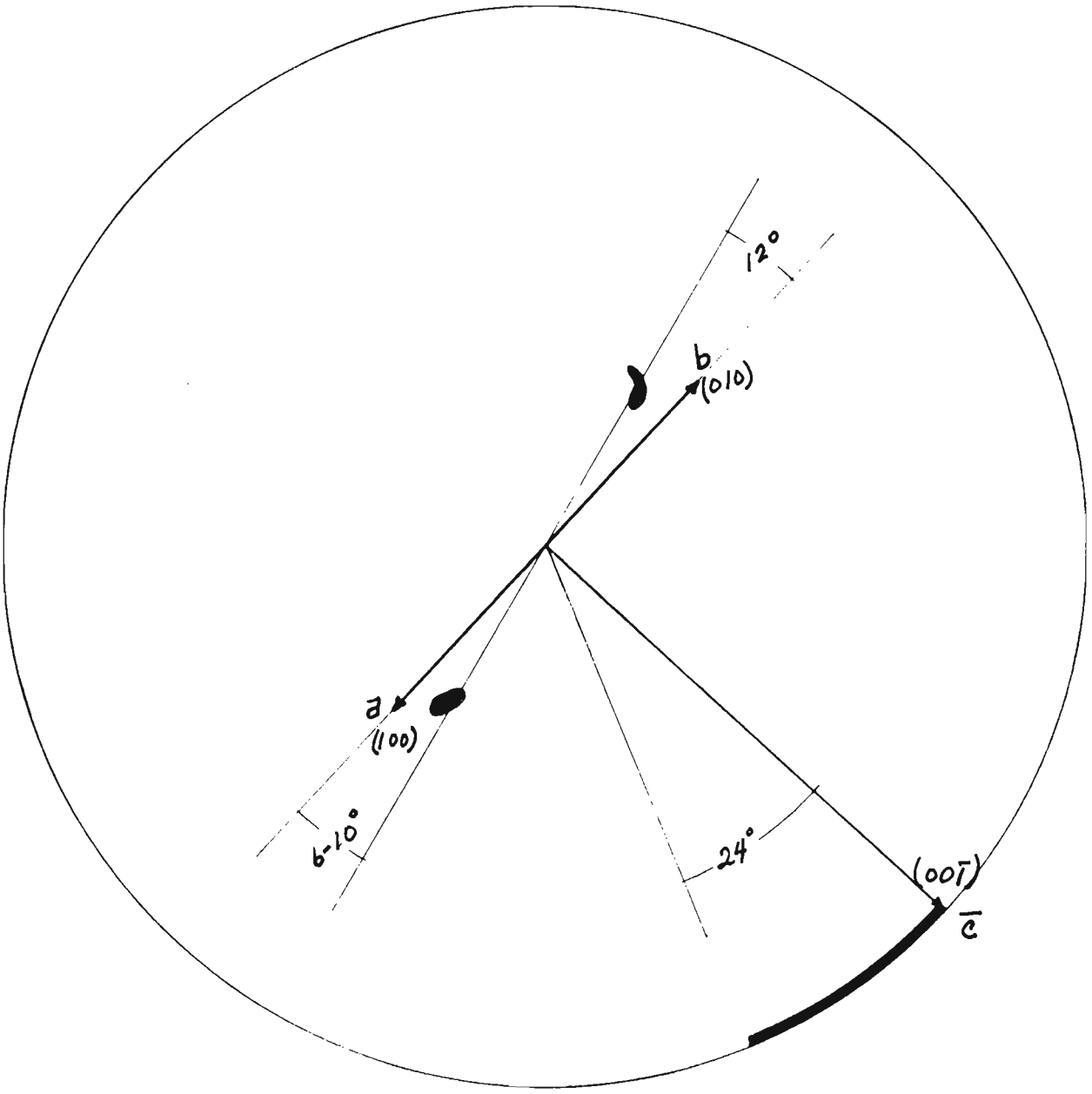

Figure 1. Stereographic Plot Showing Clevage Poles of Thorium Oxide.

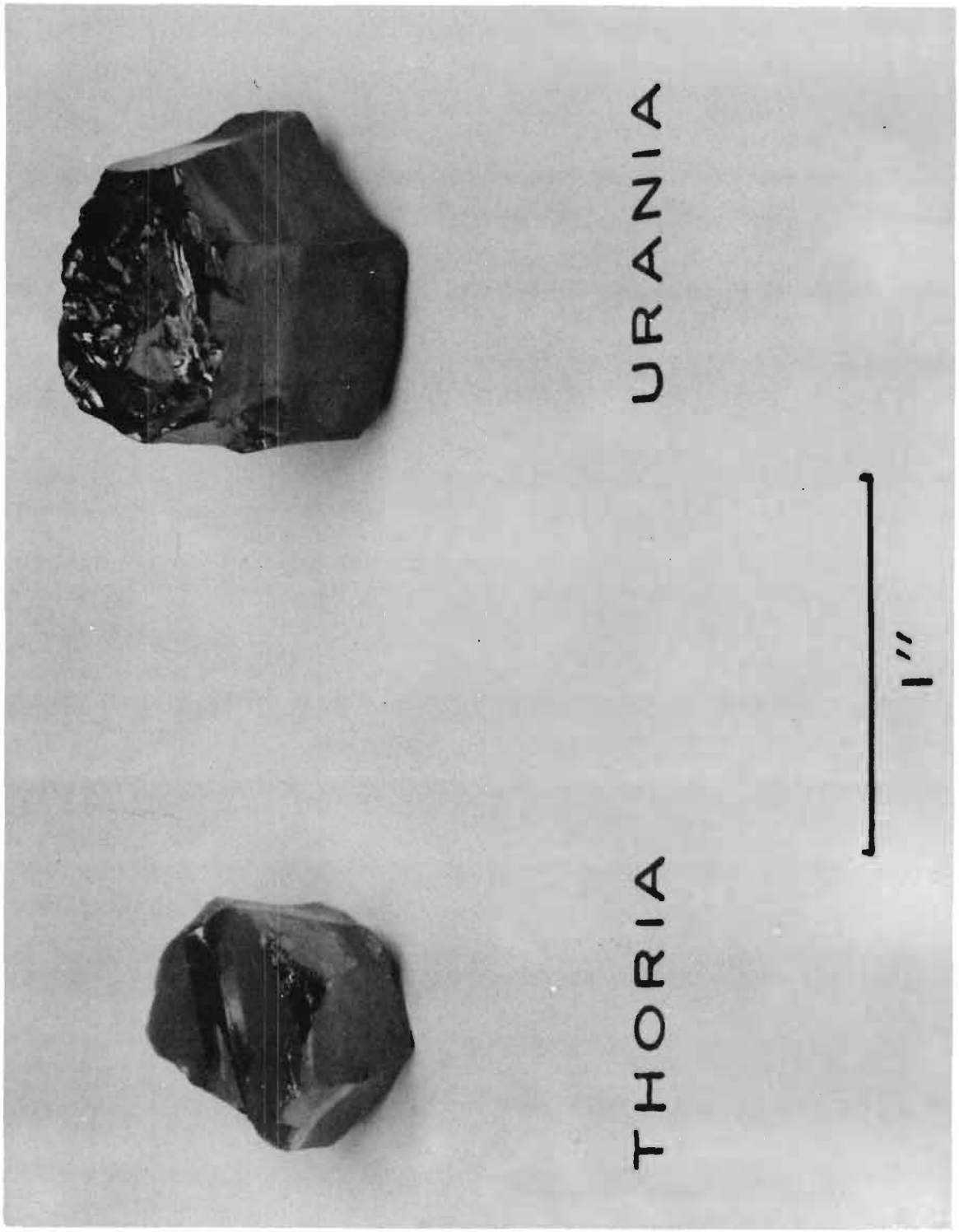

Figure 2. ThO_2 and UO_2 Crystals.

PROGRESS REPORT NO. 2

PROJECT NO. B-146

MECHANISM AND ACTIVATION ENERGY FOR DIFFUSION THROUGH SINGLE CRYSTAL AND POLYCRYSTALLINE HIGH TEMPERATURE MATERIALS

By

WILLIS E. MOODY

CONTRACT NO. AT (40-1)-2420

ATOMIC ENERGY COMMISSION

1 FEBRUARY 1960

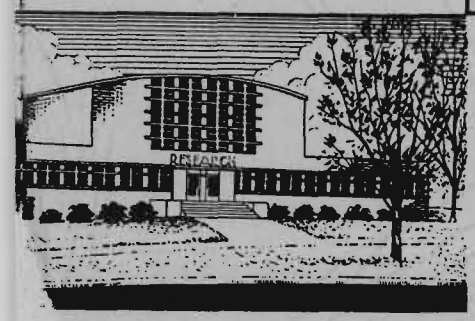

Engineering Experiment Station

Georgia Institute of Technology

Atlanta, Georgia

ENGINEERING EXPERIMENT STATION
of the
GEORGIA INSTITUTE OF TECHNOLOGY
ATLANTA, GEORGIA

PROGRESS REPORT NO. 2

PROJECT NO. B-146

MECHANISM AND ACTIVATION ENERGY FOR DIFFUSION THROUGH SINGLE CRYSTAL AND POLYCRYSTALLINE HIGH TEMPERATURE MATERIALS

By

WILLIS E. MOODY

CONTRACT NO. AT (40-1)-2420

ATOMIC ENERGY COMMISSION

1 FEBRUARY 1960

TABLE OF CONTENTS

This report contains 13 pages

LIST OF FIGURES

LIST OF TABLES

I. INTRODUCTION

This report summarizes the work performed since Progress Report No. 1, submitted under the date of 1 February 1959, through January 1960.

The objective of this program is to advance in a systematic manner the basic scientific knowledge of mass transport phenomena and imperfections in metallic oxide, ceramic, materials. Uranium dioxide and alumina were selected for this study as metallic oxides having desirable high temperature characteristics. The inert gases, helium, neon, krypton, argon and xenon, were selected as diffusing elements with which to obtain data on diffusion as a function of size. Also, as these gases are assumed to have zero valence, any complications arising from valency considerations would be eliminated.

II. SUMMARY OF WORK

The results of experimental work and equipment construction are outlined in detail in sections A to D. Considerable time has been devoted to procurement and assembly of equipment during the period of this report.

A. Tube Fabrication

Figure 1 shows examples of the alumina single crystal and polycrystalline barriers and tubes which have been fabricated. The single crystal alumina barrier can be observed more clearly in Figure 2. The alumina tubes currently being used are 98 per cent alumina and were made by American Lava Corporation, Chattanooga, Tennessee. It was necessary to set up the equipment (Figures 3 and 4) to shape the barriers. A faceting goniometer and a 100-mesh diamond grinding wheel mounted on the polishing

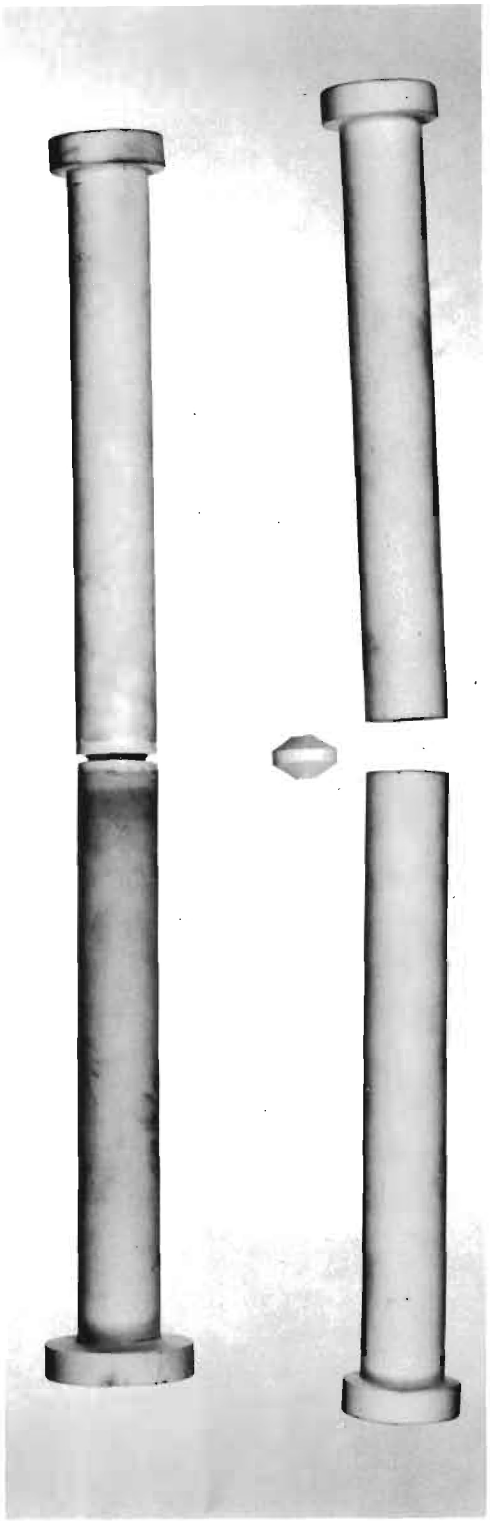

Figure 1. Alumina Tubes and Barriers.

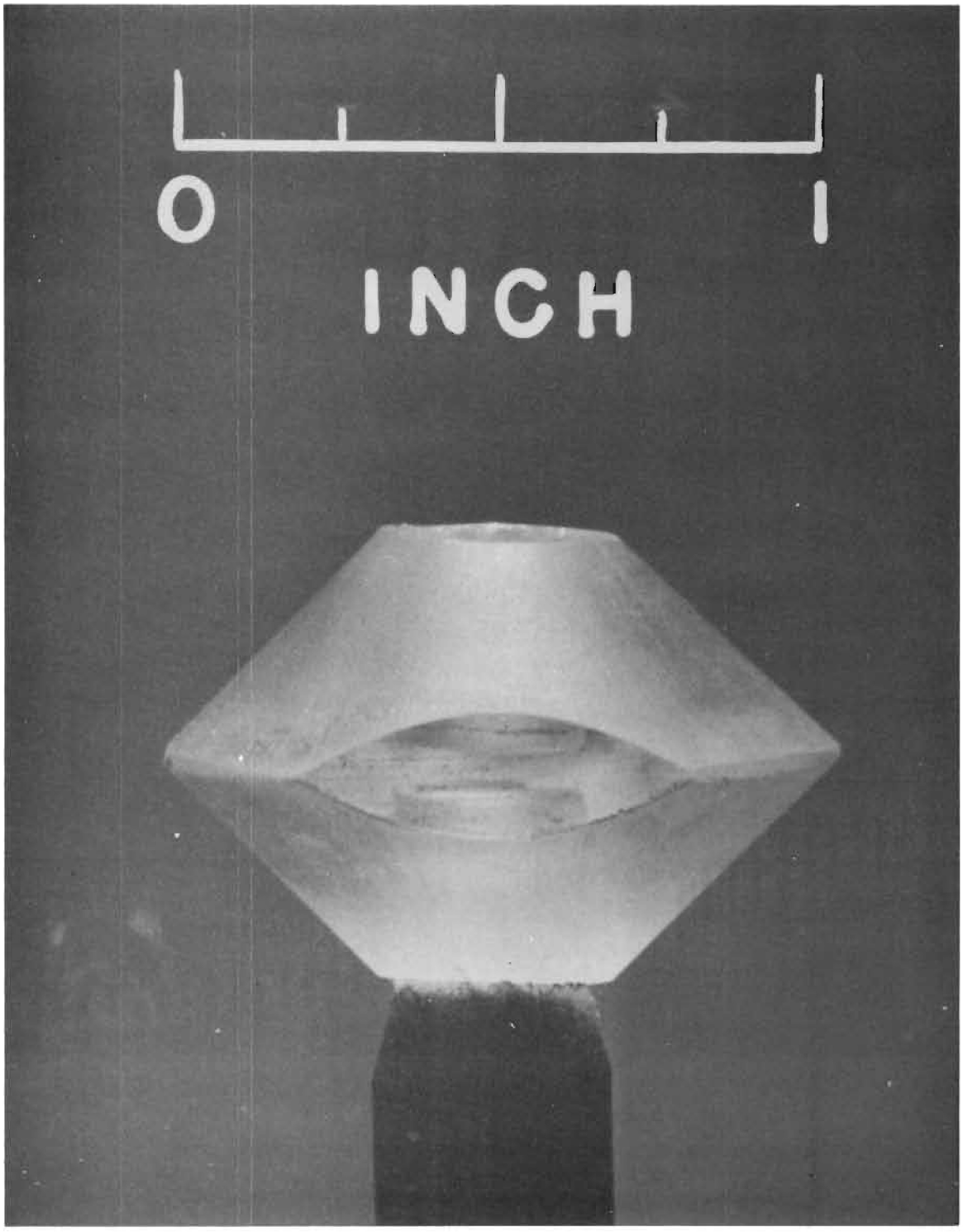

Figure 2. Single Crystal Alumina Barrier.

Figure 3. Grinding Wheel and Faceting Goniometer.

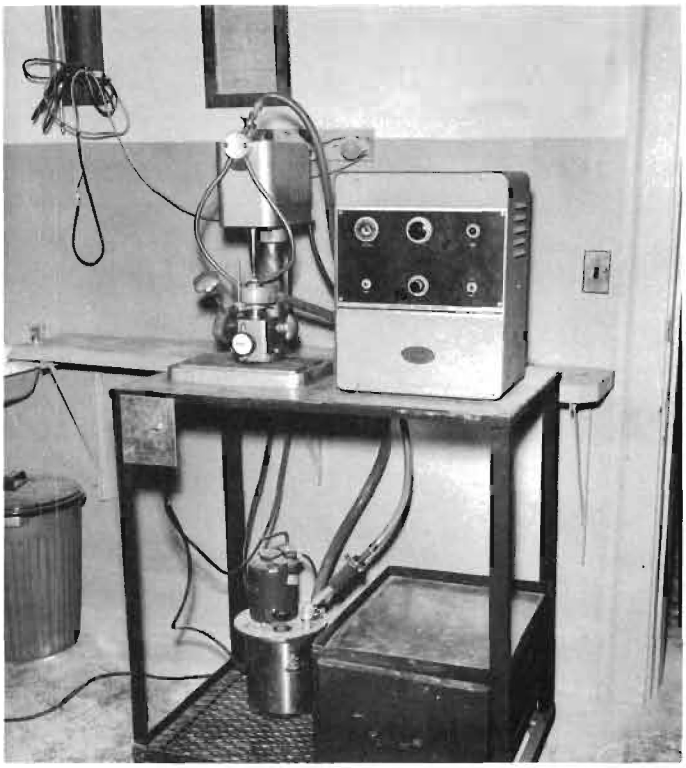

Figure 4. Sonic Grinder.

wheel proved satisfactory for shaping the exterior profile of the barriers. The polishing wheel set-up was placed in a glove box for shaping the uranium dioxide, UO_2, barriers (Figure 2). The sonic grinder (Figure 4), Raytheon Mfg. Co., Model 2-334, was very satisfactory for drilling the $\frac{1}{4}$-inch-diameter holes. Boron carbide, B_4C, is being used as the abrasive for the sonic grinder. Shaping the barrier is a somewhat slow operation which may require from 2 to 3 days for the more difficult single crystal alumina. All of the alumina barriers have been shaped in profile and drilled for a barrier thickness of 0.060 inch. A few tubes have been fabricated for the helium diffusion study. All of the alumina tubes will be fabricated as soon as a suitable barrier thickness can be estimated from the helium data. The thickness of the barrier is being determined from the equation, $2\sqrt{Dt} \approx$ thickness, that gives the relationship between time to reach steady state, diffusion coefficient, and barrier thickness. It is desirable to have the time interval required to reach steady state to not exceed 2 days and to have the thickest barrier possible. A barrier thickness of 0.060 inch has required approximately 5 hours in the polycrystalline alumina and approximately 13 hours in the single crystal alumina to reach steady state conditions with helium. A single crystal alumina barrier thickness of 0.090 inch required approximately 4 days to reach steady state conditions with helium.

The single and polycrystalline uranium dioxide blanks are ready for grinding into barriers. Because of the probability of radioactive contamination of the equipment, the uranium dioxide barriers will be fabricated after the fabrication of the alumina barriers is no longer in the experimental stage.

The source and fabrication techniques for the barrier materials are listed in Table I.

TABLE I

BARRIER MATERIALS

Barrier	Source
Polycrystalline Al_2O_3	100% Al_2O_3, hot pressed, refired to 1820°C in oxidizing atmosphere, Carborundum Co., Niagara Falls, N. Y.
Polycrystalline UO_2	100% UO_2, H_2 firing, Mallinckrodt Nuclear Corp., St. Louis, Mo.
Single Crystal Al_2O_3	Oxyhydrogen ~~Oxyacetylene~~ flame process, Linde Co., New York, N. Y.
Single Crystal UO_2	Electric arc melt growth, Norton Co., Worcester, Mass.

All of the alumina and uranium dioxide barriers and all of the alumina barrier tubes should be fabricated by the end of the present contract period. The uranium dioxide barrier tubes will be fabricated upon completion of the alumina-to-uranium-dioxide bonding or sealing material study. It is expected that the uranium dioxide tubes will be ready within the first 4 months of the next contract period.

B. Bonding Material

A large number of different materials have been investigated as bonding materials. Only the materials forming a bond at temperatures above 1500°C have been considered suitable. The most satisfactory composition for the alumina-to-alumina bond is given in Table II.

TABLE II

ALUMINA-TO-ALUMINA BONDING MATERIAL: EMPIRICAL FORMULA

0.60 CaO		
0.20 MgO	1.3 Al_2O_3	13.5 SiO_2
0.10 BaO		
0.10 SrO		

It was found to be a glass and formed a good bond when held for one hour at a temperature of 1515°C in an oxyacetylene furnace. Appreciable amounts of potassium oxide and sodium oxide have shown a great tendency to form bubbles in the bonding area. The bubbles were not visible on the surface to any extent. It is planned to try the composition in Table II with additions of uranium dioxide and thorium dioxide as a bond for uranium dioxide to alumina. These experiments and a suitable uranium-dioxide-to-alumina bond should be completed within the next 6 months.

C. Helium Diffusion

Figure 5 shows the diffusion cell and auxiliary equipment. A schematic diagram of the diffusion cell was shown in Progress Report No. 1. The cell was checked for leaks with the helium leak detector at tube temperatures up to 1000°C. A number of runs have been made with single and polycrystalline alumina barriers.

Figure 6 is a graphical presentation of the helium-alumina data. A helium leak detector on hand was calibrated and successfully used to determine the rate of flow of helium through the barrier. The detector also permitted recognition of the time when steady state conditions were achieved.

Figure 5. Diffusion Cell.

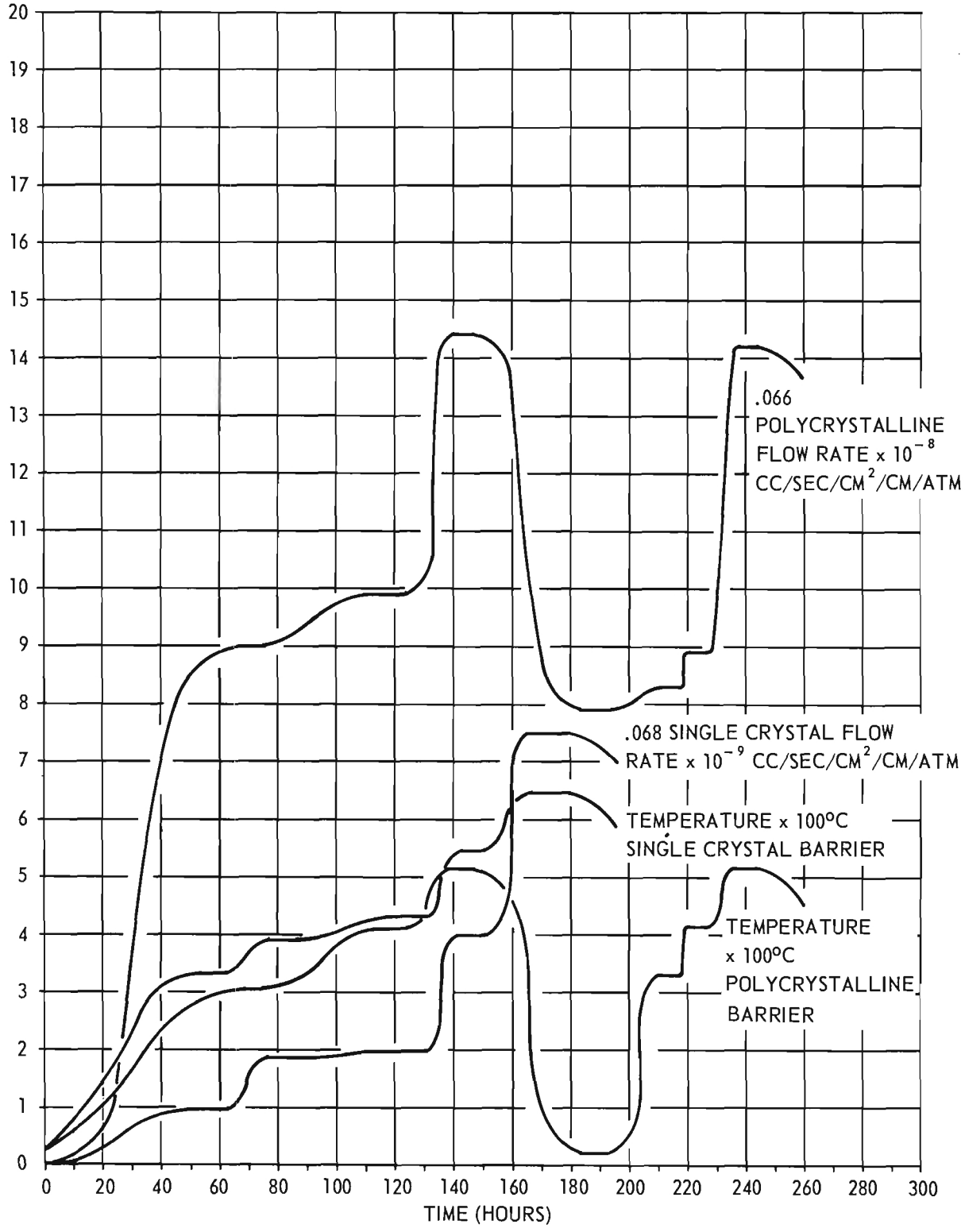

Figure 6. Helium-Alumina Data.

At the flow rates obtained, 10^{-10} to 10^{-7} (cc)/(sec)(sq cm)(cm/atm), a mass spectrometer apparently is the only suitable means for obtaining suitable accuracy of analyses and flow rates for the gases other than helium. An ionization gas chromatograph, Model 10, Barber-Coleman Co., was not satisfactory for the analysis of the helium under such low flow rates. Consideration has been given to neutron activation analysis. However, the cost involved for a large number of analyses, at about $100 each, and the time lag of 2 or more days necessary for an analysis make this method unsatisfactory. A mass spectrometer will give results immediately and with adequate accuracy for this work. A mass spectrometer is considered necessary for future work.

Figure 7 shows a plot of the D vs $\frac{1}{T}$ curve for the diffusion of helium through single and polycrystalline alumina. The activation energy for the single crystal material was 0.31 ev and for the polycrystalline material was 0.103 ev for the first cycle and 0.115 ev for the second cycle. The activation energy in the polycrystalline alumina was slightly higher when determined from the data of the second run as compared with the first. This is illustrated by the two curves for the polycrystalline alumina in Figure 7. Contrary results have been obtained by other investigators.[1] However, it should be pointed out that the data of Figure 7 must be extended before this can be considered a well-established conclusion.

The numerical value of the activation energy is of the order of magnitude that would be expected for the atom-vacancy exchange mechanism. The helium atom is smaller in size than the oxygen ion and would very

---

[1] "Atom Movements", Amer. Soc. Metals, 1951.

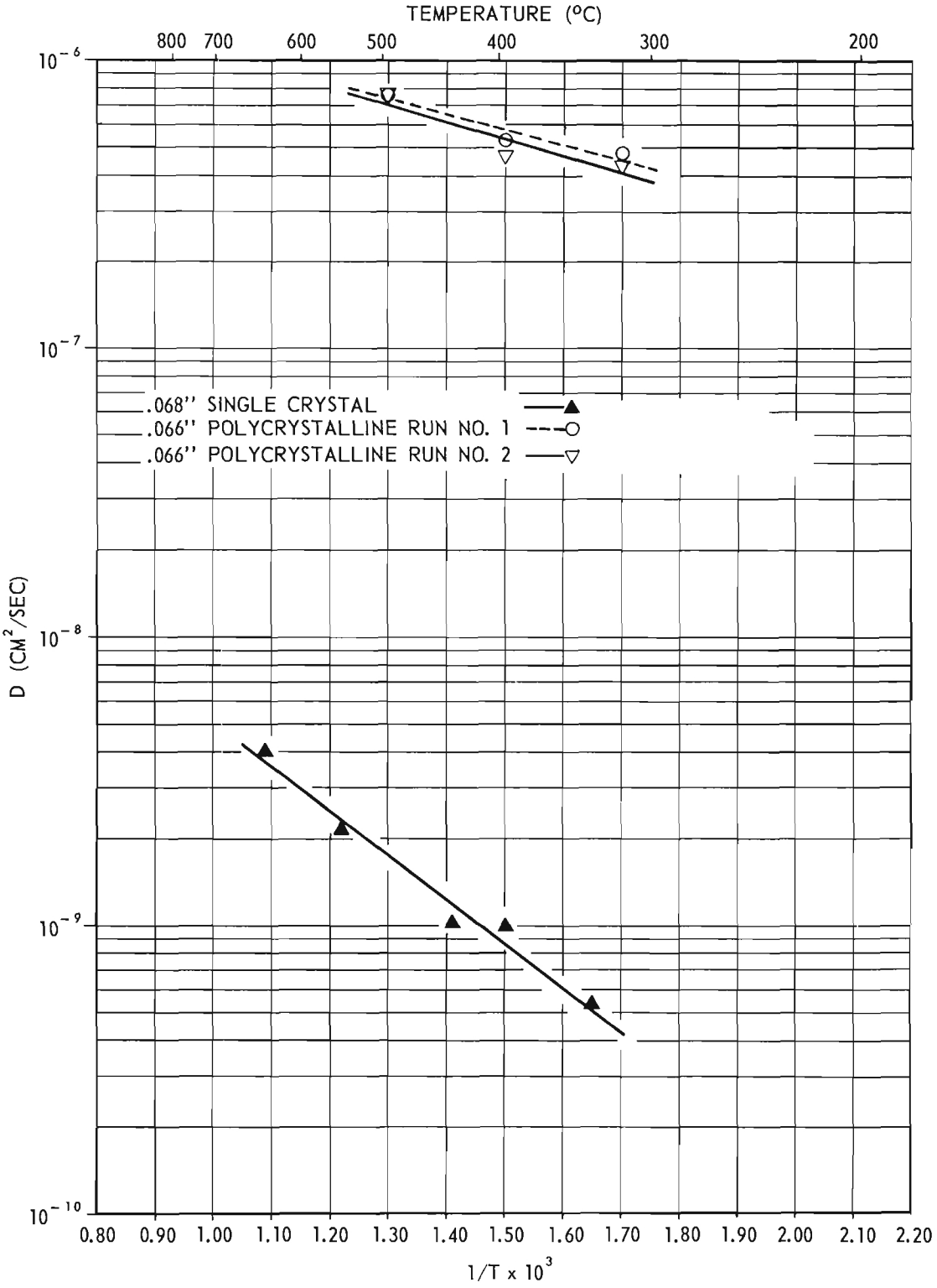

Figure 7. Diffusion of Helium through Alumina.

easily move along grain boundaries and through the lattice where holes exist in the oxygen layers.

The reproducibility of the data on helium is being evaluated at the present time.

A paper on this subject will be presented at the American Ceramic Society meeting, Philadelphia, Pennsylvania, in April 1960. The paper will be primarily on the diffusion of helium but will also present the objectives of this program.

D. Concentration Gradient and Lattice Parameters

A great deal of necessary information may be obtained by establishment of the concentration gradient. P. Gibbs[2] has postulated the existence of edge dislocations in single crystal alumina. Edge dislocation diffusion would probably show very little difference in concentration across the thickness. Schematically the concentration could vary as shown in Figure 8. The concentration lines of Figure 8 may be curved

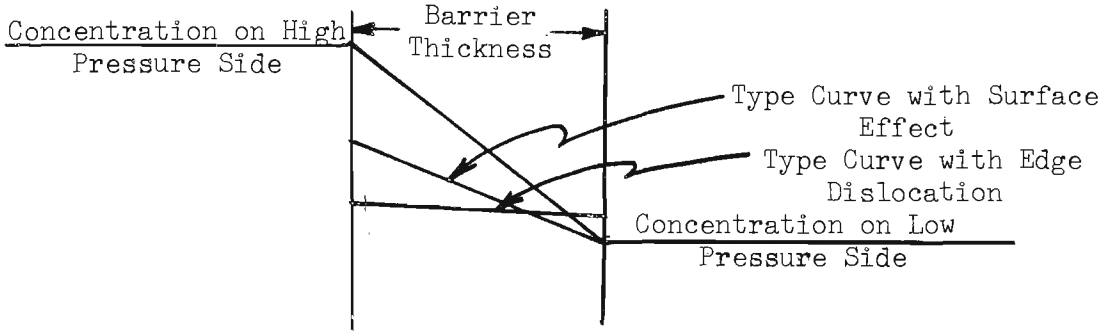

Figure 8. Schematic Probable Concentration Gradients

[2] P. Gibbs, H. B. Vanfleet, and G. S. Baker, "Macroscopic Flow of Impurity Along Dislocation", Amer. Ceramic Soc. meeting, Chicago, 1959.

(Bessel functions) rather than straight as shown. The numerical value of D will be greatly changed should there be any surface effect on the concentration gradient as illustrated in Figure 8. In other words, if the gradient were as shown in Figure 8 (surface effect curve), the numerical value of D would be considerably higher. X-ray fluorescence techniques appear to be the only satisfactory method of obtaining the gradient for argon, krypton, and xenon without using extensive equipment. From the data on argon, krypton, and xenon, an attempt will be made to estimate a curve for helium and neon. This should be possible as the main difference would be in the size of the atoms.

X-ray diffraction techniques will give information on changes in the lattice size should they occur. The alumina crystals have been shaped so as to have the C axis perpendicular to the barrier surface and the layers of close packed oxygen atoms in the plane of the barrier. It would not be unreasonable to expect the diffusing atoms to collect between planes of oxygen atoms and cause slight expansion of the lattice as movement takes place by a jump across the oxygen layers. Correlation of the gradient and lattice size data with the activation energy should establish quite accurately the mechanism of mass transport.

A suitable x-ray diffraction and fluorescence unit can be obtained from Philips Electronics, Inc., for $25,000.

Respectfully submitted,

Approved:

Willis E. Moody
Project Director

Frederick Bellinger, Chief
Material Sciences Division

PROGRESS REPORT NO. 3

PROJECT NO. B-146

MECHANISM AND ACTIVATION ENERGY FOR DIFFUSION THROUGH SINGLE CRYSTAL AND POLYCRYSTALLINE HIGH TEMPERATURE MATERIALS

By

WILLIS E. MOODY

CONTRACT NO. AT (40-1)-2420

ATOMIC ENERGY COMMISSION

1 FEBRUARY 1961

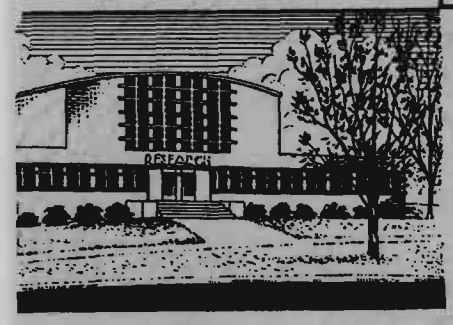

Engineering Experiment Station

Georgia Institute of Technology

Atlanta, Georgia

ENGINEERING EXPERIMENT STATION
of the Georgia Institute of Technology
Atlanta, Georgia

PROGRESS REPORT NO. 3

PROJECT NO. B-146

MECHANISM AND ACTIVATION ENERGY FOR DIFFUSION THROUGH SINGLE CRYSTAL AND POLYCRYSTALLINE HIGH TEMPERATURE MATERIALS

By

WILLIS E. MOODY

CONTRACT NO. AT (40-1)-2420

ATOMIC ENERGY COMMISSION

1 FEBRUARY 1961

TABLE OF CONTENTS

This report contains 12 pages.

LIST OF FIGURES

I. INTRODUCTION

This report summarizes the work performed since Progress Report No. 2, submitted under the date of 1 February 1960, and through January 1961.

The objective of this program is to advance in a systematic manner the basic scientific knowledge of mass transport phenomena and imperfections in metallic oxide, ceramic, materials. Alumina was selected for this study as a metallic oxide having desirable high temperature characteristics. The inert gases, helium, neon, argon, krypton, and xenon, were selected as diffusing elements with which to obtain data on diffusion as a function of size. Also, as these gases are assumed to have zero valence, any complications arising from valency considerations would be eliminated. The experimental diffusion work has been confined to helium diffusion through Al_2O_3 because of equipment limitations which did not permit working with the other inert gases. The feasibility of determining the concentration gradient for argon, and krypton in Al_2O_3 has been demonstrated with the vacuum x-ray fluorescence unit.

II. SUMMARY OF WORK

The results of experimental work are outlined in section A to D. Considerable time has been devoted to data analysis during the period of this report.

A. Helium Leak Detector

A Veeco helium leak detector, model MS-9A, was obtained for measuring the helium flow rate as it was necessary to return the borrowed unit to the local Veeco representative. Oscillations were observed on the lower scale for helium leak rate after a few weeks of operation. These oscillations were sporadic and

of sufficient amplitude to obscure the helium leak rate. After a number of attempts to eliminate the oscillations, the amplifier power supply was checked on an oscilloscope. It indicated that the 6626 (V6) gas filled voltage regulator tube was malfunctioning. A tube replacement, OA2, resulted in stabilization and elimination of the oscillations. It is understood that the Veeco Vacuum Corporation has now replaced the 6626 (V6) tube with a OA2 tube on all new models.

B. Krypton and Argon Concentration Gradient Determination

The feasibility of determining the concentration gradient of argon and krypton in Al_2O_3 has been demonstrated. A Philips Electronic Instruments Division vacuum x-ray spectrograph, Model 52360 with pulse height analyzer, with a NaCl crystal was used to detect argon K_α, and with a LiF crystal was used to detect krypton K_α. In order to set up the pulse-height analyzer for argon, it was necessary to use silver L_α, (4.154 Å) as a close substitute for argon K_α. Under these conditions the argon and krypton contents of single crystal Al_2O_3 could be detected for specimens heated to 1000° C, for 24 hours, in those atmospheres. Fig. 1 shows the heights of the peaks obtained with all x-ray conditions duplicated except as specified for specimen C. The remaining traces of argon in the vacuum are the cause of the small peak for the no-argon specimen, Fig. 1A. These same specimens were run on a helium x-ray spectrograph without a pulse-height analyzer and no significant differences could be deduced between the specimens with or without the inert gas content. It was necessary to visit the Philips Laboratory at Mount Vernon, New York to obtain use of the vacuum x-ray fluorescence equipment.

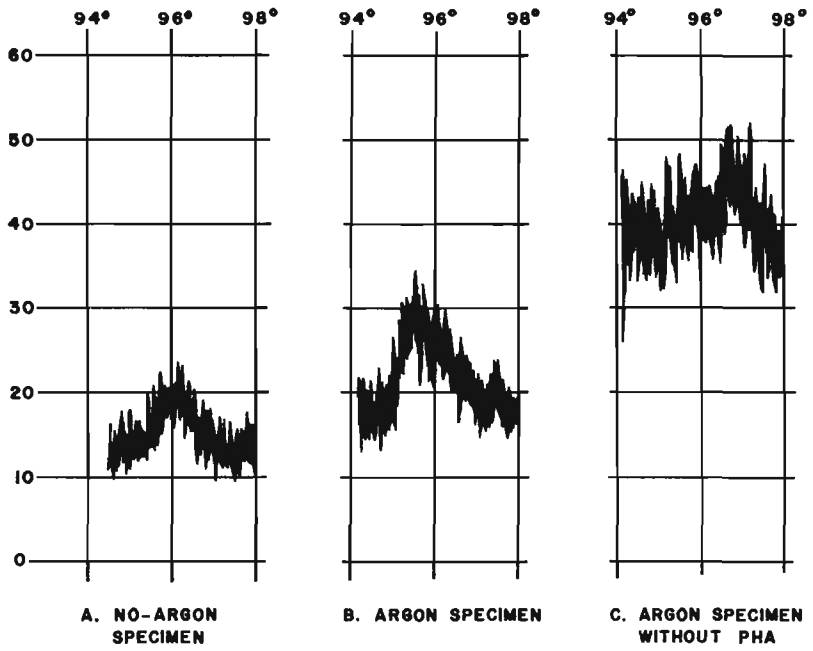

FIG. 1 ARGON AND KRYPTON X-RAY FLUORESCENCE RECORDER CURVES

C. Helium Diffusion

The experimental set-up has been given in Progress Reports Nos. 1 and 2. The experimental work has been largely confined to collection of He diffusion data and comparison of methods of analysis. The two methods of data analysis have been:

Method A. It is assumed that the concentration gradient is equivalent to the difference in concentration of He on each side of the barrier divided by barrier thickness. The diffusion coefficient is then calculated from equation (1):

$$P = -D\frac{\partial c}{\partial x} \qquad (1)$$

P = Permeability or flux

D = Coefficient of diffusion

$\frac{\partial c}{\partial x}$ = Concentration gradient

Method B. Rogers, Buritz and Alpert[1] developed a method for simultaneously measuring the diffusion coefficient, solubility, and permeability for a gas in a single sample of solid material. The method utilizes solutions of the diffusion equation which makes it possible to calculate the diffusion parameters from data in the early part of the transient period, early-time approximation, or in the steady-state gas flow, late-time approximation.

Solutions for equation (1) are obtained as follows:

1. W. A. Rogers, R. S. Buritz and D. Alpert, "Diffusion Coefficient, Solubility, and Permeability for Helium in Glass," J. App. Phy. 25(7) 868 (1954).

1. Early-time Approximation

   Slope = $d^2/4D$

   d = barrier thickness

   D = Coefficient of diffusion

   Slope = slope of line of Fig. 2

2. Late-time Approximation

   $D = d^2/6t_c$

   D = Coefficient of diffusion

   d = barrier thickness

   t_c = Characteristic time as shown on Fig. 3

3. Solubility (late-time approximation)

   P = DS

   P = Permeability

   D = Coefficient of diffusion

   S = Solubility

A very fundamental question arises in the concept of permeability and solubility. The method of Alpert assumes that the gas has a uniform solubility within the solid rather than the concentration gradient of method A. Geochemists[2] have known for many years that certain rock samples, when heated, will give off gases which could not come from any chemical reaction present. At the present time the data are being analyzed by both methods for agreement. Within experimental error there appears to be good agreement for the value of D. However, the solubility value is not consistent with what should be expected when determined by method B. However, it should be pointed out that

2. F. W. Clarke, Bull. U. S. Geol. Sur., 695, 270 (1920).

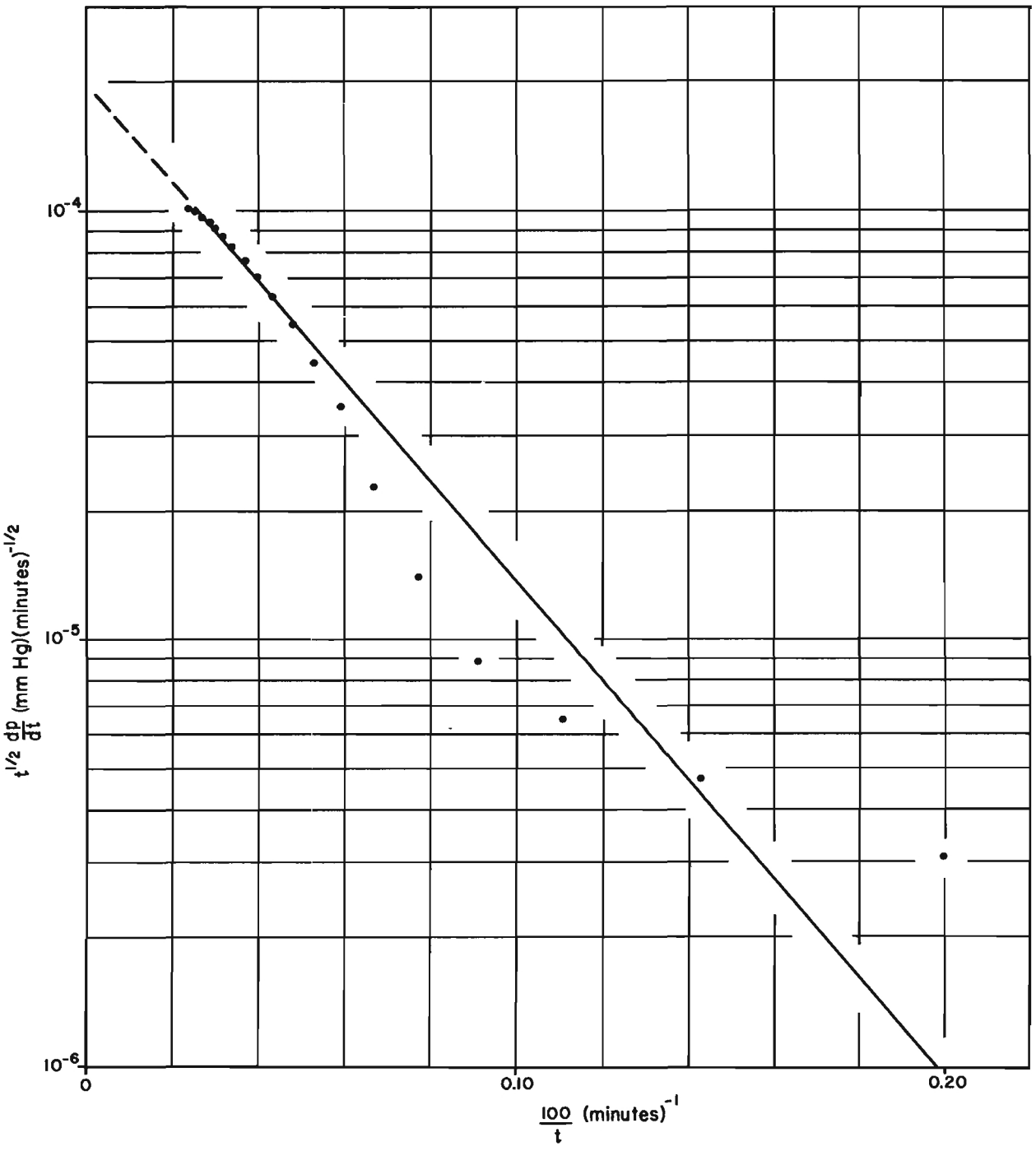

FIG. 2 DATA PRESENTATION FOR EARLY TIME APPROXIMATION.

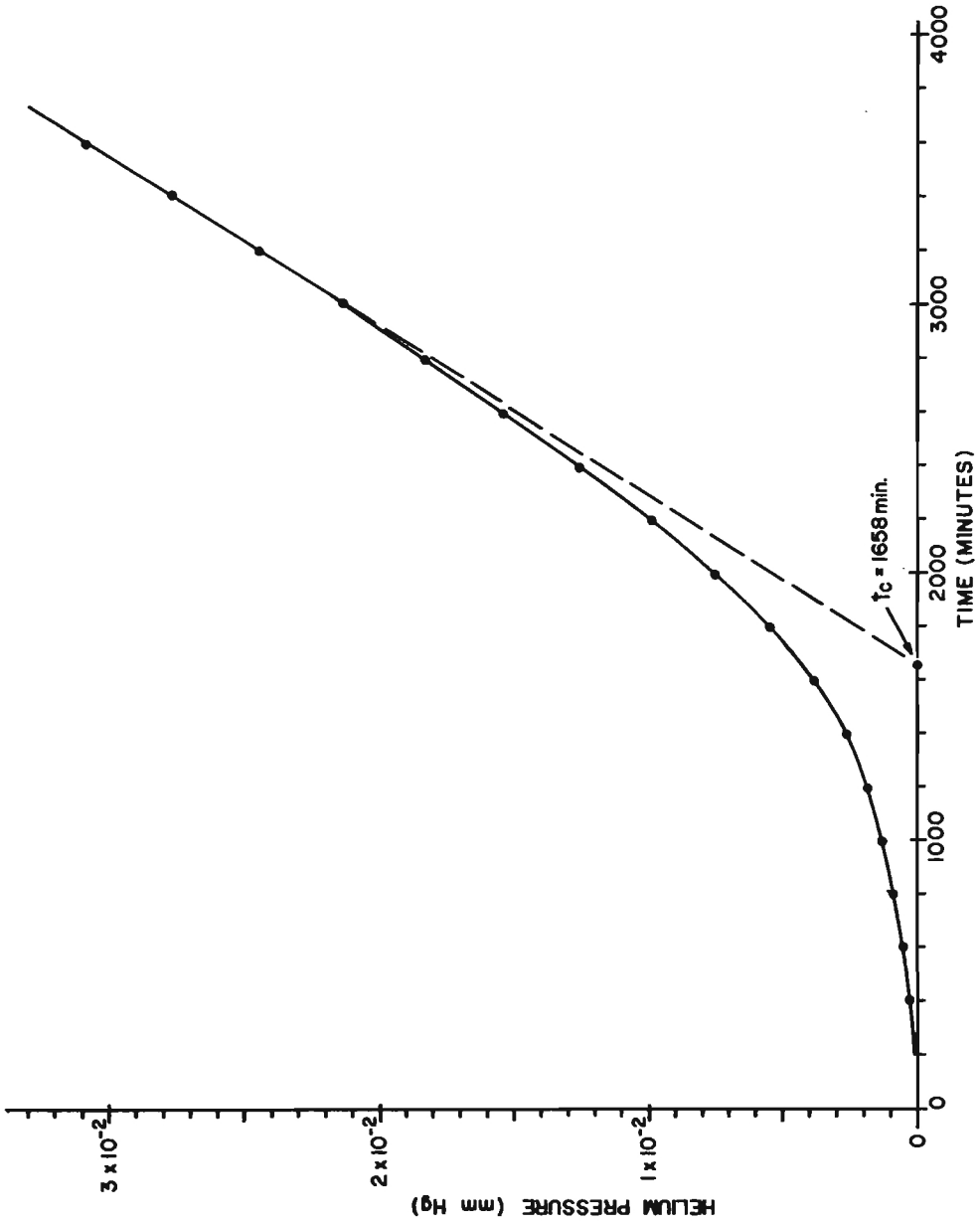

FIG. 3 DATA PRESENTATION FOR LATE TIME APPROXIMATION.

only two calculations have been made using method B. Additional samples and calculations are being made at this time so as to arrive at more conclusive results.

The experimental results for He diffusion using method A is given in Figs. 4 and 5. Two specimens of the General Electric Company product, Lucalox, Al_2O_3 were heated to 500° C and no detectable amount of Helium diffusion could be determined. The material is polycrystalline Al_2O_3 which is very close to theoretical density. The samples were not run at higher temperatures as large leaks developed in the barriers. Crandall et al.[3] have observed peaks for internal friction measurements on polycrystalline Al_2O_3 at temperatures slightly higher than the discontinuities of the curves of Figs. 4 and 5. The experimentally measured values of activation energy from Fig. 5 for the single crystal Al_2O_3 compared favorably with a calculated value, 0.20 ev., obtained by the method outlined by Moody et al.[4] for edge dislocations as illustrated in Fig. 6.

An x-ray diffraction unit has been purchased and measurements will be made on the lattice parameters of the barrier section. The x-ray diffraction studies of the lattice parameters for single crystal specimen should indicate a concentration gradient or solubility. The lattice should be expanded uniformly to some extent along the c-axis if solubility rather than a concentration gradient exists. If a concentration gradient exists, one would expect to find the lattice expanded to a much lesser extent on the low concentration side of the barrier. Measurements will be made on the surface of the barrier and as subsequent layers are removed. It would be very desirable to make a diffusion study with argon or krypton and use x-ray fluorescence techniques to determine

3. W. B. Crandall, D. H. Chung, and T. J. Gray, "The Mechanical Properties of Ultra-fine hot-pressed Alumina," Monthly Progress Report No. 287 Vol. XXV, No. 5, Ceramic Research Dept. Alfred University, New York (1960).

4. W. E. Moody, W. D. Whitehead, and W. W. Kriegel, "Activation Energy for Diffusion of ^{133}Xe through MgO-Ni Cermet Compacts." J. Am. Ceram. Soc. 43 (12)634(1960).

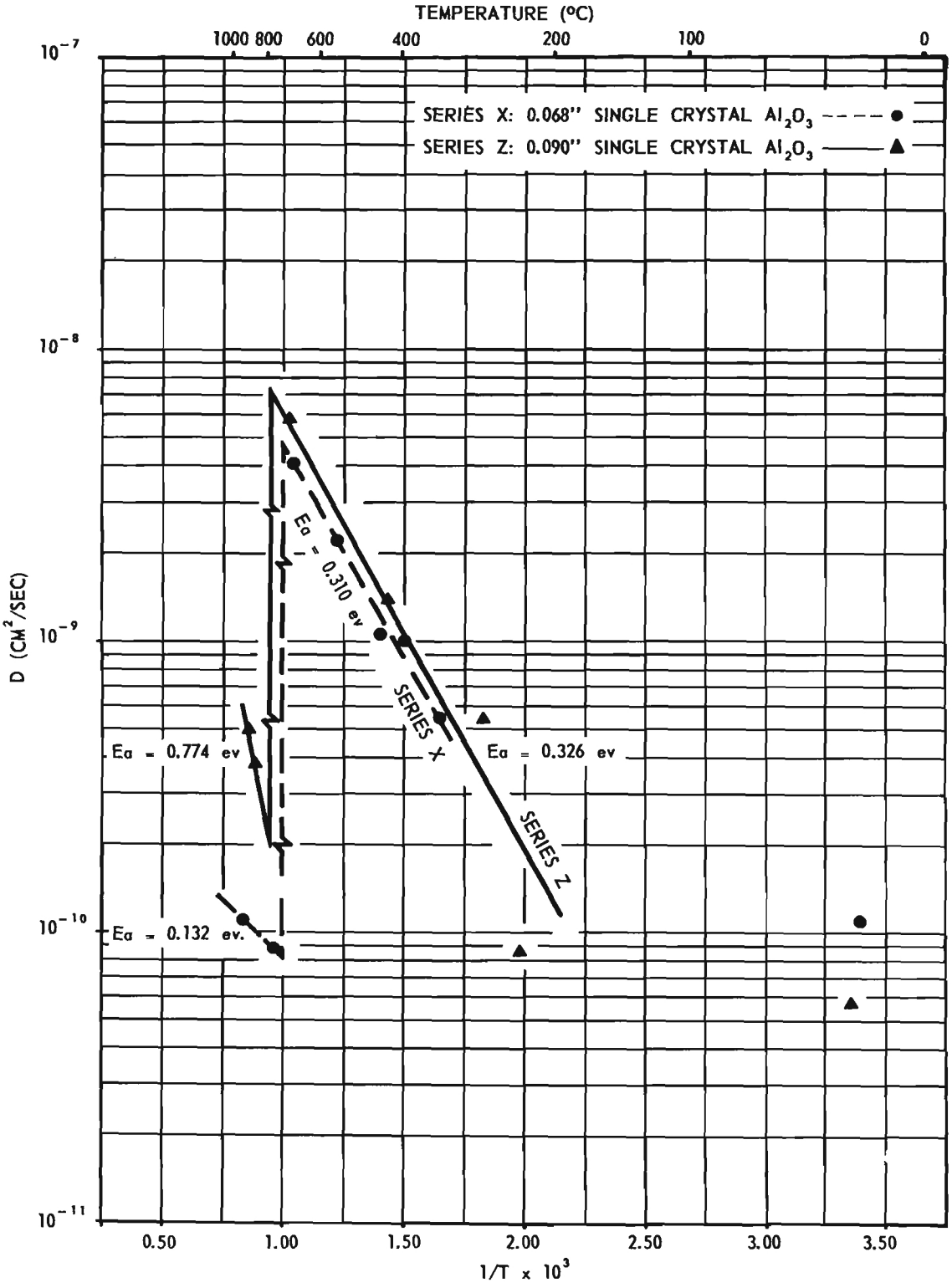

FIG. 4 HELIUM DIFFUSION THROUGH SINGLE CRYSTAL Al_2O_3

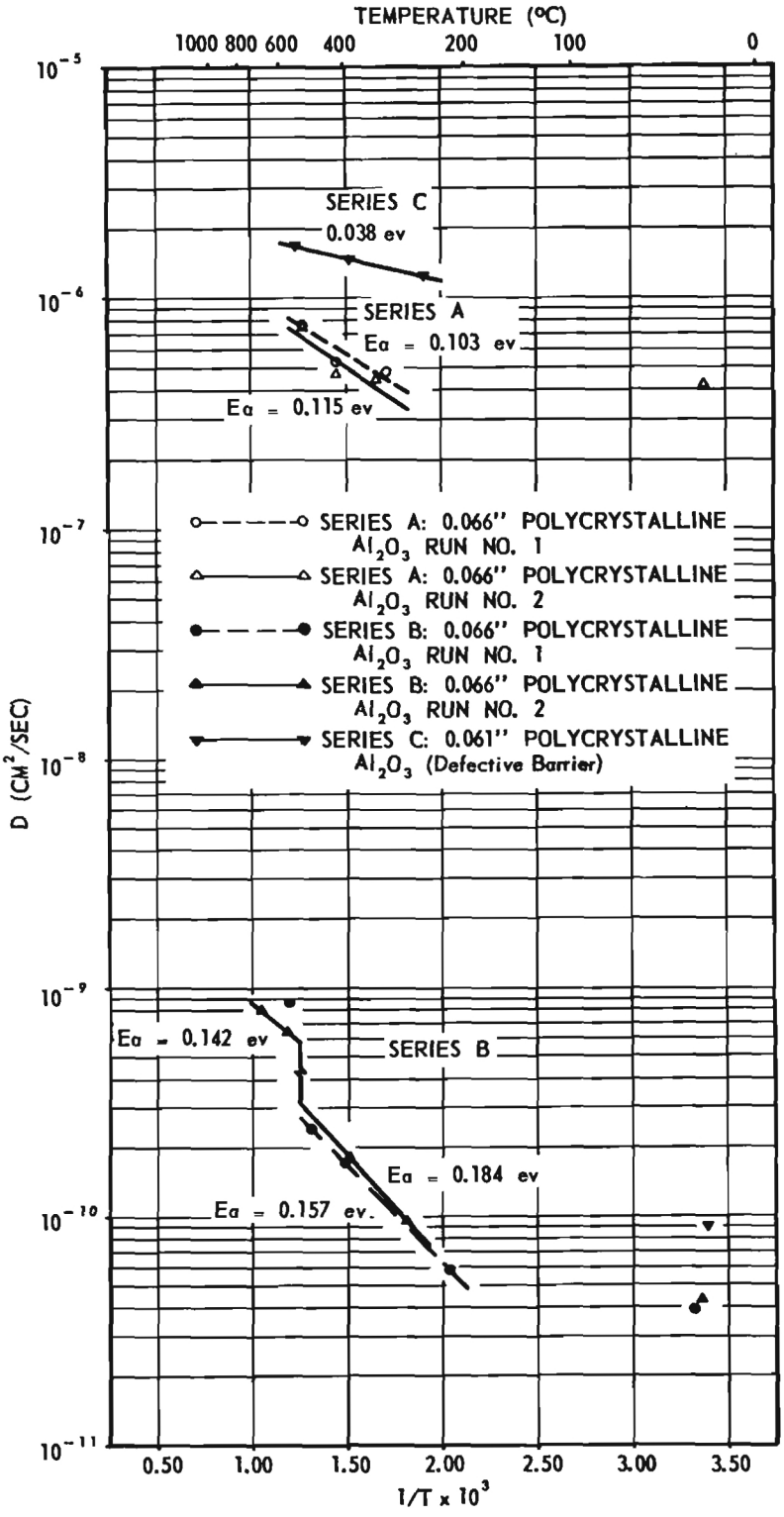

FIG. 5 HELIUM DIFFUSION THROUGH POLYCRYSTALLINE Al_2O_3

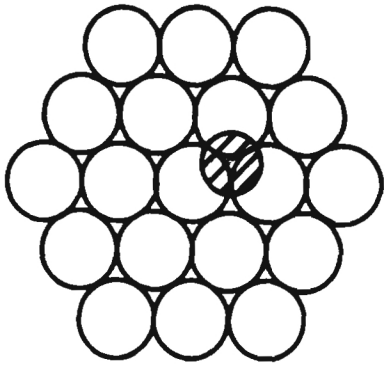

INTERSTITIAL HOLE
Ea = 5.7 ev

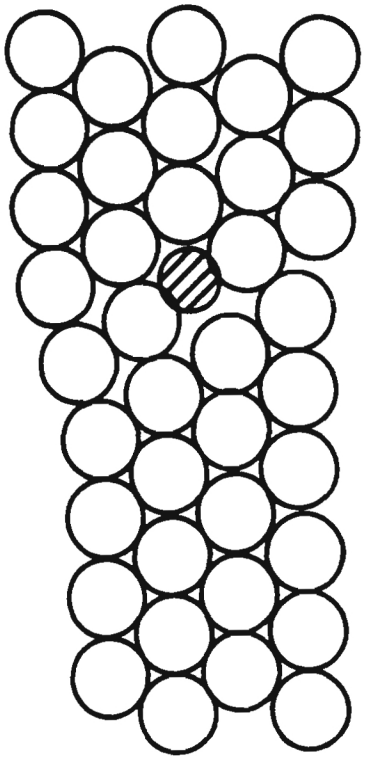

EDGE DISLOCATION
Ea = 0.2 ev

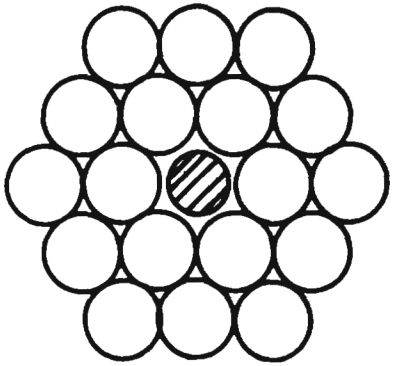

VACANCY
Ea = 0 ev

HELIUM 1.86 Å

OXYGEN 2.64 Å

FIG. 6 CALCULATED ACTIVATION ENERGIES

to what extent a concentration gradient does exist.

It is planned to continue the helium diffusion through Al_2O_3 work during the remaining contract period and during the four months renewal period. This should give sufficient time to complete the work and allow the two graduate students to complete their theses.

D. Publications

A small amount of time and effort has been spent during the past two years in preparing and revising a paper for publication on work from a previous AEC contract at North Carolina State College. A reprint of this paper is attached.

Respectfully submitted:

Willis E. Moody
Project Director

Approved:

Frederick Bellinger, Chief
Material Sciences Division

[Reprinted from the Journal of The American Ceramic Society, Vol. 43, No. 12. December, 1960.]

Activation Energy for Diffusion of ^{133}Xe Through MgO-Ni Cermet Compacts

by W. E. MOODY, W. D. WHITEHEAD, and W. W. KRIEGEL

Ceramic Engineering, Department of Mineral Industries, North Carolina State College, Raleigh, North Carolina

The ^{133}Xe was produced by irradiation of UO_2 which formed the central or core portion of small disks made from a 66% Ni and 34% MgO cermet material. Diffusion rates through this material were determined in the temperature range 800° to 1100°C. The activation energy for diffusion was determined to be 4.4 e.v. with the diffusion coefficient given by the equation $D = 1.85 \times 10^7 e^{-\frac{4.4 \text{ e.v.}}{kT}}$ sq. cm. per second. The mechanism of diffusion appeared to be of the atom-vacancy interchange type.

I. Introduction

THE diffusion of fission products through solids is of great importance in the design and construction of nuclear power reactors. Because of the dangers associated with the high-level radioactivity of fission products, it is imperative that any container material be evaluated as to its ability to retain fission products or to prevent them from escaping. The coefficients of diffusion of a particular fission-product isotope at various temperatures for different materials make it possible to calculate the amount of this isotope which will pass through any thickness of a given material. The activation energy for diffusion aids in predicting the mechanism of diffusion whereby criteria for the improvement of the retention ability of the material can be established. The criteria for improvement would consist of changes in grain boundaries, elimination of lattice vacancies, and other phenomena related to the mechanism of diffusion.

As there are several hundred fission products and an equal or greater number of materials for which a diffusion study could be conducted, a somewhat arbitrary selection of materials that might have some technological significance was made. The diffusion of ^{133}Xe through a MgO-Ni cermet was chosen. The MgO-Ni cermet has some of the properties desirable for reactor components at elevated temperatures in that it has a relatively high coefficient of thermal conductivity, oxidation resistance, and other properties given in Table I.[1] Also, the neutron-economy classification would be in the category of an intermediate,* $\sigma_t = 0.184$ sq. cm. per cc. ^{133}Xe is one of the principal fission products and constitutes[2] approximately 6.29% of the fission products generated. The high capture cross section for some of the Xe isotopes is of importance in reactor poisoning.

Table I. Properties of MgO-Ni Cermet*

Composition:	66% Ni by weight 34% MgO by weight
Calculated density:	5.95 gm./cc.
Oxidation:	1094°C. in air, 0.2 to 0.4 gm./sq. cm. weight gain for 200 hr.
Young's modulus of elasticity:	
Temp. (°C.)	Y (lb./sq. in.)
25	36,000
982	13,000
1093	9,000
1204	7,500
Porosity:	Less than 1/4%

* From footnote 1.

II. Survey of Literature

(1) Diffusion

A study of diffusion processes is related to numerous aspects of physical-chemical phenomena such as chemical kinetics, sorption, and solution equilibria. In general, the two states of flow by diffusion are the unsteady state and the steady state. From the steady state, equation (1) is obtained for the permeability constant or flux. From the unsteady state, a second equation is derived, (equation (2)), which refers to the accumulation of matter at a given point as a function of time. Both equations are differential forms of Fick's laws[3] of diffusion which were developed in 1855 and summarized by Darken.[4]

$$P = -D \frac{\partial C}{\partial x} \quad (1)$$

$$\frac{\partial C}{\partial t} = D \frac{\partial^2 C}{\partial x^2} \quad (2)$$

P = permeability constant (quantity transferred per unit time per unit area) or flux.
D = coefficient of diffusion.
C = concentration.
$\partial C/\partial x$ = concentration gradient.
$\partial C/\partial t$ = change in concentration with change in time.
$\partial^2 C/\partial x^2$ = rate of change of concentration gradient.

Numerous excellent surveys are available, e.g., those by Barrer,[5] by Carslaw,[6] and by Jost[7] dealing with specific mathematical solutions of equations (1) and (2) as applied to particular idealized geometrical configurations.

Presented at the Fifty-Eighth Annual Meeting, The American Ceramic Society, New York, N. Y., April 25, 1956 (Refractories Division, No. 37). Received July 27, 1959; revised copy received July 13, 1960.

The writers are, respectively, associate professor, School of Ceramic Engineering, Georgia Institute of Technology, Atlanta, Georgia; associate professor, Physics, University of Virginia, Charlottesville, Virginia; and professor of ceramic engineering, North Carolina State College, Raleigh, N. C.

[1] T. S. Shevlin, Engineering Experiment Station, Ohio State University, Columbus, Ohio, 1956; private communication.

* σ_t = thermal neutron absorption cross section.

[2] Reactor Handbook, Vol. 1, Physics. Technical Information Service, United States Atomic Energy Commission, 1955. 790 pp.

[3] Adolf Fick, "Über Diffusion," *Pogg. Ann.*, 94, 59 (1855).

[4] L. S. Darken, "Formal Bases of Diffusion Theory"; pp. 1–25 in Atom Movements. American Society for Metals, Cleveland, Ohio, 1951. 240 pp.

[5] R. M. Barrer, Diffusion In and Through Solids. Cambridge University Press, London, 1941. 464 pp.; *Ceram. Abstr.*, 21 [8] 179 (1942).

[6] H. S. Carslaw, Mathematical Theory of Conduction of Heat in Solids. Macmillan and Company, Ltd., London, 1921. 268 pp.

[7] W. Jost, Diffusion in Solids, Liquids, Gases. Academic Press, Inc., New York, 1952. 558 pp.; *Ceram. Abstr.*, **1953**, May, p. 94*a*.

In general, existing experimental data support equations (1) and (2) as limiting laws which are valid at sufficiently low concentrations. The coefficient of diffusion, D, as outlined by Darken,[4] is now recognized, however, to be a function of concentration as well as of the state variables.

Equation (1) was simplified for application to the problem so as to obtain equation (3), which was used to determine the D values.

$$D = \frac{\Delta s L V}{\Delta t A (C_1 - C_2)} \tag{3}$$

D = coefficient of diffusion.
Δs = number of diffused atoms.
L = thickness of cladding.
V = volume of fuel core.
Δt = time for diffusion.
A = total area through which diffusion products pass.
C_1 = concentration inside specimen core.
C_2 = concentration on outside of specimen.

The coefficient of diffusion, D, is of particular interest as it aids in an understanding of the phenomena of diffusion. From equations (1) and (2) there is a definite implication that D is a function of state variables such as temperature and composition. Barrer[5] has found that, for small concentrations, experimental diffusion measurements in metallic and nonmetallic systems have led to D values which can be expressed by a relation in the form of equation (4). The equation is of the form of the relation first proposed by Arrhenius for chemical reaction rates.

$$D = D_0 e^{-E_a/kT} \tag{4}$$

D = coefficient of diffusion.
D_0 = constant.
E_a = experimental energy of activation (activation energy).
k = Boltzmann's constant.
T = absolute temperature.

The D_0 value usually is constant for small concentrations but will vary as the concentration is altered. From calculations by means of fundamental chemical reaction rate equations, D_0 can be related to the thermodynamics of the system and, in particular, to the entropy. Empirical values of D_0 vary widely from those calculated from theoretical considerations. In the diffusion of carbon in body-centered cubic (alpha) iron the values have ranged from 0.0005 to 0.020 as compared with a calculated theoretical value of 0.026.[8] When coupled with the inherent inaccuracies associated with the experimental procedure of the present investigation, speculation concerning the values of D_0 is not warranted, and D_0 is considered as a constant.

Diffusion in solids may be described by means of three basic processes as outlined by Seitz[9]: (*a*) atom-atom interchange, (*b*) interstitial migration, and (*c*) atom-vacancy interchange. The relative probability of the three processes depends strongly on the numerical value of the activation energy of each process as associated with the particular spatial configuration of the system. The role of imperfections such as dislocations and grain boundaries is of great interest in diffusion as they provide diffusion paths of relatively low activation energy. The basic mechanism of diffusion along such paths is usually considered to be a vacancy and atom interchange. In general, for any given diffusion system, a combination of the three mechanisms constitutes the process of diffusion.

[8] C. Zener, "Theory of Diffusion"; pp. 289–314 in Imperfections in Nearly Perfect Crystals (W. Shockley, J. H. Hollomon, R. Maurer, and F. Seitz, editors). John Wiley & Sons, Inc., New York, 1952. 475 pp.

[9] F. Seitz, "Fundamental Aspects of Diffusion in Solids"; pp. 77–148 in Phase Transformations in Solids (R. Smoluchowski, J. E. Mayer, and W. A. Weyl, editors). John Wiley & Sons, Inc., New York, 1951. 660 pp.

Table II. Nuclear Properties of Isotopes in Mass 133 Decay Chain*

Isotope	Decay constant, λ (hr.$^{-1}$)	Half-life, $t_{1/2}$	Direct fission yield (%)	Total yield (%)
$^{133}_{51}Sb$		4.4 min.		
$^{133}_{52}Te$		1.1 hr.		4.5
$^{133}_{53}I$	3.18×10^{-2}	22 hr.	1.32	4.6
$^{133}_{54}Xe$	5.45×10^{-3}	5.3 days		6.29
$^{133}_{55}Cs$		Stable		

* From footnote 10.

(2) Fission Reaction and ^{133}Xe Production

The fission products are distributed among the various isotopes in the range of masses 70 to 160. The rate at which fission occurs in a nuclear reaction is given by equation (5).[10]

$$R.R. = \sigma_f N_0 F \tag{5}$$

$R.R.$ = fission per second per cc.
σ_f = fission cross section of ^{235}U (sq. cm. per atom).
N_0 = number of ^{235}U nuclei per cc.
F = neutron flux (neutrons per sq. cm. per second).

Equation (5) must be corrected for per cent yield for any particular fission product. The correction factor for ^{133}Xe is approximately 6.29%. The fission products usually belong to a decay chain which leads to a much more complicated expression for their production.[11]

^{133}Xe is the fourth member of the radioactive decay chain[10] for isotopes of mass 133 as given by equation (6).

$$^{133}_{51}\text{Sb} \rightarrow {}^{133}_{52}\text{Te} \rightarrow {}^{133}_{53}\text{I} \rightarrow {}^{133}_{54}\text{Xe} \rightarrow {}^{133}_{55}\text{Cs} \tag{6}$$

Table II[10] lists the nuclear properties of interest in the decay chain. The short half-life of Sb and Te simplified the diffusion calculations for the present investigation to the parent and daughter relation between I and Xe respectively as given by equation (7).

$$N_2 = \frac{\lambda_1}{\lambda_2 - \lambda_1} N_1^0 (e^{-\lambda_1 t} - e^{-\lambda_2 t}) + N_2^0 e^{-\lambda_2 t} \tag{7}$$

N_2 = number of daughter atoms.
λ_1 = decay constant of parent, ^{133}I.
λ_2 = decay constant of daughter, ^{133}Xe.
N_1^0 = number of initial parent atoms.
N_2^0 = number of initial daughter atoms.
t = elapsed time.

(3) Quantitative Measurements from ^{133}Xe Radioactivity

The gamma-ray spectrometer (Fig. 1) is an apparatus for measuring the gamma-ray energy and intensity from a source and is used to make a qualitative and quantitative determination for any particular isotope. In general, the gamma-ray spectrometer[12] is based on the principle of radiation detection in scintillating crystals by the absorption of energy which results in flashes of light (scintillations) being emitted in the crystal. The number of photons of light or intensity of the flash of light is a function of the energy of the gamma ray.

[10] Gerhart Friedlander and J. W. Kennedy, Introduction to Radiochemistry. John Wiley & Sons, Inc., New York, 1949. 398 pp.

[11] J. R. Donaldson, "Theoretical Study of Fission-Product Gaseous Activity From a Homogeneous Reactor," *U. S. Atomic Energy Comm.*, **LRL–153**, 15 pp. (1954).

[12] B. Kahn and W. S. Lyon, "Use of Scintillation Spectrometer in Radiochemical Analysis," *Nucleonics*, 11 [11] 61–63 (1953).

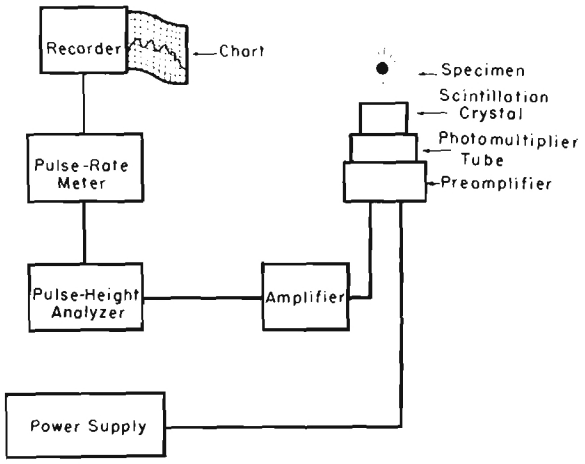

Fig. 1. Schematic representation of gamma-ray spectrometer.

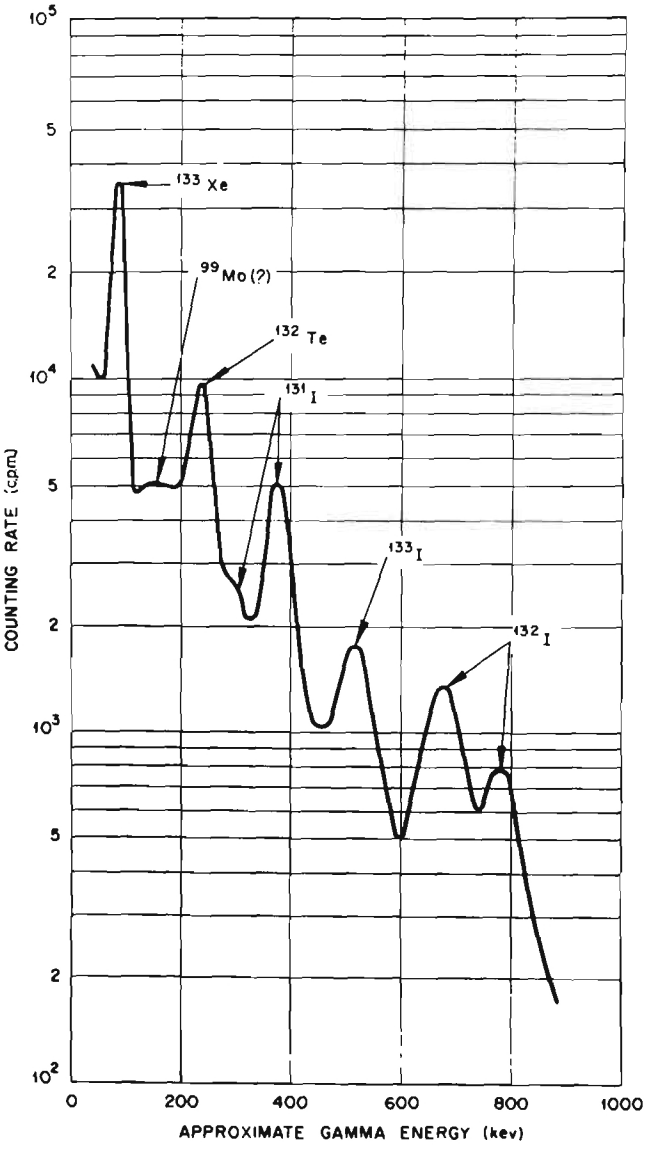

Fig. 2. Schematic curve from gamma-ray spectrometer.

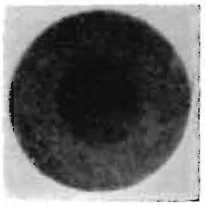

Fig. 3. Radiograph of specimen of MgO-Ni cermet.

There are three basic absorption processes for gamma rays in scintillation crystals: (1) photoelectric effect, (2) Compton scattering, and (3) pair production. The absorption results in scintillations which are proportional in amplitude to the energy of the gamma ray and proportional in number to the number of gamma rays. Absorption by the photoelectric effect will give a maximum energy pulse which "stands out" or is the isotope-identifying pulse. In a plot of the intensity versus gamma-ray energy, the area under any photoelectric peak is a quantitative measure of the activity of an isotope with a gamma-ray energy as designated by the point on the curve of maximum intensity. By means of a quantitative calibration for the geometry factor, half-life measurements, gamma-ray energy calibration, and area measurement, a qualitative and quantitative determination for any particular isotope can be made. A schematic gamma-ray spectrometer curve or chart of a mixture of isotopes is shown in Fig. 2.

III. Experimental Procedure and Data

The cermet specimens were fabricated as a configuration with the UO_2 located in the central core section as shown in the radiograph of Fig. 3. The UO_2, MgO, and Ni core mixture is the darker central portion. The outer portions were of the MgO-Ni cermet. Dimensions of the specimens are presented in Table III, and the microstructure of the MgO-Ni structure is shown in Fig. 4.

The specimens were sealed in an aluminum container and irradiated in the X-10 Graphite Reactor, Oak Ridge National Laboratory, for a period of 7 days. The thermal neutron flux was 5×10^{11} neutrons per sq. cm. per second. It was estimated that the temperature of the specimens reached 150° to 200°C. during irradiation. Careful analysis of an acid and water wash of the specimens after irradiation indicated that no detectable diffusion occurred during irradiation. The number of radioactive ^{133}I and ^{133}Xe atoms generated was 8.57×10^{10} and 2.57×10^{11} atoms, respectively, as given by equations (5) and (7).

Neutron activation of the Ni and Mg caused the specimens to be quite radioactive. The radioactivity at contact was approximately 8 roentgens, which necessitated special handling techniques during processing.

After irradiation, the specimens were sealed in a quartz glass container tube as shown in Fig. 5. Aluminum silicate wool insulators were placed on each side of the specimen to prevent excessive heating of the specimen during the sealing of the glass container. The portion of the process tube containing the specimen was heated in a furnace at designated temperatures for a time interval of 24 hours unless otherwise specified in the data. The stem portion of the glass container was immersed in liquid nitrogen for 4 hours after heating. The boiling point of nitrogen, −195.8°C., was well below the melting point of Xe, −140°C. The diffused gaseous fission products condensed in the stem were sealed off from the specimen section of the container tube and analyzed as soon as possible with the aid of a gamma-ray spectrometer. The specimens were removed from the container tube and given an acid and water wash which was also analyzed. The amount of ^{133}Xe found in the larger portion of the container tube, in the aluminum silicate wool, and in the washes was so slight that it did not affect the calculations. The amount

Table III. Physical Dimensions of Specimens

Specimen composition (wt. %)	Core composition	Amount natural UO_2 (mg.)	Cladding thickness (cm.)	Core thickness (cm.)	Core diam. (cm.)	Specimen thickness (cm.)	Specimen diam. (cm.)
MgO 34 Ni 66	UO_2 + MgO + Ni	3.3	0.0635	0.0635	0.44	0.1905	1.11

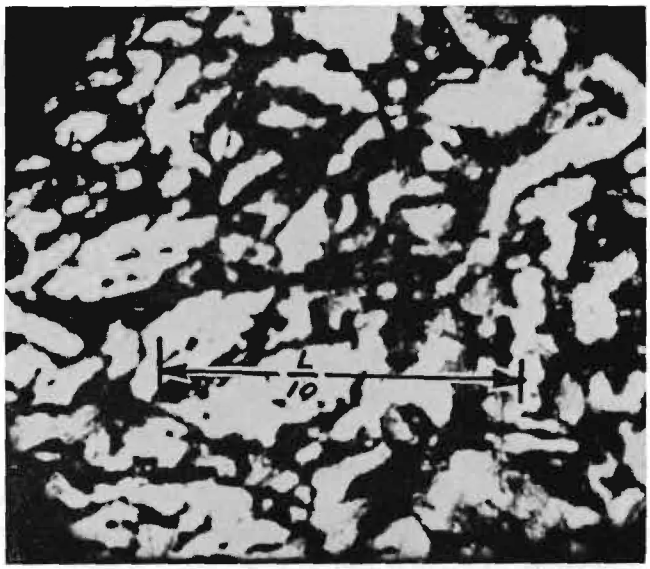

Fig. 4. Microstructure of MgO-Ni cermet. Light grains are Ni and dark grains are MgO. $L/10$ = one-tenth distances Xe atoms diffuse to outside of specimen. (×1000.)

of ^{133} Xe condensed in the sealed stem constituted the major portion by a factor of approximately 100.

A specimen made from powdered UO_2 encased in glass wool was processed at 900°C. in the usual manner. Approximately 65% of the ^{133}Xe calculated to have been generated was collected in the liquid-nitrogen trap. The collecting system therefore appeared to be adequate to within 30%.

It was necessary to calibrate the gamma-ray spectrometer (Fig. 6) with respect to gamma-ray energy and counting efficiency; $^{199}_{79}$Au, $^{203}_{80}$Hg, $^{137}_{55}$Cs, and $^{60}_{27}$Co isotopes were selected for the calibration procedure.

The voltage scale at amplifier gains of 8 and 16 was calibrated as to distance from point of zero distance on the recorder chart to photoelectric peaks from isotopes of known gamma-ray energies. Figure 7 is the calibration curve for the gamma-ray energy. The voltage scale on the pulse-height analyzer and the rotation of the chart from the recorder were synchronized so as to give the gamma-ray energy as a function of the chart-rotation distance.

The calibration for counting efficiency was accomplished by means of a strip of gold foil which approximated the geometrical configuration of the quartz glass stem. The lower end of the gold strip or glass-stem specimen was placed

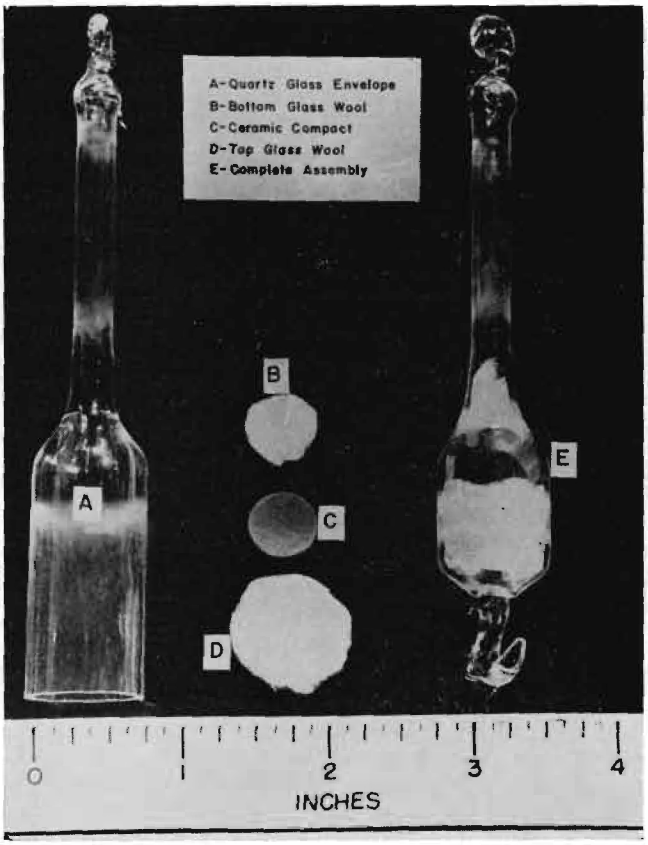

Fig. 5. Quartz glass envelope.

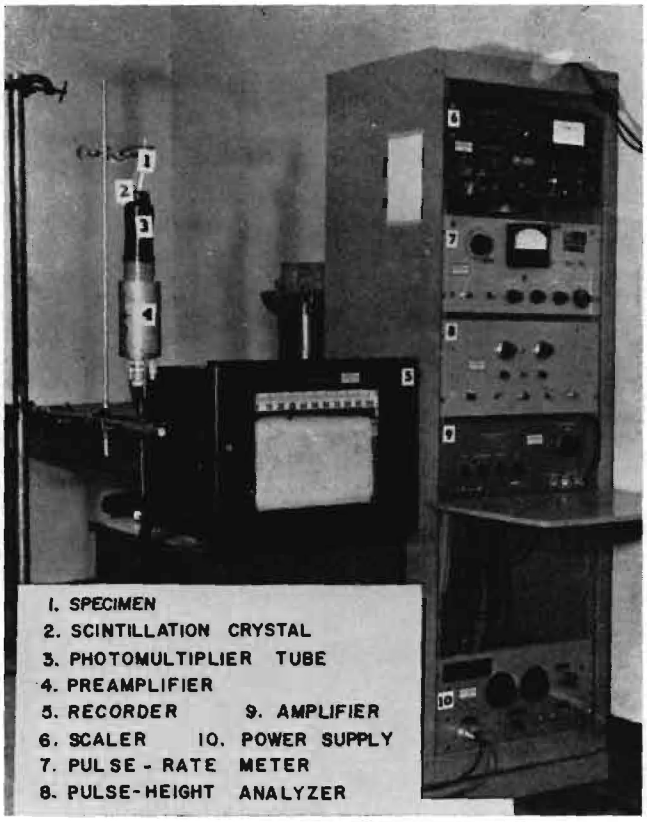

Fig. 6. Gamma-ray spectrometer.

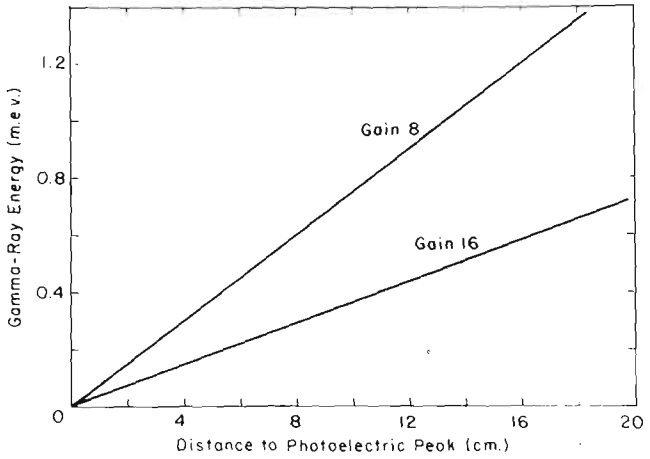

Fig. 7. Gamma-ray energy vs. chart-distance calibration.

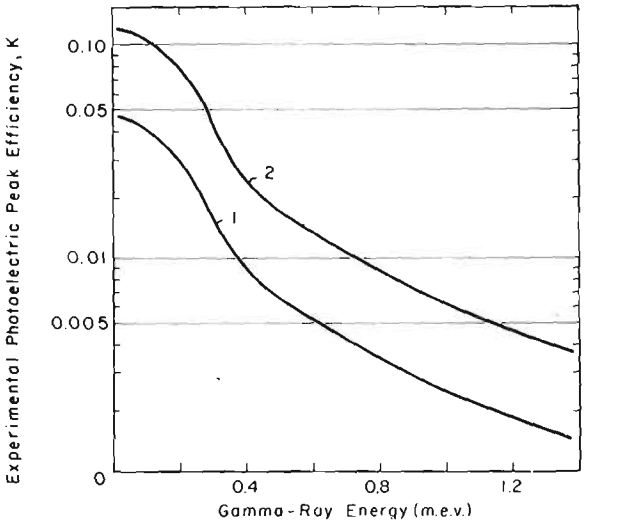

Fig. 8. Photoelectric peak efficiency vs. gamma-ray energy for NaI(Tl) crystal. (1) Experimental curve from gold strip at contact with crystal and (2) data from Kahn and Lyon (footnote 12).

next to the top of the crystal. It was assumed that the shape of the counting-efficiency curve versus gamma-ray energy was the same as given by Kahn and Lyon[12] for a NaI (Tl) crystal. The detector in the gamma-ray spectrometer was a cylindrical thallium-activated sodium iodide crystal. Figure 8 shows the results obtained with the gold strip-specimen calibration. The strength of the radioactive source in disintegrations per second was determined by equation (8).

$$S = \frac{A}{K\Delta V} \tag{8}$$

S = number of disintegrations per second for isotope source.
A = area under photoelectric peak (counts volts per second).
K = experimental photoelectric peak efficiency (counts per disintegration).
ΔV = channel width on voltage scale (volts).

The K variable for any gamma-ray energy was determined from Fig. 8, and it had dimensions of counts per

Table IV. Conversion Factor, r, for Area

Counting range: Counting-rate meter setting (ct./sec.)	Counting range: Recorder-chart range (ct./sec.)	Area conversion factor, r (ct. volt/sec. sq. cm.)
5	2.5	0.262
25	12.5	1.31
50	25	2.62
250	125	13.1
500	250	26.2
2,500	1,250	131.0
5,000	2,500	262.0
25,000	12,500	1310.0

disintegration. The gamma-ray spectrometer was set for a 2-volt channel width. Also, the spectrometer electronic arrangement was such as to obtain maximum recorder deflection at one-half the maximum deflection of the pulse-rate meter. The recorder-chart counting rate therefore was one-half the counting rate set into the pulse-rate meter. The area under the chart curve was measured with a planimeter in square centimeters and a conversion factor was determined for each counting rate on the chart. The A variable, when corrected by the conversion factor, had dimensions of counts volts per second. The conversion factor, r, for the A variable, from area in square centimeters to counts volts per second, is given in Table IV. Equation (8) then reduces to equations (9) and (10).

$$S = \frac{(A \text{ sq. cm.})}{(2 \text{ volts})} \frac{(r \text{ ct. volt/sec. sq. cm.})}{(K \text{ ct./dis.})} \tag{9}$$

$$S = \frac{(A \text{ sq. cm.})\,(r)}{2K} = S \text{ dis./sec.} \tag{10}$$

The S value was converted to the number of ^{133}Xe atoms by equation (11).

$$N = \frac{S}{\lambda^*} = \frac{S}{1.51 \times 10^{-6}} \text{ atoms} \tag{11}$$

N = number of atoms.
λ^* = radioactive decay constant for ^{133}Xe.

The experimental data obtained for each specimen are given in Table V.

As the diffusion path through the edge of the specimen was much greater than through the sides, the area, A, was assumed to be the total area adjacent to the UO_2 core. The diameter of the area adjacent to the UO_2 core was measured from the radiograph of Fig. 3, which is the darker central area. The concentration was considered as zero at all times on the outside of the specimen. The total number of atoms of ^{133}Xe present at the time of removal from the furnace was considered as the concentration in the core of the specimen. The values of D, the coefficient of diffusion, as calculated from equation (3) and from the experimental data of Table V, are given in Table VI. Figure 9 is a graphical presentation of the D values.

The slope of the straight line of Fig. 9 is a function of the activation energy. The activation energy was evaluated from equation (4).

IV. Discussion of Results

The coefficients of diffusion, D, when plotted versus temperature were such as to give a close approximation to a straight line (Fig. 9). The activation energy, E_a, was calculated from Fig. 9 to be 4.4 e.v. The single relatively high value of D at 1000°C. could be attributed to a structural defect such as a crack in specimen No. 6. In general, the lowest value of D at any given temperature should be the most representative, as a structural or any other type of defect would tend to cause D to be higher than that of a

Table V. Diffusion Data

Specimen No.	Heating temp. (°C.)	Heating time (hr.)	Elapsed time from flux to furnace removal (hr.)	Elapsed time from furnace to gamma-ray spectrometer analysis (hr.)	^{133}Xe and ^{131}I present at removal from furnace (atoms)	^{133}Xe and ^{131}I diffused through at removal from furnace (atoms)	^{133}Xe and ^{131}I present in gamma-ray spectrometer analysis of tube stem (atoms)
1	800	24	50	24.4	Xe 2.52×10^{11} I 1.73×10^{10}	Xe 5.04×10^{6}	Xe 4.33×10^{6} I trace
2	900	24	25	47.5	Xe 2.67×10^{11} I 3.86×10^{10}	Xe 1.09×10^{7}	Xe 8.26×10^{6} I trace
3	900	24	49	28.3	Xe 2.52×10^{11} I 1.74×10^{10}	Xe 1.97×10^{7}	Xe 1.65×10^{7} I trace
4	1000	24	48	27.4	Xe 2.51×10^{11} I 1.89×10^{10}	Xe 3.25×10^{8}	Xe 2.76×10^{8} I trace
5	1000	24	72	27.4	Xe 2.31×10^{11} I 8.57×10^{9}	Xe 4.43×10^{8}	Xe 3.75×10^{8} I trace
6	1000	24	52.5	6	Xe 2.50×10^{11} I 1.63×10^{10}	Xe 7.02×10^{9} I 9.5×10^{8}	Xe 6.98×10^{9} I 7.79×10^{8}
7	1000	24	52.5	6.8	Xe 2.50×10^{11} I 1.63×10^{10}	Xe 3.62×10^{8} I 3.01×10^{8}	Xe 4.04×10^{8} I 2.41×10^{8}
8	1000	24	52.5	21.8	Xe 2.50×10^{11} I 1.63×10^{10}	Xe 3.05×10^{8} I 2.7×10^{8}	Xe 4.04×10^{8} I 1.35×10^{8}
9	1100	18	30	6.3	Xe 2.63×10^{11} I 3.26×10^{10}	Xe 4.04×10^{9} I 3.63×10^{9}	Xe 4.52×10^{9} I 2.94×10^{9}
10	1100	18	30	6.8	Xe 2.63×10^{11} I 3.26×10^{10}	Xe 7.55×10^{9} I 2.20×10^{9}	Xe 7.66×10^{9} I 1.76×10^{9}
11	1100	18	30	7.3	Xe 2.63×10^{11} I 3.26×10^{10}	Xe 6.00×10^{9} I 3.93×10^{9}	Xe 6.48×10^{9} I 3.10×10^{9}

Table VI. Calculated Coefficients of Diffusion

Specimen No.	Temp. $\left(\frac{1}{T°K} \times 10^{3}\right)$	Coefficient of diffusion, D (sq. cm./sec.)
1	0.932	9.37×10^{-13}
2	.852	1.92×10^{-12}
3	.852	3.66×10^{-12}
4	.784	6.07×10^{-11}
5	.784	9.00×10^{-11}
6	.784	1.32×10^{-9}
7	.784	6.78×10^{-11}
8	.784	5.72×10^{-11}
9	.727	9.60×10^{-10}
10	.727	1.80×10^{-9}
11	.727	1.43×10^{-9}

perfect specimen. The value for the single specimen at 800°C. was considered to be quite inaccurate, as the ^{133}Xe which diffused through the cladding was of such magnitude as to allow only an estimate of its quantity.

The crystalline structure of Ni is face-centered cubic whereas that of MgO is edge-, body-, and face-centered cubic. Phase changes of appreciable magnitude in the Ni or MgO, and probable grain-boundary formation of NiO, should bring about inflections in the curve of Fig. 9. The inflections would be caused by a change in the crystalline structure, which would cause an associated change in the coefficient of diffusion. Figure 9 indicates no inflections, which was as expected since the phase equilibrium diagrams for Ni, MgO, and MgO-NiO indicate no phase changes in the temperature interval of this investigation.

The path traversed by the migrating ^{133}Xe atom was considered as being direct to the surface for the calculation of the coefficient of diffusion. The equation for the coefficient of diffusion was determined to be equation (12).

$$D = 1.85 \times 10^{7} e^{-\frac{4.4 \text{ e.v.}}{kT}} \text{ sq. cm./sec.} \qquad (12)$$

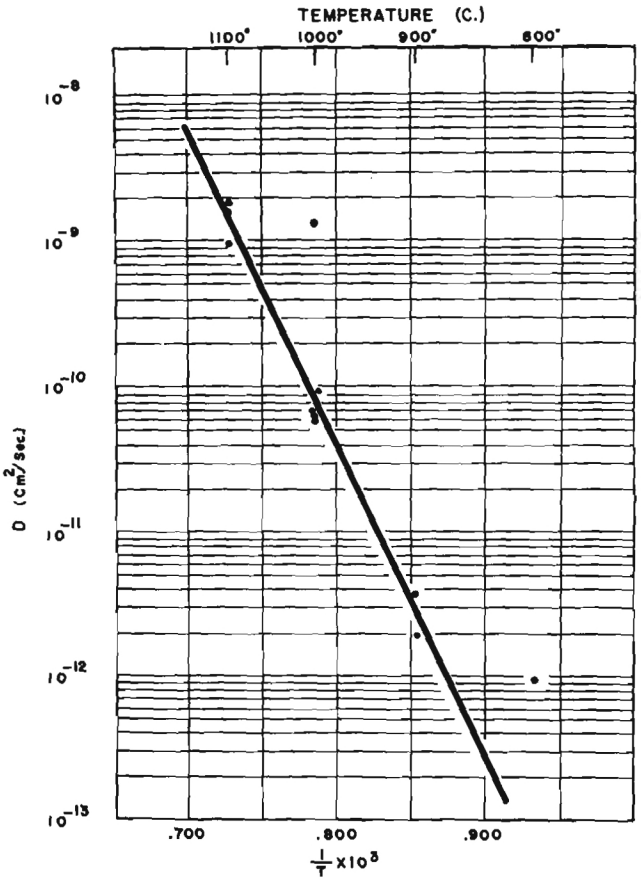

Fig. 9. Diffusion of ^{133}Xe in MgO-Ni cermet.

The value of 1.85×10^7 sq. cm. per second for D_0 is quite high in comparison with values of approximately 0.01 sq. cm. per second which are usually found. As there are many variables, such as grain boundaries, grain size, and experimental accuracy, which affect the D_0 value, it is beyond the limits of this investigation to elaborate extensively on the numerical value of D_0. The effect of the nuclear reactor irradiation and fission energy on the steady-state concentration gradient was not known. There is some indication that these variables did affect the concentration gradient, as the curve of Fig. 9 appears to be a straight line even with a variation in the time of heating for diffusion. It is obvious that D_0 would be substantially increased during irradiation owing to the creation of vacancies.

From Fig. 4, it can be observed that there are approximately 50 grains of MgO and 50 grains of Ni along the direct path. If the diffusion occurred along the grain boundaries and the grains were considered to be spherical, the path traversed by the migrating atoms would be on the order of 1.5 times as long as by the direct path. Thus, the coefficient of diffusion, D, as calculated in this investigation could be low by a factor of 1.5. The activation energy, E_a, would remain unchanged, as it is a function of the ratio of D evaluated at two points. Also, as outlined for the previous example, any linear experimental error that may have occurred would not affect the activation energy calculation.

Evans[13] gives the atomic radii of Ni, Ni^{2+}, Mg^{2+}, O^{2-}, and Xe as 1.24, 0.78, 0.78, 1.32, and 2.20 a.u., respectively. The Xe atom is approximately eight times as large by volume and twice as large in diameter as any of the other atoms or ions. As the Xe atom is much larger than any of the other atoms or ions, a relatively high value for the activation energy for diffusion would be expected. The experimental value of 4.4 e.v. is relatively high as compared with the calculated theoretical values for the self-diffusion of copper.[9] The value is not high enough, however, to give consideration to the atom-atom interchange diffusion mechanism. The relative size of the Xe atom, slightly larger than the Ni unit cell and approximately one-half the volume of the MgO unit cell, also is such as to cause a complete disruption of the lattice structure and to rule out the atom-atom interchange mechanism.

The activation energy associated with creating an interstitial atom is usually high. The necessity for traversing 100 grain boundaries or more by an atom in a direct diffusion path would tend to eliminate the interstitial diffusion mechanism on the bases of the 4.4-e.v. experimental activation energy. The relative size of the Xe atom also would place interstitial diffusion in the category of being an impossibility.

The value of 4.4 e.v. is of the order of magnitude of the value expected with the atom-vacancy interchange diffusion mechanism. It would seem to be most probable that the migration followed a path along the grain boundaries, as they were sources of vacancies. The 4.4-e.v. value was also in agreement with an approximate classically calculated value of somewhat greater than 3.5 e.v. The classical calculated value was obtained by considering the Xe atoms as tunneling through the Ni structure with the tunnel being formed by a missing Ni atom, and imaginary springs based on Young's modulus of elasticity holding the Ni atoms in place. The Ni phase was selected for the calculation as it appeared to be the continuous phase (Fig. 4). The potential barrier was assumed to consist of a plane of atoms or a series of faces (e.g., a plane of (011) faces) with the Xe atom on one side and moving to the opposite side during the diffusion jump. A hole or tunnel was created in the face by the removal of an atom, thereby creating a vacancy. The activation energy was considered as being that which was required to compress the atoms and thereby enlarge the hole or vacancy in the plane of atoms to such an extent as to allow the Xe atom to pass through. The fundamental equation was as follows:

$$\frac{\text{Force}}{\text{Area}} = Y\frac{(\Delta L)}{(L)} \tag{13}$$

Area $= \lambda^2$, where λ is diameter of Ni atom and equal to 2.4×10^{-8} cm.
Force $= k\Delta\lambda$, where k is a constant for imaginary spring and $\Delta\lambda$ is movement in compression or in tension as Xe atom passes through.
Y = Young's modulus of elasticity for Ni $= 30 \times 10^6$ lb. per sq. in.
ΔL = change in length.
L = total length.

This leads to

$$\frac{k\Delta\lambda}{\lambda^2} = Y\frac{\Delta L}{L} \tag{14}$$

where

$$k = Y\lambda \tag{15}$$

The work required to move one Ni atom to a position $\lambda/2$ away from its equilibrium site to allow the Xe atom to pass through the Ni atom plane was as follows:

$$\text{Work} = \text{force} \times \text{distance} \tag{16}$$

$$\text{Work} = \int_0^{\lambda/2} kx\,dx = \left[\tfrac{1}{2}kx^2\right]_0^{\lambda/2} = \frac{Y\lambda^3}{8} \tag{17}$$

The activation energy was computed to a close approximation by a summation of the work required to move the nearest and next nearest neighbors a distance of $\lambda/2$ in compression in one direction and in tension in other directions. The value obtained for the activation energy was 3.5 e.v. This is somewhat low, as the complete effect of the movement of all the atoms was not determined. It is believed, therefore, that the calculated value of 3.5 e.v. compares very favorably with the experimental value of 4.4 e.v.

A similar activation-energy calculation for the MgO phase was not made because the Young's modulus of elasticity would lead to erroneous results as it is not representative of the bond strength.

V. Conclusions

(1) For small concentrations, the order of magnitude for the coefficients of diffusion of ^{133}Xe migration in a MgO-Ni cermet can be determined experimentally at temperatures above 800°C. by means of radioactive tracer techniques.

(2) The equation for the coefficient of diffusion of ^{133}Xe migration through a MgO-Ni cermet was determined to be

$$D = 1.85 \times 10^7\, e^{-\frac{4.4\text{ e.v.}}{kT}} \text{ sq.cm./sec.} \tag{12}$$

(3) The activation energy calculated from the experimental data on diffusion of ^{133}Xe through a MgO-Ni cermet was 4.4 e.v.

(4) The most probable basic mechanism for the diffusion of ^{133}Xe through a polycrystalline MgO-Ni cermet (34% MgO and 66% Ni) was of the atom-vacancy interchange type.

(5) In all probability the migration occurred along grain boundaries, as they constitute sources of vacancies.

Acknowledgment

In addition to the sponsorship given by the Ceramic Laboratory, Oak Ridge National Laboratory, the writers wish to express special thanks to J. R. Johnson and J. M. Warde for suggestions and assistance and to T. S. Shevlin for preparing the test specimens.

[13] R. C. Evans, Introduction to Crystal Chemistry, 2d revision. Cambridge University Press, London, 1948. 412 pp.

FINAL REPORT

PROJECT NO. B-146

MECHANISM AND ACTIVATION ENERGY FOR DIFFUSION THROUGH SINGLE CRYSTAL AND POLYCRYSTALLINE HIGH TEMPERATURE MATERIALS

By

WILLIS E. MOODY
Professor, School of Ceramic Engineering

CONTRACT NO. AT (40-1)-2420

UNITED STATES ATOMIC ENERGY COMMISSION

DECEMBER 1961

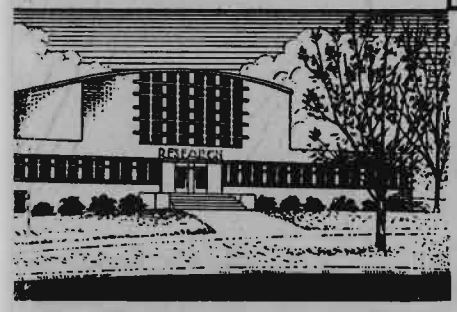

Engineering Experiment Station
Georgia Institute of Technology
Atlanta, Georgia

ENGINEERING EXPERIMENT STATION
and School of Ceramic Engineering
of the Georgia Institute of Technology
Atlanta, Georgia

FINAL REPORT

PROJECT NO. B-146

MECHANISM AND ACTIVATION ENERGY FOR DIFFUSION THROUGH SINGLE CRYSTAL AND POLYCRYSTALLINE HIGH TEMPERATURE MATERIALS

By

WILLIS E. MOODY
Professor, School of Ceramic Engineering

CONTRACT NO. AT (40-1)-2420

UNITED STATES ATOMIC ENERGY COMMISSION

DECEMBER 1961

ABSTRACT

The diffusion coefficients, D, and activation energies, E_a, for helium passing through single and polycrystalline Al_2O_3 were determined in the temperature range of 300° to 900° C. The coefficients of diffusion of helium in single crystal and polycrystalline Al_2O_3 can be experimentally determined from approximately 300° C and above by means of a mass spectrometer. The most probable basic mechanism for diffusion in a single crystal Al_2O_3 as indicated by the experimentally determined activation energy value, 0.32 ev, was an atom-vacancy interchange type occurring along edge dislocations. It was found that D for polycrystalline Al_2O_3 occurred in the range of 10^{-7} cm^2/sec to 10^{-11} cm^2/sec for densities greater than approximately 3.70 gm/cc. The experimentally determined activation energy, 0.13 to 0.83 ev, indicated the most probable basic mechanism for diffusion through polycrystalline Al_2O_3 to be an atom-vacancy interchange type occurring mainly along grain boundaries. Annihilation of imperfections was the probable cause of discontinuities in the curves for the values of D for single and polycrystalline Al_2O_3.

The feasibility of determining the concentration gradient for argon and krypton in Al_2O_3 has been demonstrated with a vacuum x-ray fluorescence unit.

TABLE OF CONTENTS

This report contains 61 pages.

LIST OF FIGURES

LIST OF TABLES

Final Report, Project No. B-146

I. INTRODUCTION

The Final Report summarizes the information developed and accomplishments of a 3-year program. Work was initiated on 1 July 1959 under Atomic Energy Commission Contract No. AT (40-1)-2420. Three Progress Reports were submitted under the dates of 1 February, 1959, 1960, and 1961. The work was carried out under the direction of Dr. Willis E. Moody in the laboratories of the School of Ceramic Engineering and of the Engineering Experiment Station.

The objective of this program was to advance in a systematic manner the basic scientific knowledge of mass transport phenomena and imperfections in metallic oxide, ceramic, materials. Alumina was selected as a metallic oxide, having desirable high temperature characteristics, and capable of being formed as a single crystal and as a polycrystalline material. The inert gases, helium, neon, argon, krypton, and xenon, were considered for the diffusing gas for two reasons. First, as these gases are assumed to have zero valence, any complications from valency considerations would be eliminated. Second, the range of atomic size of these gases should permit obtaining data on diffusion as a function of atomic size. Due to measurement equipment limitations, the work reported herein was confined to the study of helium diffusion.

Towards the close of the contract period, x-ray fluorescent equipment became available. Sufficient work was done to demonstrate the feasibility of employing this technique to determine the concentration gradient of argon and krypton in alumina.

II. SURVEY OF LITERATURE

A. Inert Gases

Helium gas is the lightest of all the inert gas series and remains atomic, rather than assuming a molecular configuration, in the gaseous state. It has an atomic radius of 0.93 Å, which approximates the size of many metal atoms and other types of ions. It has been suggested[1] that helium will not diffuse through the close-packed structure of some metals because of a lack of chemical affinity.

In the case of the more open lattice structures, typical of which are ceramic oxides, diffusion of gases has been found to be a function of the atomic size if no chemical affinity exists.[1] However, imperfections such as edge dislocations and other surface conditions may provide adequate entrance sites for atoms or ions to enter the close-packed structure. It should be pointed out that the conditions necessary for an atom and/or ion to pass through the theoretical surface are not well understood or defined to any extent.

Table I lists the properties of the helium gas used in this work. The relative sizes of the inert gas atoms are given in Table II.

B. Alumina Structure

The compound alpha-Al_2O_3 falls into a general group designated by the form R_2O_3. In this group, there is a definite gradient of sizes of the metal ions composing the compounds. In general, the greater the charge on the ion,

---

1. P. S. Flint, The Diffusion of Hydrogen through Materials of Construction, KAPL - 659, Knolls Atomic Power Laboratory, 1951, p. 9.

TABLE I

PROPERTIES OF AMARILLO GRADE A HELIUM[2, 3]

Atomic Number	2
Atomic Weight	4.003
Melting Point	-272.2° C (26 atmospheres)
Boiling Point	-268.9° C (1 atmosphere)
Purity	99.99^{+} %
Chief Impurities	H_2, Ne, N_2, O_2, A, CO_2 (18.2 ppm total)
Purity Measurement	Mass Spectrometer
Atomic Radius	0.93 Å
Atomic Velocity at 300° K	1.252×10^5 cm/sec
Atomic Velocity at 600° K	1.92×10^5 cm/sec
Atomic Velocity at 900° K	2.36×10^5 cm/sec

TABLE II

INERT GAS ATOMIC SIZE[4]

Element	Radius (Å)	Volume (Å^3)
He	.93	3.36
Ne	1.59	16.8
A	1.91	29.1
Kr	2.01	33.9
Xe	2.20	44.6

2. C. D. Hodgman, Handbook of Chemistry and Physics, 41st Edition, Chemical Rubber Publishing Company, 1960, p. 3089.

3. C. G. Kirkland, Determining Trace Impurities in Grade-A Helium, RI-5644, Bureau of Mines, United States Department of the Interior, 1960.

4. Wyckoff, Crystal Structures, Interscience Pubs. Inc., 1 (II) 14 (1951).

the smaller will be its atomic radius. With small metal ions that have r_R/r_O less than 0.60, oxygen ions can approach nearer to a close-packing, and such metallic and close-packed sesquioxides are often found in the arrangement typified by Cr_2O_3. Its symmetry is rhombohedral with a unit cell containing two molecules and having dimensions given in Table III. The space group is $D_{3d}^6(R\bar{3}\,c)$.

In this structure each aluminum ion has three oxygen ions at a distance of 1.89 Å and three more at 1.93 Å. The nearest O - O distance is 2.49 Å.

This arrangement is probably best viewed as a slightly distorted hexagonal close-packing of molecules in which aluminum ions occur above and below the midpoints of the oxygen ion triangles of the close-packed oxygen layers. Six oxygen ions surround each aluminum ion, and each oxygen ion is surrounded by four aluminum ion sites. Two-thirds of the octahedral sites are occupied by aluminum ions while the remaining ones are vacant to fulfill the conditions of net electrical neutrality and stiochiometry of the compound. Aluminum ions and holes are arranged so as to give a maximum separation of like charges and a minimum separation of unlike charges,[5,6] Figs. 1 and 2. The packing would be perfect if α were 53° 47' instead of the measured value of about 55° 17', and all the oxygen ions were equidistant from the aluminum ions.[4]

Fig. 1 represents a plan view of the α-Al_2O_3 structure looking down on the aluminum ions and holes over the close-packed oxygen ion layer. Fig. 2 shows a schematic diagram of the aluminum ion and hole distribution in a

---

5. M. L. Krunberg, "Plastic Deformation of Sapphire," Acta Metallurgica 5, (1957) 507-511.

6. A. F. Wells, Structural Inorganic Chemistry, Oxford University Press, 1950, pp. 364-389.

TABLE III

ALPHA-ALUMINA CRYSTAL DIMENSIONS[4]

AND PHYSICAL DATA

Form	α-Al_2O_3
Symmetry	Rhombohedral
a_o	4.76280
b_o	- - - -
c_o	13.00380
α	31 degrees
Coordination Number of Al to O	6:4
Remarks	Cr_2O_3 type
Melting Point	2050° C
Dislocation Annealing Temperatures	900° C - Basal Plane
	2000° C - Prismatic Plane
Parting	Rhombohedral Planes
Slip	Prismatic and basal
Theoretical Density	3.98 gm/cc

simple hexagonal lattice. The simple rhombohedral cell is also shown. A close examination of these figures reveals no straight line path through the lattice. For any gas penetration to take place, some sort of activated, step-by-step diffusion process would be necessary to supply energy for motion.

Several other forms of alumina are found in nature or occur through artificial means. Beta and zeta forms contain small amounts of alkali and alkaline earth oxides. Gamma types, of which there are many subdivisions

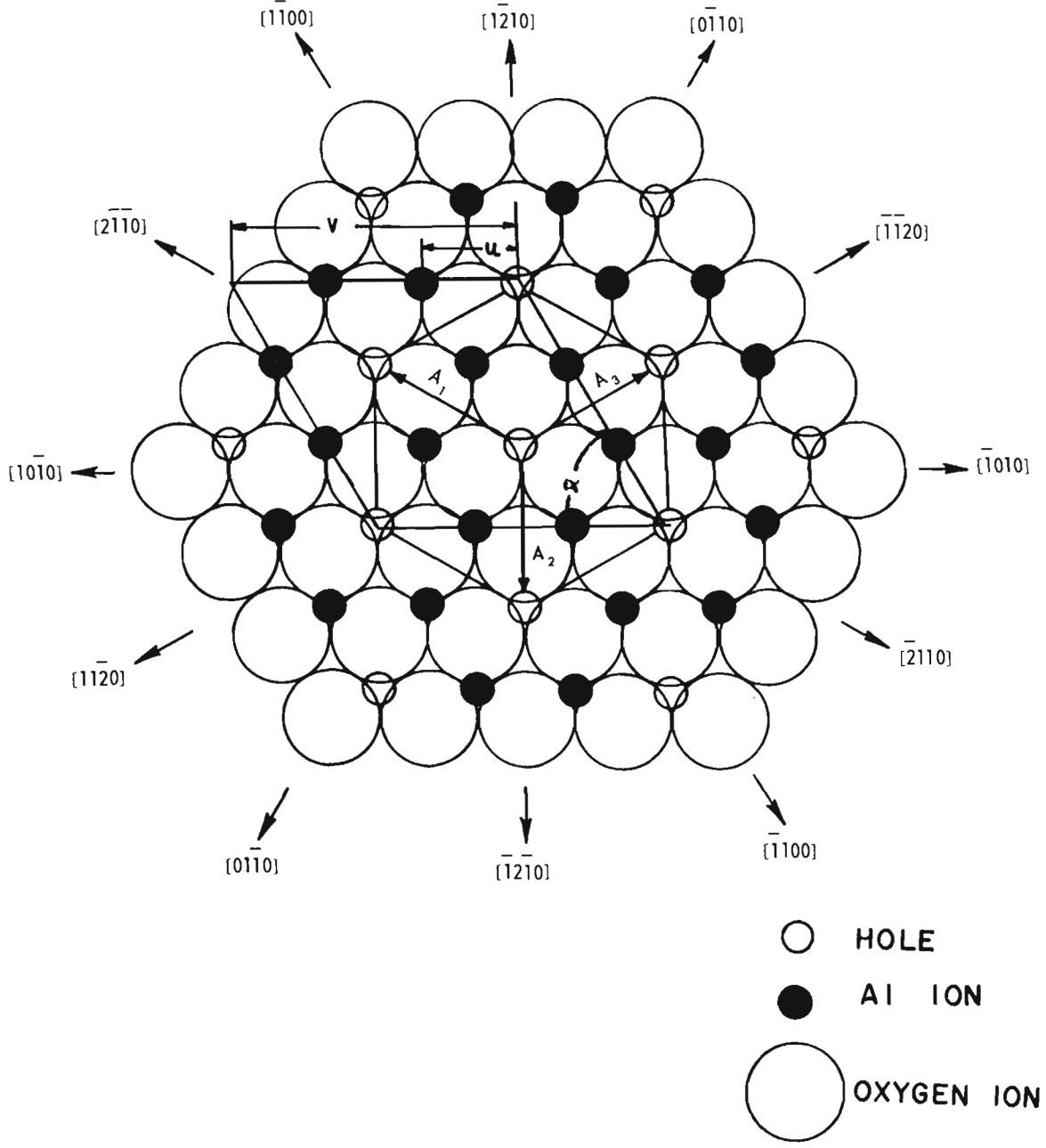

Figure 1. Basal Plane Al_2O_3.

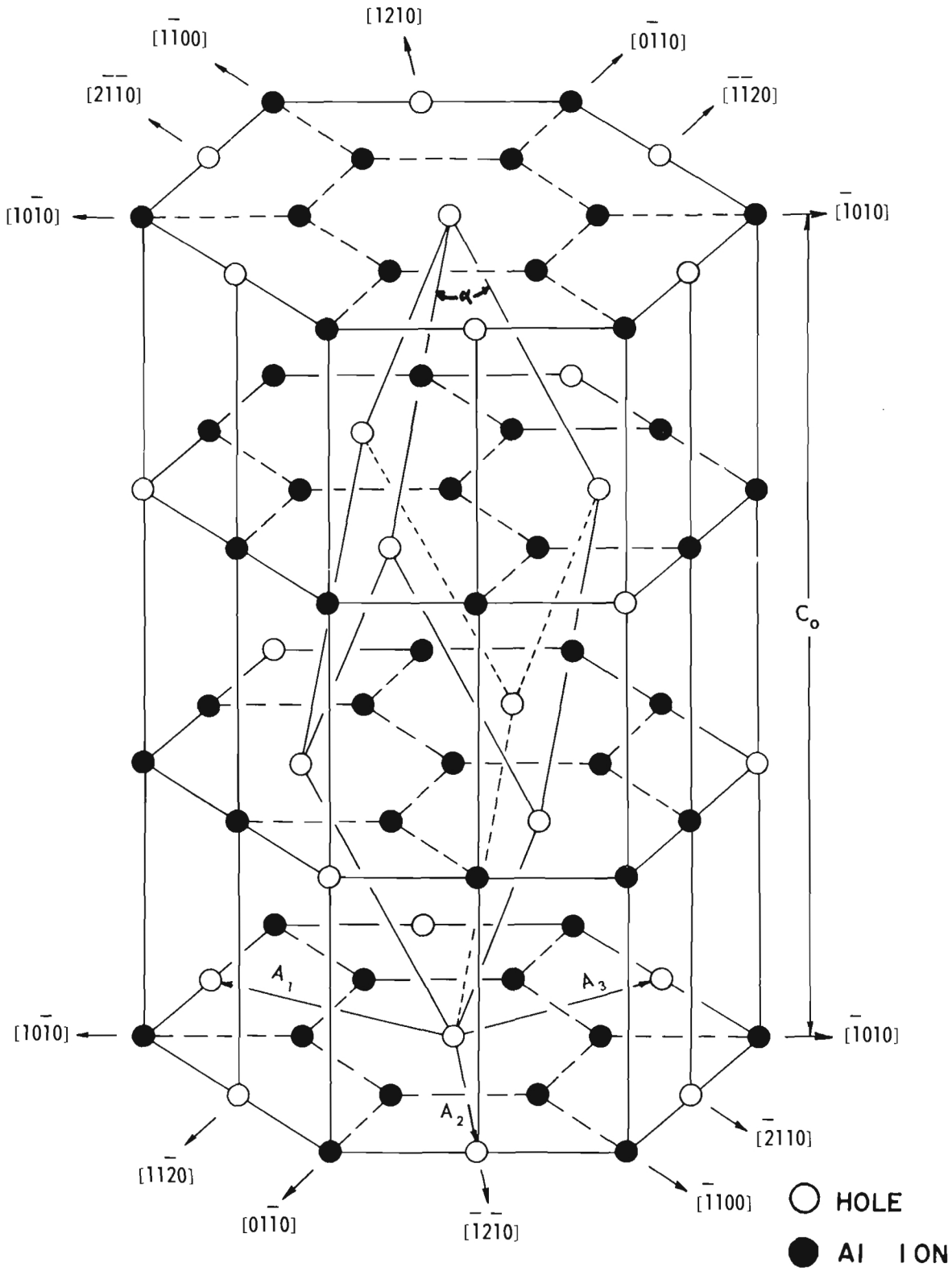

Figure 2. Aluminum Ion and Hole Distribution in the Simple Hexagonal Lattice.

(chi, gamma, eta, delta, kappa, theta), all are structures that originally contained water and revert to the alpha form upon heating.[7] Studies thus far reveal that the alpha crystalline form is stable from room temperature to 2000° C and exhibits no inversions or phase changes upon heating.[8]

A polycrystalline material behaves quite differently from its single crystal counterpart. There are several reasons for this lack of correspondence. The presence of internal surfaces or grain boundaries can and does affect the various properties of a solid. The term "sintered alumina"[9] became established in the literature in 1932 when Kohl described a new material called "sinterkorund" made from a Bayer alumina material either by slip casting or dry pressing and firing to 1800° C. He considered the firing and cooling step to be a recrystallization process.

In all cases, grain boundaries represent regions of misfit between two or more crystalline surfaces. The atoms in the boundary region are shared by adjacent lattices, but the force field in which the atoms find themselves is by no means uniform, and the region is in stress and permanent strain. Generally, a grain boundary is at a higher potential energy state than its surroundings. In summation, the properties of a polycrystalline substance that depend upon or are a function of the ionic bonds are affected by the presence of a boundary in the sense that the region is a lattice imperfection. It represents a discontinuity in the potential field, but it is not a barrier

---

7. A. S. Russell, Alumina Properties, Technical Paper No. 10 (revised), Alcoa, 1956, 10 pp.

8. D. S. Klein, Measurement of the Crystallographic Thermal Expansion of Alpha-Alumina and Beryllia to Elevated Temperatures Emphasizing Anisotropic Effects, National Aeronautical Administration, NAA - SR-2542, 1958, 24 pp.

9. H. N. Baumann, "Crystal Habits of Alpha-Alumina in Alumina Ceramics," Bulletin of the American Ceramic Society 37, No. 4, 179-184 (1958).

that completely blocks electronic interchange. Mechanical properties depend upon ionic movements, and grain boundaries represent areas sufficiently different to modify the behavior of the material.

Crandall et al.[10] observed internal friction peaks for polycrystalline Al_2O_3 at 1080° C for high purity material and at 700° C for a material with a one per cent silica addition.

According to Tucker and Gibbs,[11] single crystals of Al_2O_3 normally contain approximately 10^7 dislocations/cm^2.

C. Theory of Diffusion

To fully appreciate the mathematics of diffusion, one must have a working knowledge of kinetics, thermodynamics, solubility phenomena, and steady state and nonsteady state flow. Numerous references are given in the literature dealing with the mathematical solutions of various systems that might be employed, such as plane surfaces, cylinders, and spheres.

The basis for the mathematics of diffusion lies with the two differential forms of Fick's Laws[12] dealing with steady and nonsteady state flow. They may be written:

$$J = -D \frac{\partial C}{\partial X} \qquad (1)$$

---

10. W. B. Crandall, D. H. Chung, and T. J. Gray, "The Mechanical Properties of Ultra-fine hot-pressed Alumina," Monthly Progress Report No. 287, Vol. XXV, No. 5, Ceramic Research Dept., Alfred University, New York, 1960.

11. R. N. Tucker and P. Gibbs, "Impurity Penetration Along Dislocation Lines in α - Al_2O_3," Jour. Appl. Physics 29, No. 9, 1374-1375 (1958).

12. R. M. Barrer, Diffusion In and Through Solids, Cambridge University Press, 1951, pp. 1-51 (461 pp.).

where: J = current density, or quantity of substance passed per unit area per unit time per unit thickness

D = diffusion coefficient

$\frac{\partial C}{\partial X}$ = concentration gradient.

Fick's second law may be derived from the first with the use of the particle continuity equation which results in:

$$\frac{\partial C}{\partial T} = D \frac{\partial^2 C}{\partial X^2} \qquad (2)$$

where: $\frac{\partial C}{\partial T}$ = change of concentration with change in time

$\frac{\partial^2 C}{\partial X^2}$ = rate of change of concentration gradient.

The general theory of diffusion is based upon analogy to the flow of heat through solid media, as is exemplified in the classical works of Fourier and Lord Kelvin. However, new phenomena are observed in the actual diffusion processes of molecules and ions in and through solids which are not found in systems concerned with the flow of heat alone. Consequently, these phenomena require limitations to be imposed much more frequently on mass transfer systems than on heat transfer systems.

A quantitative consideration of the theory of diffusion involves an understanding of the diffusion equation, permeability, and the relationship between permeability, solubility, and diffusion coefficient.

There are two general types of gas flow through a solid: (A) diffusion processes and (B) molecular flow processes.

1. Diffusion Processes

There are three classical mechanisms by which an atom or an ion

may diffuse through a crystal. They are shown in Fig. 3 and are as follows:(13)

1. Atom A and atom B may interchange places. They would move past each other in the lattice to reach the new sites.
2. Atom B may diffuse through interstitial sites in the lattice.
3. The diffusing atom may move by occupying vacant sites in the lattice.

The first mechanism involves breaking the bonds which surround atoms A and B. This requires an energy equal to the bonding energy of the material and is the most unlikely to occur. Experimental evidence seems uniformly to support this assumption.

The second mechanism involves a smaller amount of energy, but the number of interstitial sites available usually limits the process. The ion moves out of its normal site into the interstitial position and is accompanied by some lattice distortion due to the size of the ions and ion-ion energy interaction.

The mechanism requiring the least amount of energy is shown in Part 3 of Fig. 3. Crystals usually possess vacant lattice sites or missing atoms or ions, and these would be available as vacancies. It is necessary to overcome bonding forces on three sides of the atom for it to be moved. The new site is available with little additional energy expenditure.

In polycrystalline materials where grain boundaries represent areas of unequal energy potential, but not actual holes, small amounts of energy

---

13. F. Seitz, "Fundamental Aspects of Diffusion in Solids," pp. 77-148, Phase Transformations in Solids (R. Smoluchowski, J. E. Mayer, and W. A. Weyl, editors). John Wiley & Sons, Inc., New York, 1951. 660 pp.

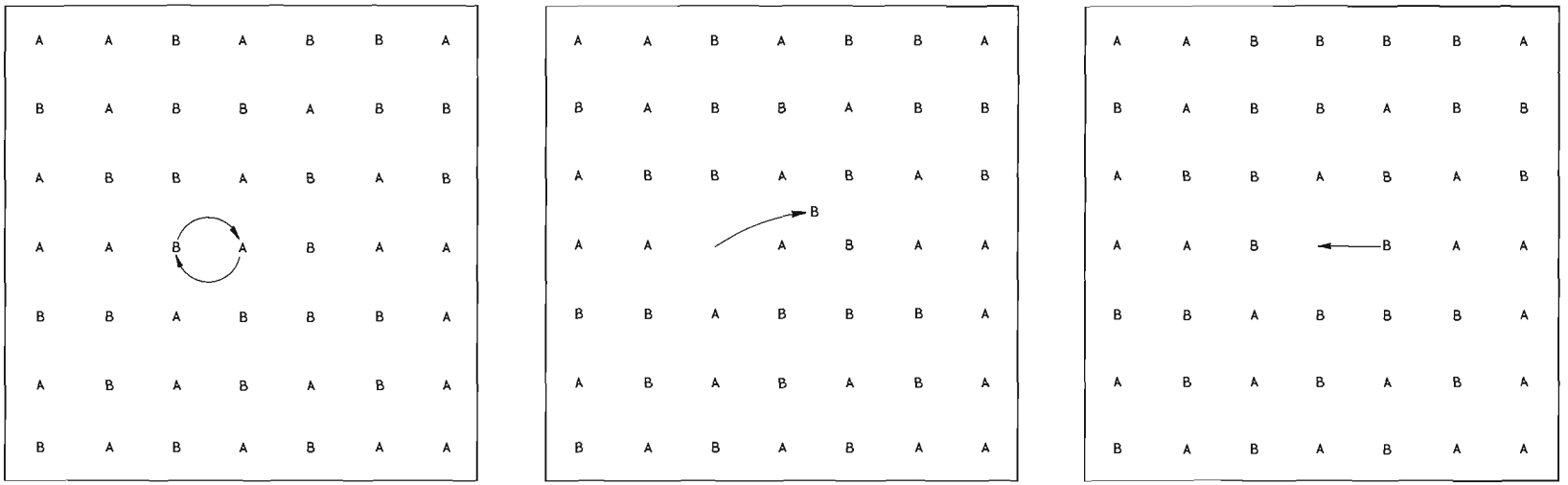

Figure 3. The Three Basic Mechanisms of Diffusion.

supplied to a diffusing atom could cause the area to become a diffusing path. Grain boundaries and dislocations may also consist of holes in which the diffusing path is well defined.

The two methods of data analysis have been:

Method A. It is assumed that the concentration gradient is equivalent to the difference in concentration of He on each side of the barrier divided by barrier thickness. The diffusion coefficient is then calculated from a simplification of equation (1) to:

$$D = \frac{M\ LV}{\Delta t\ A\ (C_1 - C_2)} \qquad (3)$$

A = area diffusing gas passes through

C_1 = concentration on high pressure side

C_2 = concentration on low pressure side

L = barrier thickness

V = unit volume

Δt = time for diffusion

M = number of diffused atoms

D = coefficient of diffusion.

Method B. Rogers, Buritz and Alpert[14] developed a method for simultaneously measuring the diffusion coefficient, solubility, and permeability for a gas in a single sample of solid material. The method utilizes solutions of the diffusion equation which makes it possible to calculate the diffusion parameters from data in the early part of the transient period, early-time approxi-

14. W. A. Rogers, R. S. Buritz and D. Alpert, "Diffusion Coefficient Solubility, and Permeability for Helium in Glass," J. App. Phy. 25, No. 7, 868 (1954).

mation, or in the steady-state gas flow, late-time approximation. This technique requires a continuous recording of the pressure build-up of the diffusing gas on the low pressure side of the barrier.

Solutions for equation (1) are obtained as follows:

1. Early-time approximation

   Slope = $d^2/4D$

   d = barrier thickness

   D = coefficient of diffusion

   Slope = slope of line of Fig. 4.[14]

2. Late-time approximation

   $D = d^2/6t_c$

   D = coefficient of diffusion

   d = barrier thickness

   t_c = characteristic time as shown on Fig. 5.[14]

3. Solubility (late-time approximation)

   P = DS

   P = permeability

   D = coefficient of diffusion

   S = solubility.

a. Activation Energy. It has been experimentally determined that values of D may be expressed by a relation of the following form:

$$D = D_o \exp(-E_a/kT) \qquad (4)$$

where: D_o = diffusion constant

E_a = activation energy

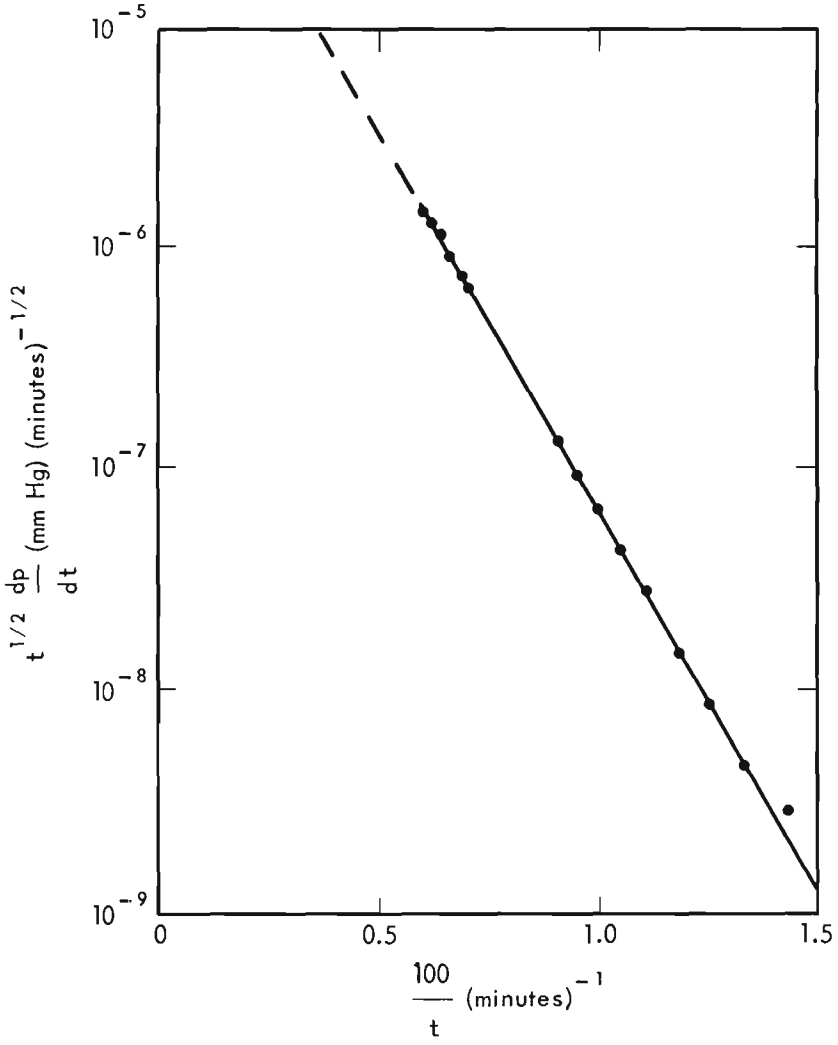

Figure 4. Data Presentation for Early Time Approximation.

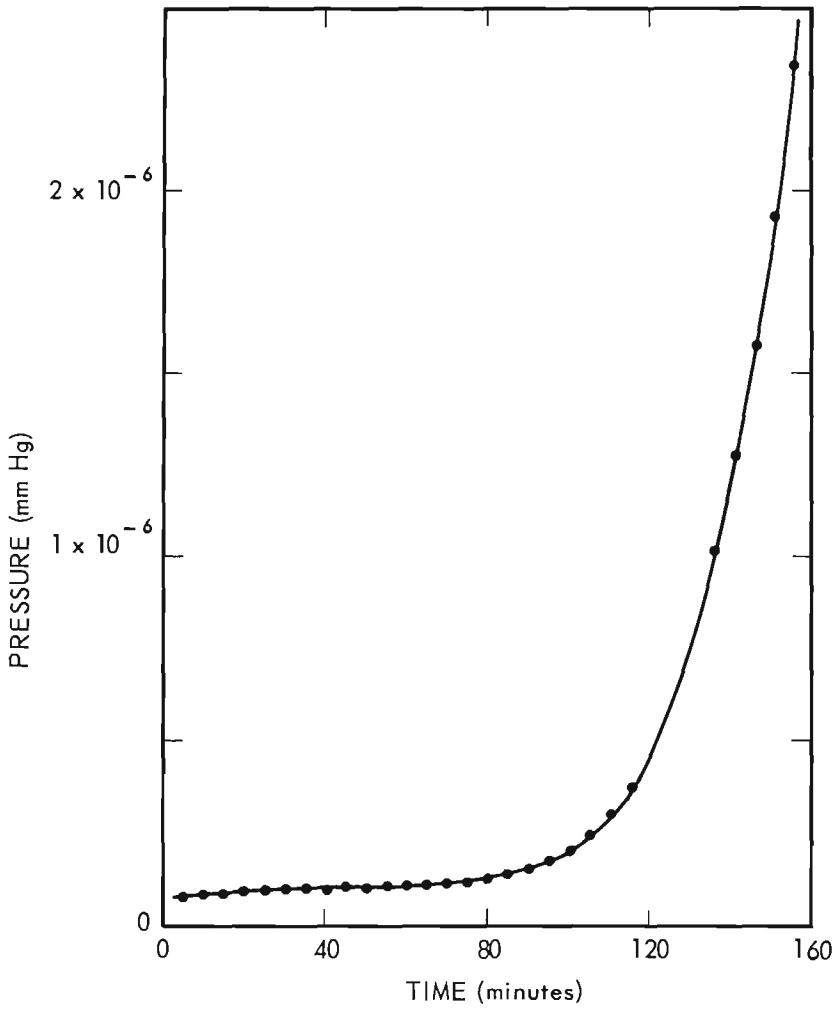

Figure 5. Data Presentation for Late Time Approximation.

k = Boltzmann constant

T = absolute temperature.

The activation energy of a system may be defined as the energy that must be put into a system in order to start a reaction, rearrange a structure, or shift atoms. The rate at which diffusion takes place is a function of the activation energy for the particular diffusion process.

If the natural logarithm is taken of equation (4), an arithmetic plot of ln D versus 1/T will yield a straight line. The magnitude of the slope of the line will be a function of the activation energy and the Boltzmann constant. Thus:

$$\ln D = \ln D_o \quad \frac{E_a}{k} \quad \frac{1}{T} \qquad (5)$$

Fig. 6 shows a schematic representation of a barrier which has to be overcome by the activation energy.

Moody et al.[15] have calculated a classical activation energy by considering the atoms as tunneling through the structure with the tunnel being formed by a missing atom and imaginary springs based on Young's modulus of elasticity holding the atoms in place. A hole or tunnel was created in the plane by the removal of an atom, thereby creating a vacancy. The activation energy was considered as being that which was required to compress the atoms and thereby enlarge the hole or vacancy in the plane of atoms to such an extent as to allow the diffusing atom to pass through. The fundamental equation was as follows:

---

15. W. E. Moody, W. D. Whitehead, and W. W. Kriegel, "Activation Energy for Diffusion of ^{133}Xe through MgO-Ni Cermet Compacts," J. Am. Ceram. Soc. 43, No. 12, 634 (1960).

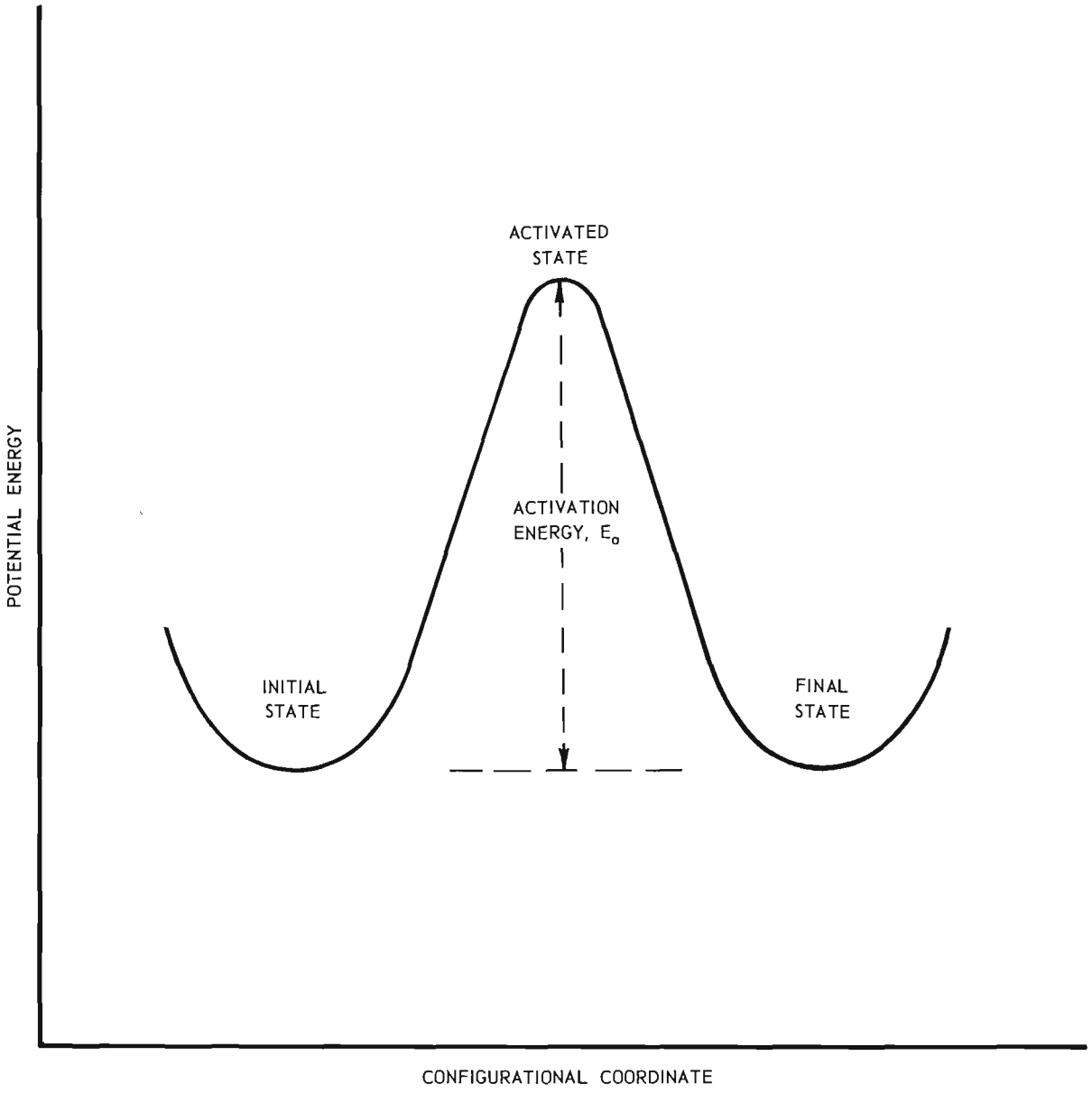

Figure 6. Potential Energy Curve Showing the Activated State.

$$\frac{\text{Force}}{\text{Area}} = Y \frac{(\Delta L)}{(L)} \tag{6}$$

where: Area $= \lambda^2$, where λ is diameter of missing atom

Force $= k\Delta\lambda$, where k is a constant for imaginary spring and $\Delta\lambda$ is movement in compression or in tension as diffusing atom passes through

Y = Young's modulus of elasticity, lb./sq. in.

ΔL = change in length

L = total length.

This leads to

$$\frac{k\Delta\lambda}{\lambda^2} = Y \frac{\Delta L}{L} \tag{7}$$

where

$$k = Y\lambda \tag{8}$$

The work required to move one atom to a position $\lambda/2$ away from its equilibrium site to allow the diffusing atom to pass through the atom plane was as follows:

$$\text{Work} = \text{force X distance} \tag{9}$$

$$\text{Work} = \int_0^{\lambda/2} kx\, dx = \left[\frac{1}{2} kx^2\right]_0^{\lambda/2} = \frac{Y\lambda^3}{8} \tag{10}$$

The activation energy was computed to a close approximation by a summation of the work required to move the nearest and next nearest neighbors a distance of $\lambda/2$ in compression in one direction and in tension in other directions.

b. The Diffusion Constant. There have been many values of the diffusion constant published in the literature. These values have been accepted at face value with little speculation as to the significance of the constant. Zener[16] has approached the problem of evaluating D_o mathematically in the following manner. The normal diffusion equation for small concentrations is given by equation (4). D may also be described by the three dimensional random walk problem:

$$D = \frac{1}{6} \sum_i \tau_i \, \delta l_i^2 \qquad (11)$$

where τ_i is the rate at which a jump is made of type i and δl_i is the jump distance. The crux of the problem of evaluating D_o values lies in the definition of τ_i.

τ_i may be expressed by:

$$\tau = v \exp. (-\Delta G/KT) \qquad (12)$$

where v is the frequency of vibration leading to the saddle point, and ΔG is the isothermal work moving across the saddle. K is the Boltzmann constant, and T is the absolute temperature at which the potential barrier exists. We separate ΔG into its components by:

$$\Delta G = \Delta H - T\Delta S \qquad (13)$$

From thermodynamics:

$$\Delta H = d \left(\frac{\Delta G}{T} \right) d \left(\frac{1}{T} \right) \qquad (14)$$

16. C. Zener, "Theory of D_o for Diffusion in Metals," Journal of Applied Physics 22, No. 4, 372-375 (1951).

We define:

$$\frac{H}{K} = \frac{-d \ln D}{d\left(\frac{1}{T}\right)} \tag{15}$$

Thus, equation (15) may be written in component form:

$$\tau = v \exp(\Delta S/K) \exp(-H/KT) \tag{16}$$

with

$$\Delta S = \frac{d\Delta G}{dT} \tag{17}$$

Equation (17) may now be examined on the right side. Formerly ΔS was considered to be either plus or minus; plus corresponding to a loosening of the lattice, and minus corresponding to a tightening of the lattice.

Equation (17) does not allow for this. ΔG does not increase with temperature (at least it is unlikely) and this casts doubt upon experiments with negative values of ΔS. The above derivation assumes that all lattice sites are equivalent.

When the matrix is not homogeneous, the possibility exists that there are certain paths along which diffusion will have a lower energy of activation than through the bulk of the matrix. Since at any one time only a fraction of the atoms will be in this path, the associated D_o will be lower than the value that corresponds to homogeneous diffusion. If the major portion of the diffusion occurs along these paths, ΔS may be smaller than theoretical and may even be negative.

In this manner, low or even negative values of D_o may be explained by inhomogeneities which furnish short circuit diffusion paths. Grain boundaries

are a major source of such paths along with dislocations. Zener postulates that if these inhomogeneous areas were removed, values of ΔS would become positive and values of D_o would be approximately 10^{-2} cm^2/sec.

2. Molecular Flow Processes

Molecular flow processes have been reviewed by Barrer[12] and are of four major types:

(1) Molecular Effusion: If one has an orifice of area A with a diameter small compared to the mean free path of the gas, the number of molecules or atoms effusing in a unit time is given by the kinetic theory equation:

$$\frac{dN}{dt} = \frac{AN_o (P_1 - P_2)}{\sqrt{2\pi MRT}} \qquad (18)$$

Where N_o is Avogadro's Number, M is the mass of a mole of the material, R is the gas constant, T is the absolute temperature, and $(P_1 - P_2)$ is the pressure differential. Equation (18) gives the flow rate through a hole in a thin plate of area A in atoms/sec. At a constant temperature for a given gas, flow rate is linearly proportional to the square of the radius of the hole, the effusion pressure, and Avogadro's number. For varying temperatures, flow rate is dependent upon the square root of the temperature, the square of the radius, and the effusion pressure.

(2) Molecular Streaming or Knudsen Flow:[17] When the path is of considerable length, molecules or atoms will collide with its walls on the way through. If all the collisions were perfectly elastic, the flow through the tube would be identical with the effusion velocity through a thin plate and would be independent of the tube length. Knudsen, therefore, assumed that for each of N molecules striking the wall, a fraction, f, was emitted with a random

17. Von Wilhelm Klose, "Uber die Stromung verdunnter Gas durch Kapillaren," Annalen der Physik, Leipzig 11, Series 5, 73-93 (1931).

velocity distribution, and (1-f) was specularly reflected. Some are returned in the direction from which they came and more return the greater length of the tube. Knudsen showed that the net rate of flow in molecules or atoms per second is given by:

$$\frac{dN}{dt} = \frac{1}{2} B \frac{1}{\sqrt{2\pi MR}} \left(\frac{P_1}{\sqrt{T_1}} - \frac{P_2}{\sqrt{T_2}} \right) \frac{1}{L} \left(\frac{2-f}{2} \right) \qquad (19)$$

where L is the length of the tube. B is a constant dependent upon the shape of the tube. For a capillary tube of circular cross section the constant B takes on the value $16/3\ r^3\pi$, where r denotes the radius of the capillary. Equation (19) is the general Knudsen equation. For a given gas, the flow rate is linearly proportional to the cube of the radius, the pressure differential from one end of the capillary to the other, the length of the capillary and the friction factor for atoms rebounding from the walls of the capillary as well as the square root of the temperature.

(3) Poiseuille or Streamline Flow: For a compressible fluid obeying the perfect gas law, Poiseuille's law may be written:

$$\frac{dN}{dt} = \frac{16r^4\pi}{128L} \int \frac{1}{\eta RT}\ pdp \qquad (20)$$

where η is the viscosity of the fluid, which for an isothermal process with η = a constant becomes:

$$\frac{dN}{dt} = \frac{16r^4\pi}{128L\eta}\ \frac{1}{RT}\ \left(\frac{P_1^2 - P_2^2}{2} \right) . \qquad (21)$$

This may also take the form:

$$\frac{dN}{dt} = \frac{16r^4\pi}{128L\eta} \frac{1}{RT} \bar{\rho} (P_1 - P_2) \qquad (22)$$

where $\bar{\rho} = \frac{1}{2}(P_1 + P_2)$ is the mean pressure in the tube. Also:

$$\frac{dN}{dt} = \frac{16r^4\pi}{128L\eta} \frac{\bar{\rho}}{M} (P_1 - P_2) \qquad (23)$$

since $\frac{(P_1 + P_2)}{2} \frac{M}{RT} = \bar{\rho}$, the mean density of the gas.

Two corrections may be applied to Poiseuille's formulas. Part of the pressure difference is used to overcome friction and the remainder produces kinetic energy of motion. There may be specular reflection from the surface of the capillary in the boundary layer of gas of thickness Λ where Λ is equal to the mean free path. The coefficient of slippage is then $(\frac{2-f}{2})\Lambda$. Barrer applies both of these corrections to equation (20) and the new equation becomes:

$$\frac{dN}{dt} = \frac{1}{L} \frac{3\pi^2 r^3}{4} \frac{1}{\sqrt{2\pi MRT}} (P_1 - P_2) (\frac{2-f}{2}) \qquad (24)$$

which is the equation given for Knudsen Molecular Streaming except for the numerical constants, which are somewhat different. Flow rate is linearly proportional to the pressure and to the other system constants.

(4) Turbulent Flow: The types of flow known as streamline change when a certain mass velocity W is reached. A quantity, R, called the Reynolds Number, is defined by:

$$R = \frac{r_h W \rho}{\eta} \qquad (25)$$

where r_h denotes the ratio, $\frac{\text{cross section}}{\text{periphery}}$, and is the so-called hydraulic

radius, which for circular tubes is one-quarter of the diameter, d. The symbols ρ and η have the significance of fluid density and viscosity, respectively. It has been determined that for circular tubes, streamline equations do not hold when R is greater than 580. The differential equation of flow is:

$$-\frac{dp}{dx} = \frac{B\rho W^2}{2r_h} \qquad (26)$$

where B is a constant and varies for different shapes of tubes. Mass velocity, or flow rate, is a complex function of the square root of the Reynolds number, fluid density, and hydraulic radius at a constant temperature.

D. Diffusion through Alumina

Studies on the penetration of gases in polycrystalline alumina have been conducted recently by several sources. Hayes et al.[18] and Kingery et al.[19] have investigated this phenomenon from 25° to 1800° C. Table IV lists values of helium permeabilities of some ionic type crystals.

Hayes et al., working in temperature regions up to 1700° C with oxygen and nitrogen as the diffusing gas, have found that a combination of Knudsen flow and diffusion along the grain boundaries is the probable mechanism. He also found that the most elevated temperatures greatly shorten the life of the alumina, and a massive breakdown of structure occurs. The samples employed by Hayes were of a density of approximately 3.5 gm/cm^3, and the method of analysis

---

18. D. Hayes, D. W. Budworth and J. P. Roberts, Permeability of Ceramics to Gas at High Temperatures, Progress Reports 1 through 7, Ceramics Division, Houldsworth School of Applied Science, University at Leeds, 1960.

19. W. D. Kingery and Y. Oishi, "Self Diffusion of Oxygen in Single and Polycrystalline Alumina," Journal of Chemical Physics 33, 480-486 (1960).

TABLE IV

HELIUM PERMEABILITIES OF IONIC CRYSTALS[12]

Substance	Permeability at °C in $Cc/Hr/Cm^2/Mm$ thickness/Atm. Pressure
Quarts (cut perpendicular to optic axis)	$< 0.05 \times 10^{-8}$
Mica (cleavage plate)	$< 0.06 \times 10^{-9}$
Calcite (cleavage plate)	$< 0.05 \times 10^{-8}$
Fluorite	$< 0.20 \times 10^{-8}$
Rocksalt	$< 0.20 \times 10^{-6}$
Selenite (cleavage plate)	$< 0.70 \times 10^{-9}$
Beryl (cut perpendicular to optic axis)	$< 0.10 \times 10^{-8}$
Beryl (cut parallel to optic axis)	$< 0.15 \times 10^{-7}$

was based on pressure build-up techniques rather than a diffusion products analysis.

Kingery et al. studied the self diffusion of O^{18} in the lattice of single and polycrystalline alumina and found the probable mechanism of diffusion to be movement along holes produced by defects. He found the diffusion rate in polycrystalline alumina to be somewhat higher with a slightly lower activation energy than that found in single crystals. He made no assumptions from his data regarding ion-ion interaction. At temperatures less than 1450° C, variable results were obtained, possibly because of structure sensitive diffusion. At higher temperatures grain boundary diffusion played an important role.

III. PROCEDURE

A. Barrier and Tube Fabrication

Figure 7 shows examples of the alumina single crystal and polycrystalline barriers and tubes which were fabricated. The single crystal alumina barrier can be observed more clearly in Figure 8. The barrier and other materials and sources are given in Table V, VI, and VII. The properties of the single crystal Al_2O_3 were essentially the same as those in Table I. UO_2 was investigated to some extent as a possible barrier material. It was difficult at that time to obtain large specimens of dense polycrystalline UO_2, and so it was abandoned as a barrier material. A limited investigation was made on the cleavage and fracture of UO_2 and ThO_2 and a copy of the published report is presented in Appendix A of this report. The alumina tubes used were 98 per cent alumina and were made by Coors Porcelain Company, Golden, Colorado, and American Lava Corporation, Chattanooga, Tennessee. A faceting goniometer and a 100-mesh diamond grinding wheel mounted on the polishing wheel proved satisfactory for shaping the exterior profile of the barriers. The polishing wheel setup was placed in a glove box, Fig. 9. The sonic grinder (Fig. 10), Raytheon Mfg. Co., Model 2-334, was very satisfactory for drilling the 1/4-inch-diameter holes. Boron carbide, B_4C, was used as the abrasive for the sonic grinder. Shaping the barrier was a somewhat slow operation which required from 2 to 3 days for the more difficult single crystal alumina. The dimensions of the barriers are given in Table VIII. All density determinations were made with a mercury volumeter and a standard analytical balance.

A large number of different materials were investigated as bonding materials. Only the materials forming a bond at temperatures above 1500° C were

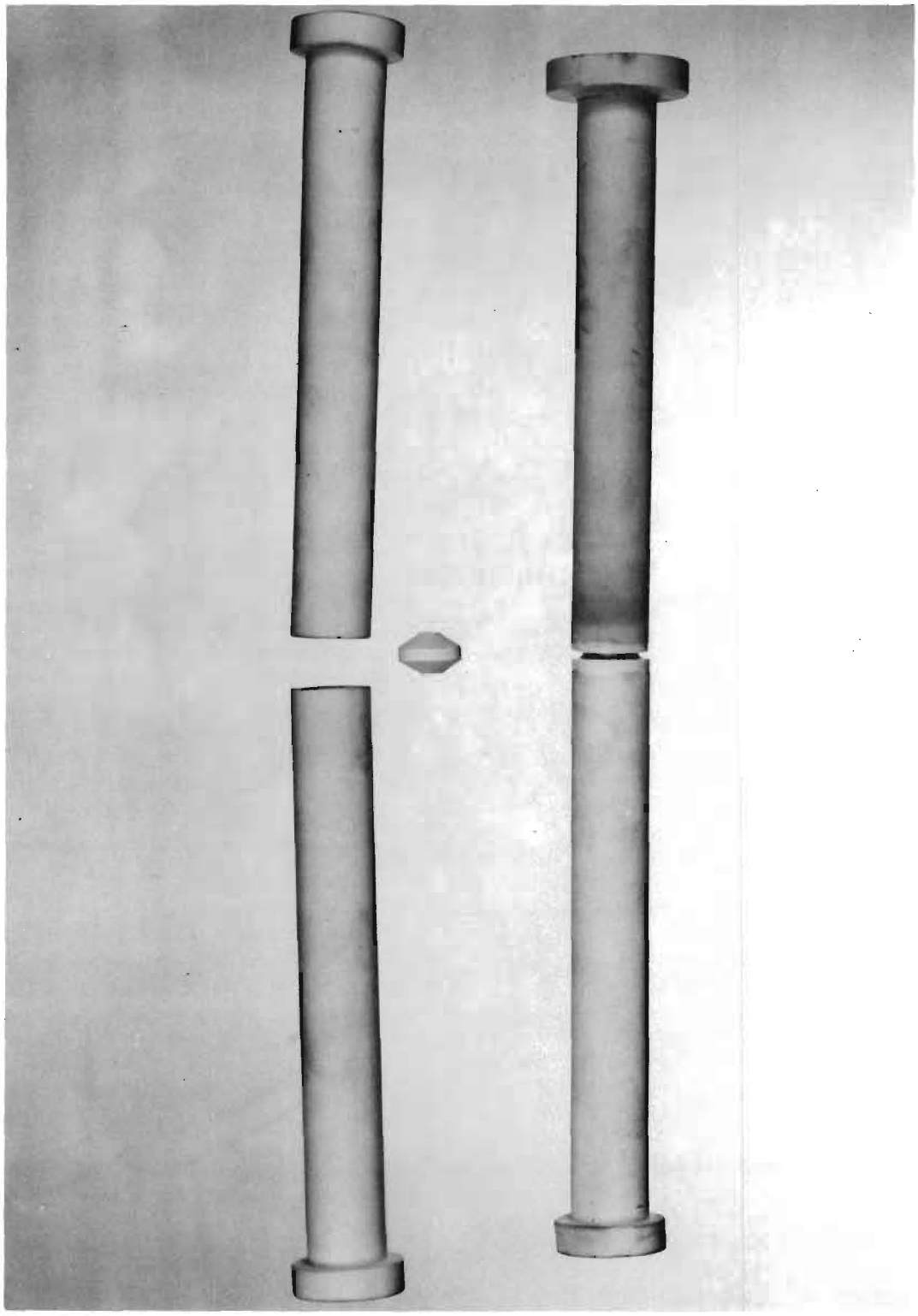

Figure 7. Alumina Tubes and Barriers.

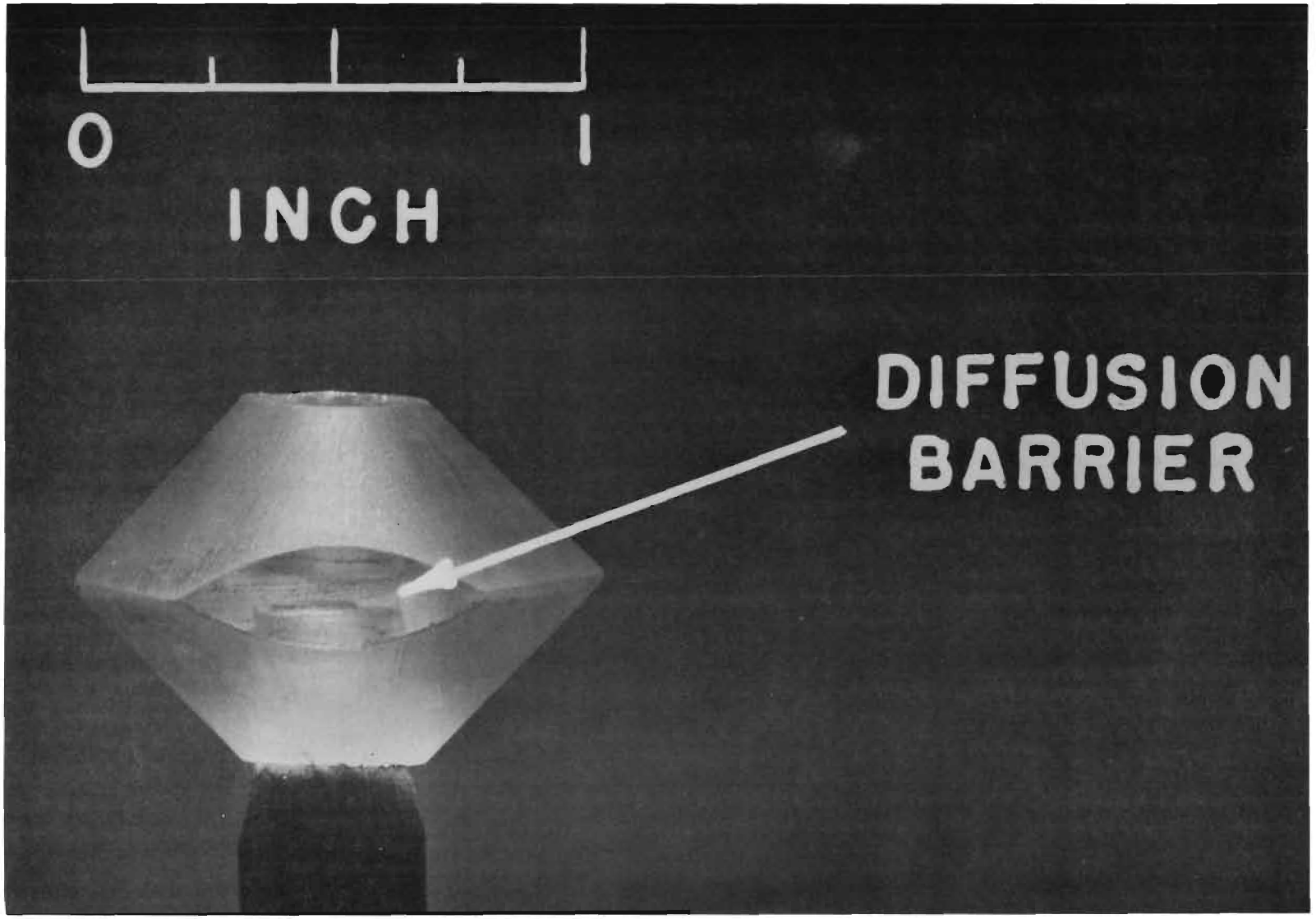

Figure 8. Single Crystal Alumina Barrier.

TABLE V

BARRIER MATERIALS

Barrier	Source
Polycrystalline Al_2O_3	1. Tucalox, General Electric Co. 2. 100% Al_2O_3, hot pressed, refired to 1820° C in oxidizing atmosphere, Carborundum Co., Niagara Falls, N. Y.
Polycrystalline UO_2	100% UO_2, H_2 firing, Mallinckrodt Nuclear Corp., St. Louis, Mo.
Single Crystal Al_2O_3	Oxyhydrogen flame process, Linde Co., New York, N. Y.
Single Crystal UO_2 and ThO_2	Electric arc melt growth, Norton Co., Worcester, Mass.

TABLE VI

PROPERTIES OF LUCALOX ALUMINA

Crystal Form	alpha - Al_2O_3
Purity	99.9^+ % Al_2O_3
Structure	Polycrystalline
Density	3.98 gm/cc^{-1} avg.
Porosity	Gas Tight, essentially zero
Melting Point	2040° C
Chief Impurity	MgO
Average Grain Size Before Sintering	$\sim$ 3 μ
Average Grain Size After Sintering	$\sim$ 7 μ

TABLE VII

PROPERTIES OF CARBORUNDUM CO. ALUMINA

Crystal Form	alpha - alumina
Purity	99.1^{+} % pure
Chief Impurity	Na_2O
Structure	Polycrystalline
Density	3.70 to 3.90 gm/cc
Porosity	Gas tight, essentially zero
Melting Point	2015° C (average)
Average Grain Size Before Hot Pressing	$\sim$ 20 to 30 μ
Average Grain Size After Hot Pressing	$\sim$ 40 to 50 μ

considered suitable. The most satisfactory seal compositions for the alumina-to-alumina bond are given in Table IX; composition A for bonding polycrystalline specimens and composition B for bonding single crystal to polycrystalline material. A limited study was made on UO_2 to Al_2O_3 bonding materials. The first attempt to make such a bond was not successful in that the bond did not react to any appreciable extent with the UO_2 (Fig. 11). The bond consisted of components which will form solid solutions or eutectics with both UO_2 and Al_2O_3. The specimens, Fig. 11, were fired to 1700° C in a hydrogen atmosphere. The composition of the bond was as follows:

Figure 9. Grinding Wheel and Faceting Goniometer.

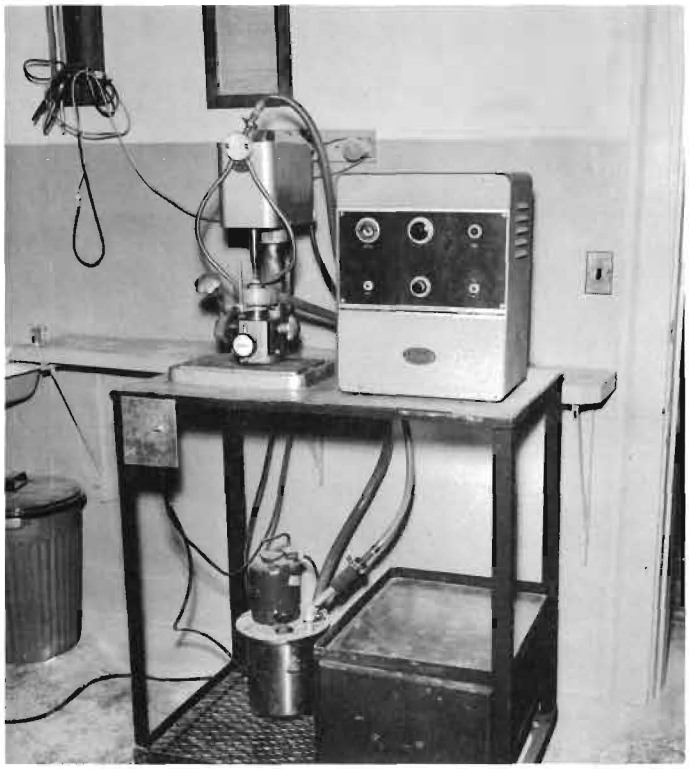

Figure 10. Sonic Grinder.

TABLE VIII

PHYSICAL DIMENSIONS OF SPECIMENS

Series*	Crystal Form	Barrier Thickness (Cm)	Barrier Diameter (Cm)	Test Thermal Treatment (Cycles)	Density
A	Polycrystalline	0.168	0.635	2	- -
B	Polycrystalline	0.168	0.635	2	- -
C	Polycrystalline	0.155	0.635	1	- -
F	Polycrystalline	0.076	0.635	1	3.901
G	Polycrystalline	0.109	0.635	1	- -
H	Polycrystalline	0.107	0.635	1	3.875
J	Polycrystalline	0.180	0.635	1	3.703
X	Single Crystal Barrier ⊥ to C axis	0.173	0.635	1	Approx. Theoretical
Z	Single Crystal Barrier ⊥ to C axis	0.229	0.635	1	Approx. Theoretical

*Letters missing from A through P, and Y denote specimens that developed cracks in barrier before diffusion runs could be completed sufficiently for data analysis.

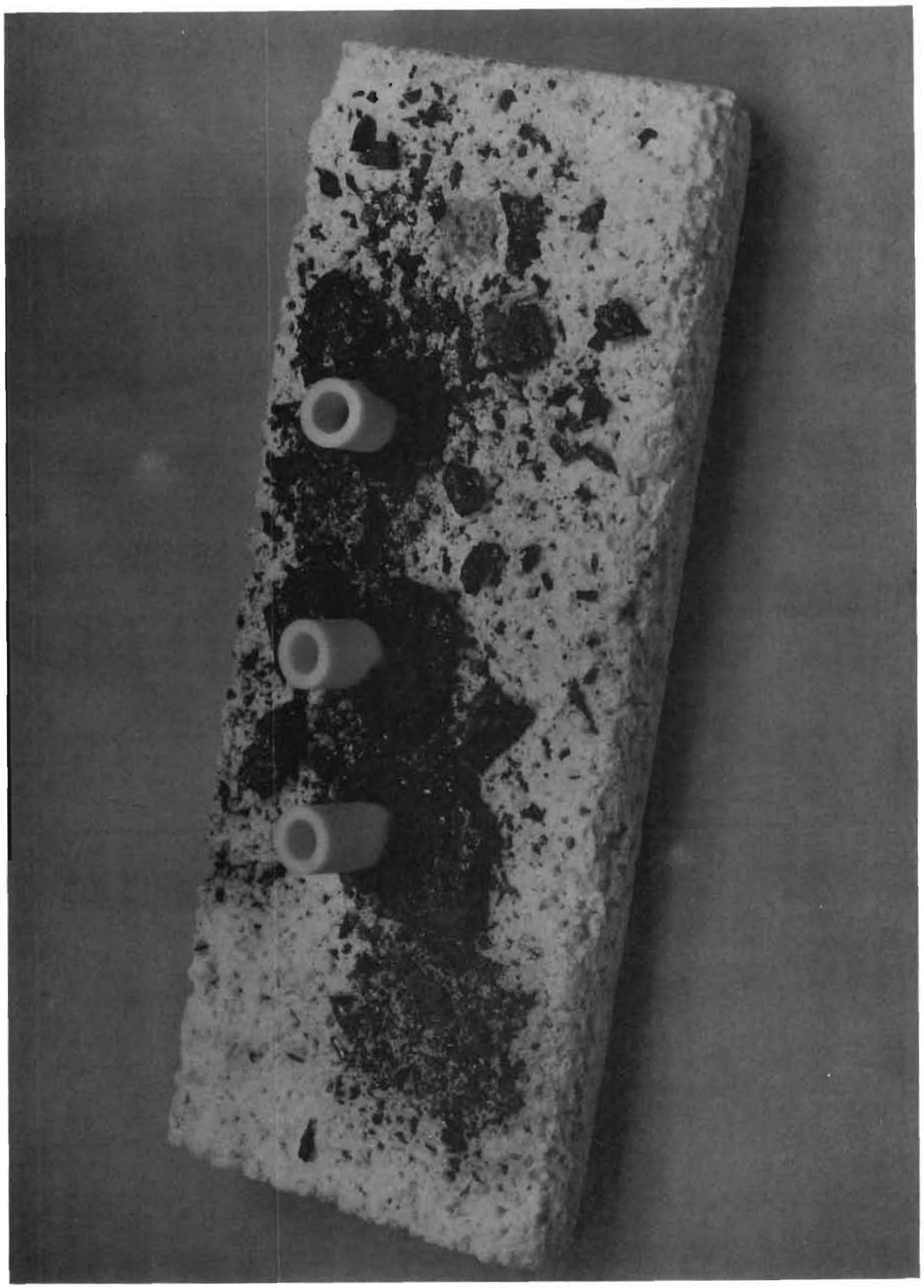

Figure 11. Al_2O_3 Bonding to UO_2.

TABLE IX

SEAL COMPOSITIONS IN MOLES

A. Polycrystalline			B. Single Crystal		
0.60 CaO			.740 K_2O		
0.20 MgO	1.3 Al_2O_3	13.5 SiO_2	.252 Na_2O	1.85 Al_2O_3	6.42 SiO_2
0.10 BaO			.010 CaO		
0.10 SrO					

Material	% wt
UO_2	40
TiO_2	5
ThO_2	10
Al_2O_3*	45
	100%

*Composition same as Coors Composition of tube:

94% Al_2O_3

2% MgO and CaO

4% SiO_2

From Figure 11, it can be observed that the UO_2 cracked away from the original flat surface as obtained by cutting slabs with a diamond saw. This may have been caused by a too rapid cooling rate or by occluded gases as the slabs were a polycrystalline material. Subsequent firings at very slow rates tended to give a much better bond between the Al_2O_3 and UO_2. Figure 12 shows some of the better bonds developed with long firing schedules at the designated

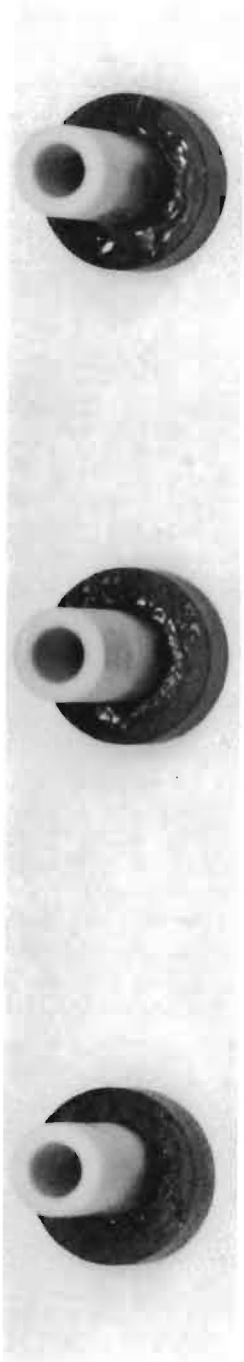

Figure 12. Al_2O_3 Bonding to UO_2.

temperatures. Additions of UO_2 were made to a base seal composition as follows:

Material	% wt
Potassium Feldspar	57.2%
Silica	34.5%
Kaolin Clay	8.3%
	100%

UO_2 additions of 25, 50, and 75% as shown in Figure 12.

This technique was discontinued as suitable specimens of UO_2 were not readily available for barrier materials.

B. Diffusion Cell

The diffusion cell system is shown in Fig. 13, and Fig. 14 is a schematic diagram of the system. It was designed to operate in pressure ranges on the order of 10^{-5} mm Hg to a lower limit of 2×10^{-6} mm Hg. This last figure represents the lower limit of the pressures obtainable with the mass spectrometer pumping station. The other side of the barrier was maintained at one atmosphere pressure of helium, Amarillo grade A. The furnace volume surrounding the assembly could be pumped down to the micron range, and it could be continually purged with a gas of zero helium content such as nitrogen.

The vacuum on the high vacuum side of the barrier was obtained from the pumping station included in the mass spectrometer unit. The station consisted of a mechanical pump, oil diffusion pump, and a cold trap charged with liquid nitrogen. Pressures inside the system were measured with a cold cathode discharge gauge located at the mass spectrometer tube, and an ion gauge and thermocouple gauge located at the end of the furnace assembly. The mass spectrometer

Figure 13. Diffusion Cell.

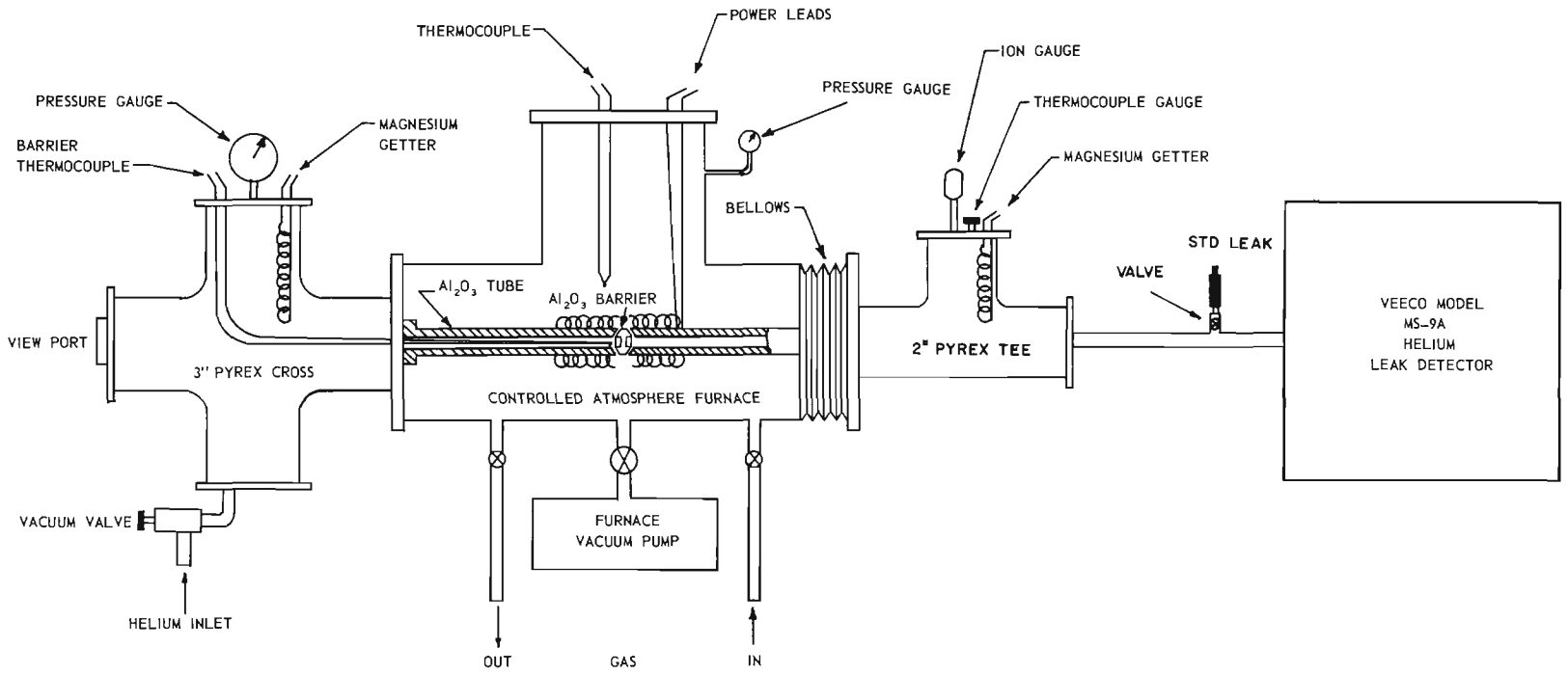

Figure 14. Diffusion Cell Schematic.

was a standard Veeco Model MS-9A helium leak detector with an 0A2 tube in the amplifier. All permanent connections in the system were silver soldered, and critical "0" ring connections were lubricated with Apiezon L high vacuum grease. Furnace "0" rings, not in the high vacuum assembly, were lubricated with Celvacene heavy vacuum grease.

The barrier and tube assembly was surrounded by a Kanthal resistance heating element powered, optionally, by a saturable reactor and temperature controller, or by a powerstat. Thermocouples were placed inside and on the exterior of the assembly at the barrier.

The entire system was checked for leaks after assembly with a helium leak detector and helium probe. Usually a minimum of 3 days was required to pump down and degas the system to operating pressures of about 10^{-5} mm Hg.

The electrical stability of the entire system, including the heating element, recorders, and the mass spectrometer with its pumping station, was maintained with Sola constant-voltage transformers. These transformers insured constant specimen temperature at all temperature levels and constant pumping speeds in the mass spectrometer unit. The apparent sensitivity of the instrument would have varied with the pumping rate of the station if the pumping rate had been held constant. Sensitivity checks that did not vary beyond the limits of error set by the manufacturer as well as the constant temperature held on the specimen confirmed the stability of the electrical system.

A base line was established in the system before helium gas was admitted. The base line represented the lower limits of the sensitivity of the mass spectrometer, about 3×10^{9} atoms/sec. Both sides of the barrier were at pressures of approximately 10^{-5} mm when the base line was established. Helium at one atmosphere was admitted to the high pressure side of the barrier and the

high vacuum side of the system was continuously sampled with the mass spectrometer to determine the presence of any diffusion products. Records were made of the pressure on the high vacuum side of the barrier, as well as the barrier temperature.

The mass spectrometer had been calibrated to detect flow rates of helium down to 1.5×10^{-10} std. cc/sec.$^{-1}$, or 2.5×10^{9} atoms/sec, with the aid of a Veeco Model SC-4 Sensitivity Calibrator. The instrument was recalibrated twice a day during the duration of each run.

When a steady state had been reached between leak rate, temperature, and pressure, after approximately 72 hours, the system was considered at equilibrium, and a higher temperature level was obtained. The temperature levels investigated were room temperature and 100° C temperature levels from 300° C to the operating limits of the furnace, approximately 1000° C. After the helium reached a steady flow at each temperature level, it was removed to observe the time necessary for the flow rate to decrease. Extremely fast times are indicative of Knudsen or turbulent flow rather than diffusion.

Fig. 15, Series J, is a typical example of the flow rates and temperatures-vs.-time types of curves obtained for the various barrier materials. Details of how this system was operated are given in Fig. 15.

One polycrystalline Al_2O_3 barrier was analyzed by the early-time and late-time approximation technique. There was very good agreement between the values obtained and those found from the more reliable steady-state method for the coefficient of diffusion. However, the values of solubility for helium were not realistic and could have been erratic due to small errors in the value of D.

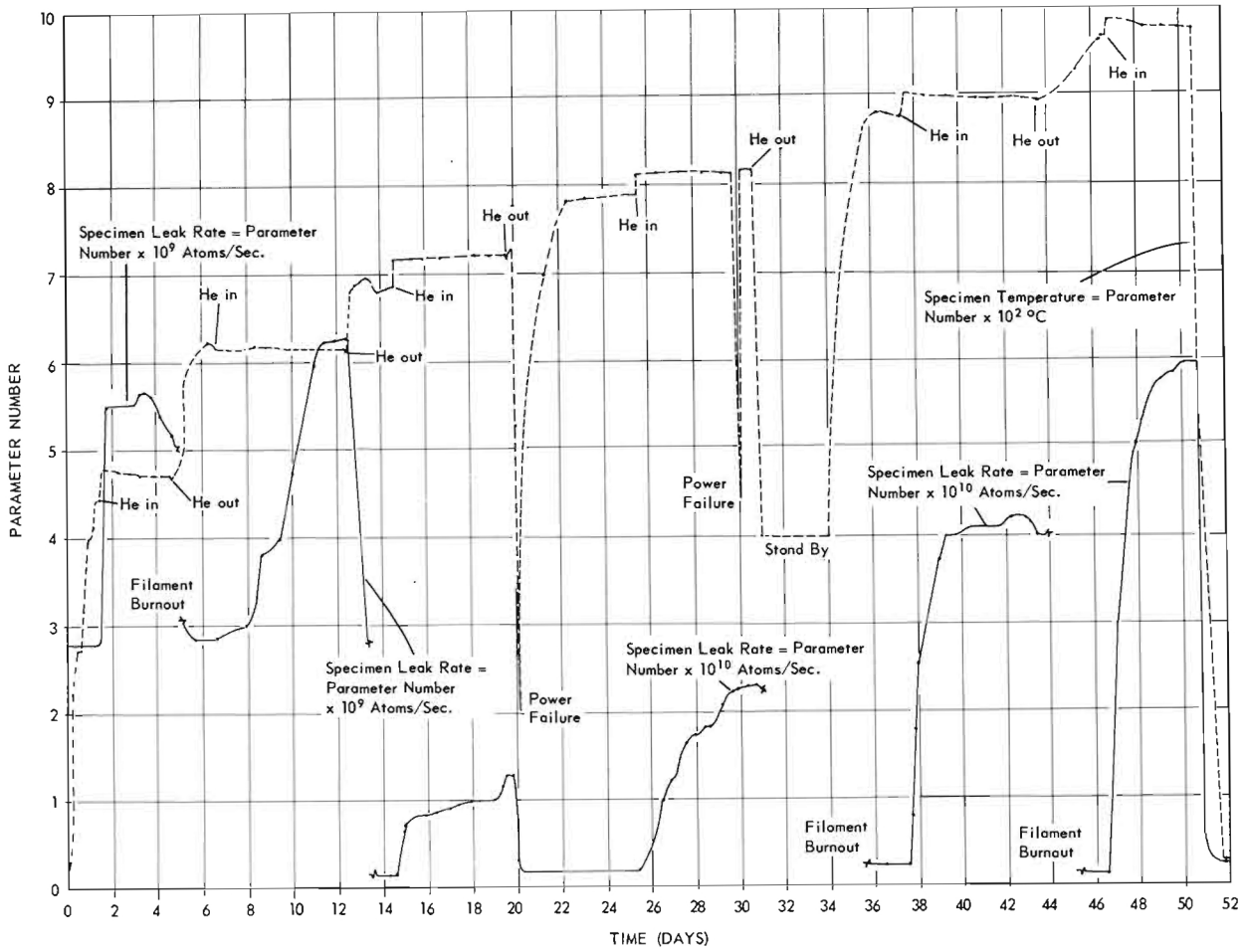

Figure 15. Data Presentation on Series J.

C. Krypton and Argon Concentration Gradient Determination

The feasibility of determining the concentration gradient of argon and krypton in Al_2O_3 was demonstrated. A Philips Electronic Instruments Division vacuum x-ray spectrograph, Model 52360 with pulse height analyzer, was used with a NaCl crystal to detect argon K_α, and with a LiF crystal to detect krypton K_α. In order to set up the pulse-height analyzer for argon, it was necessary to use silver L_α, (4.154 Å) as a close substitute for argon K_α. Under these conditions the argon and krypton contents of single crystal Al_2O_3 could be detected for specimens heated to 1000° C, for 24 hours, in those atmospheres. Fig. 16 shows the heights of the peaks obtained with all x-ray conditions duplicated except as specified for specimen C. The remaining traces of argon in the vacuum are the cause of the small peak for the no-argon specimen, Fig. 16A. These same specimens were run on a helium x-ray spectograph without a pulse-height analyzer and no significant differences could be deduced between the specimens with or without the inert gas content. It was necessary to visit the Philips Laboratory at Mount Vernon, New York, to obtain use of the vacuum x-ray fluorescence equipment.

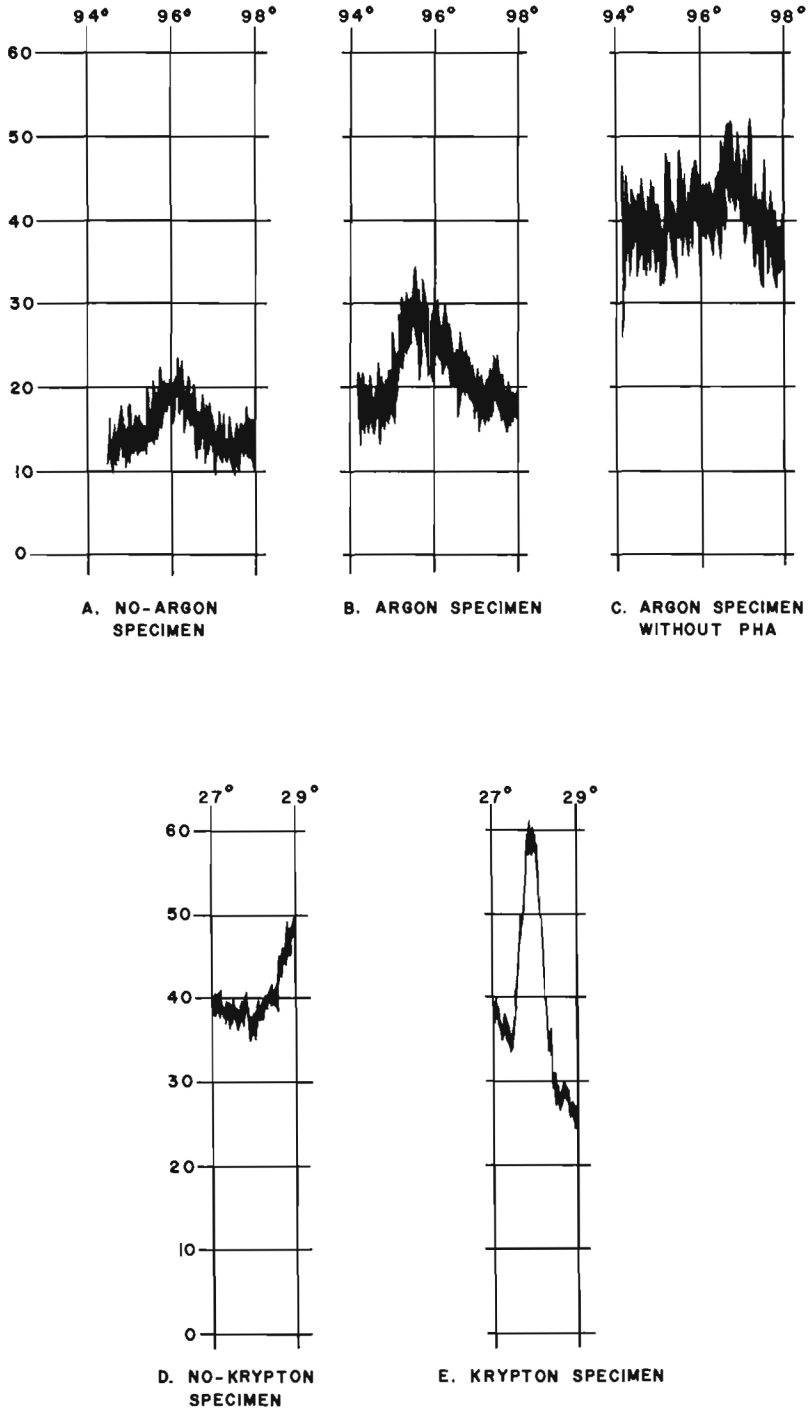

Figure 16. Argon and Krypton X-Ray Fluorescence Recorder Curves.

IV. DISCUSSION OF RESULTS

A. Coefficient of Diffusion and Activation Energy

The crystalline structure of Al_2O_3 is close packed rhombohedral with the plane of highest atomic density normal to the c-axis. According to Tucker and Gibbs[11] single crystals of Al_2O_3 normally contain 10^7 dislocations/cm^2. Since there are no apparent phase transformations in Al_2O_3 between 25° and 1000° C, any grain boundary growth in the polycrystalline Al_2O_3 and any appreciable change in the number of dislocations in the single crystal should produce a change in the diffusion coefficient, D, values. The physical dimensions of the specimens and the diffusion data for a typical run are given in Table VIII and Fig. 15, respectively.

The ln values of the coefficients of diffusion, D, approximate a straight line when plotted versus the reciprocal of temperature for all the diffusion runs except Series G. The slope of the line is a function of the activation energy. Although a discontinuity in the diffusion coefficient occurs at an elevated temperature, the values approximate separate straight lines with varied slopes above and below the temperature as shown in Figs. 17, 18, and 19. The coefficient of diffusion equations are given in Table X. The calculated activation energy, Moody, et al. method,[15] Fig. 20, for interstitial diffusion of helium through the basal plane of the Al_2O_3 lattice was 5.7 ev while a value of 0.2 ev was calculated for an edge dislocation activation energy. Fig. 20 shows the relative sizes of the inert gas series of atoms relative to the edge dislocation.

The path traversed by the diffusing helium atom was considered as being between the barrier surfaces for the calculation of the coefficient of

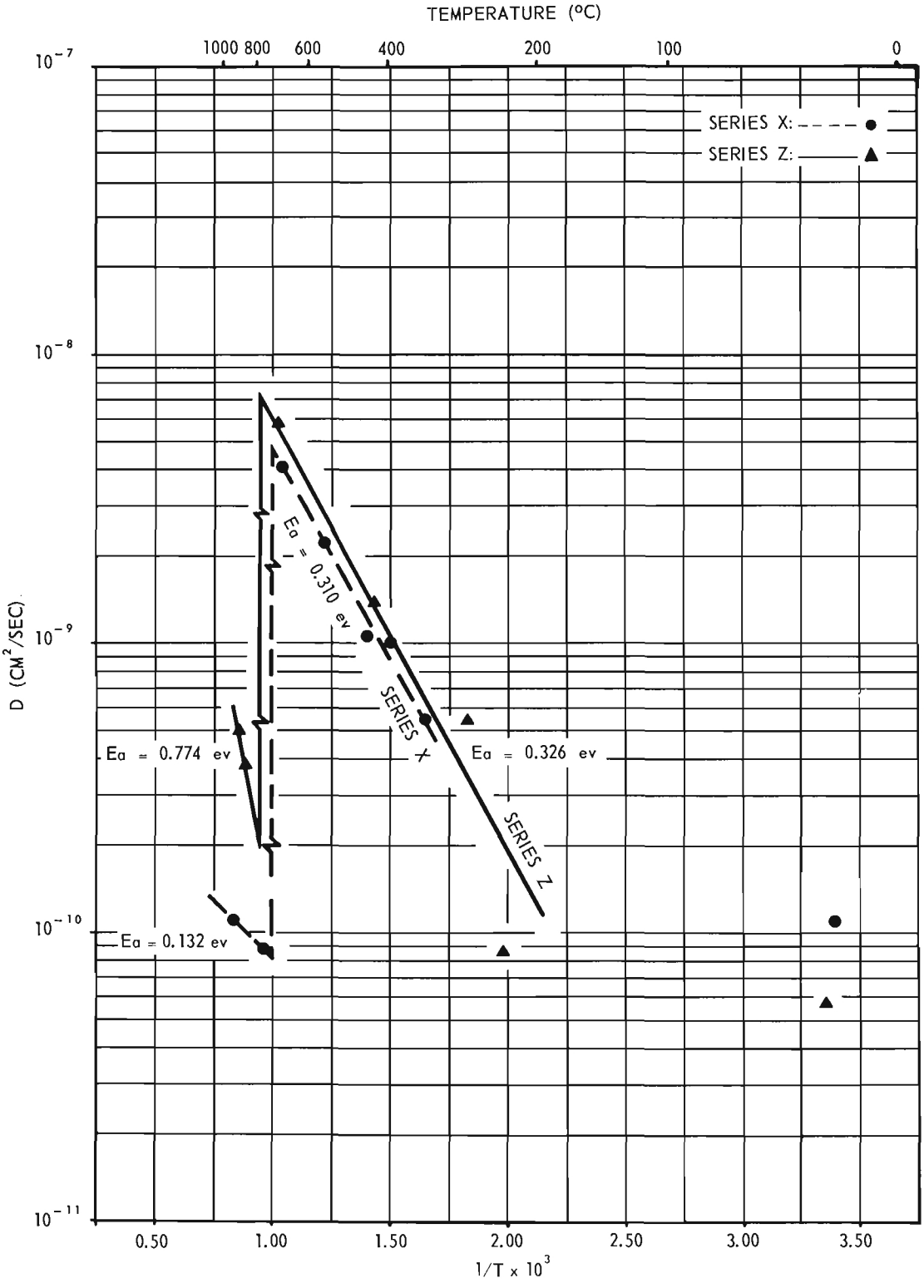

Figure 17. Helium Diffusion through Single Crystal Al_2O_3 Perpendicular to C-Axis.

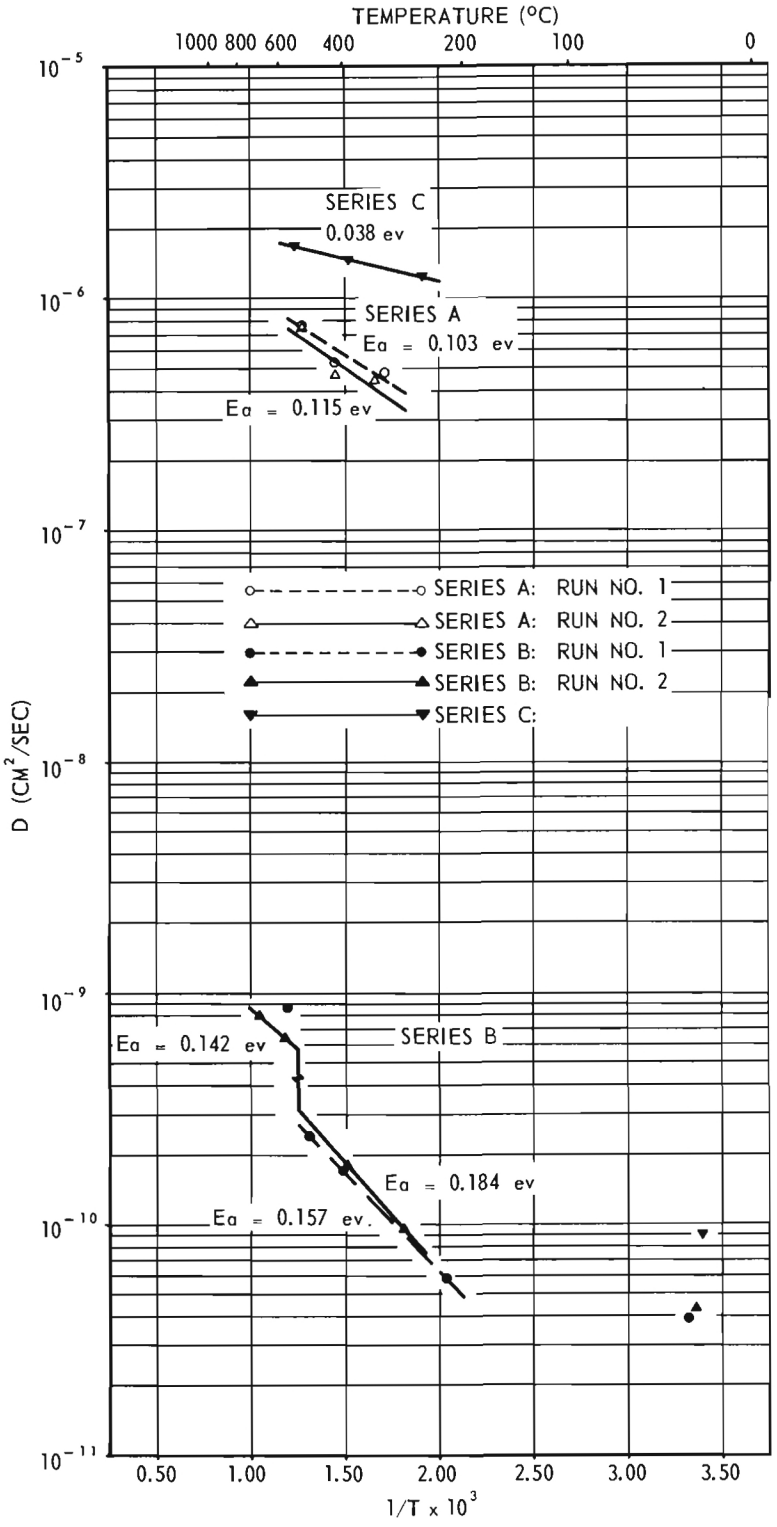

Figure 18. Helium Diffusion through Polycrystalline Al_2O_3.

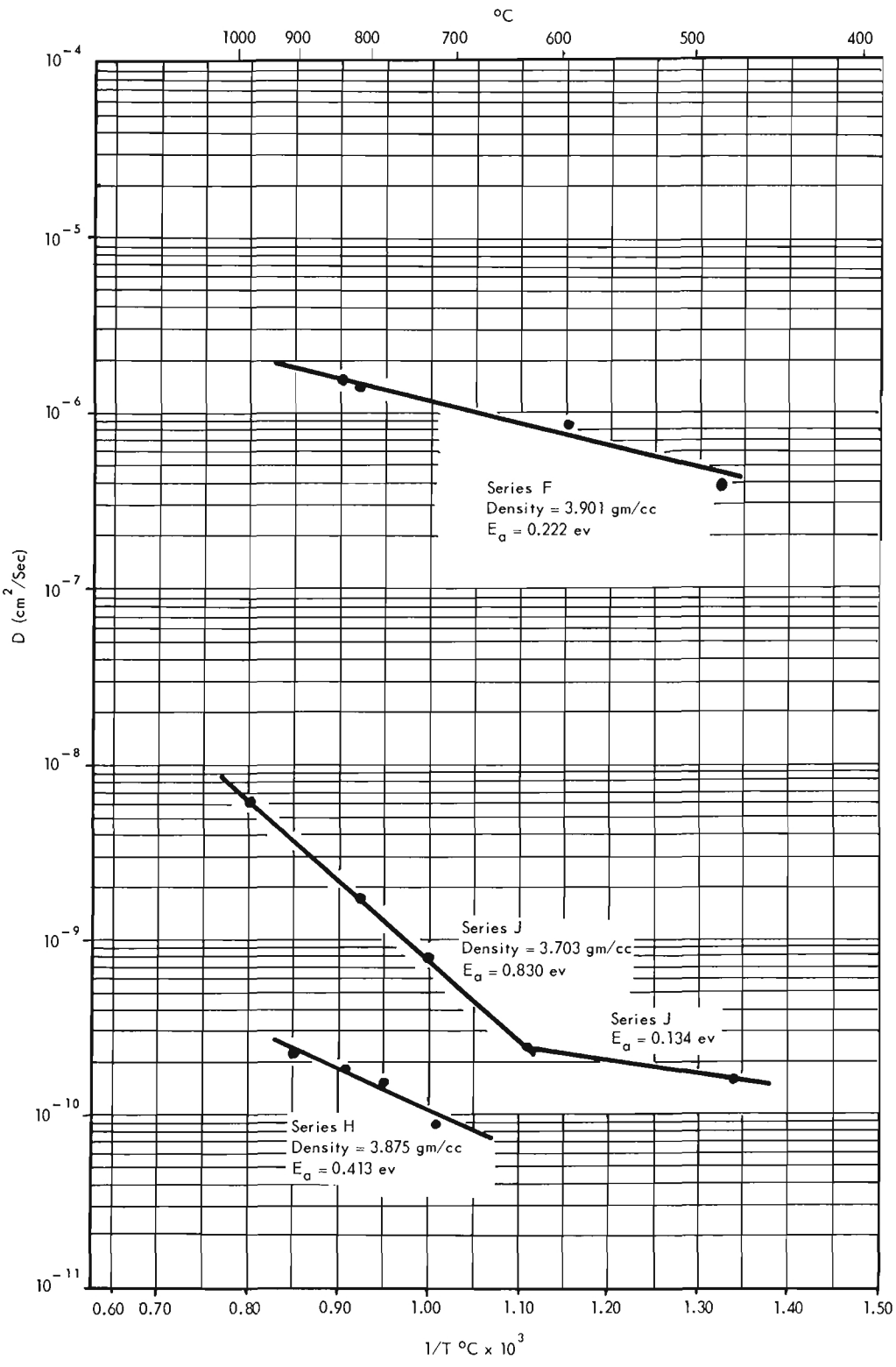

Figure 19. Helium Diffusion through Polycrystalline Al_2O_3.

TABLE X

DIFFUSION COEFFICIENT EQUATIONS

Series	$D = D_o e^{-\frac{Q}{kT}}$
$A_{(1st\ Run)}$	$D = 9.5 \times 10^{-6}\ cm^2/sec\ e^{-\frac{0.103\ ev}{kT}}$
$A_{(2nd\ Run)}$	$D = 7.2 \times 10^{-6}\ cm^2/sec\ e^{-\frac{0.115\ ev}{kT}}$
$B_{(1st\ Run)}$	$D = 3.7 \times 10^{-8}\ cm^2/sec\ e^{-\frac{0.157\ ev}{kT}}$
$B_{(2nd\ Run,\ Before\ Inflection)}$	$D = 2.2 \times 10^{-8}\ cm^2/sec\ e^{-\frac{0.184\ ev}{kT}}$
$B_{(2nd\ Run,\ After\ Inflection)}$	$D = 2.3 \times 10^{-8}\ cm^2/sec\ e^{-\frac{0.142\ ev}{kT}}$
C	$D = 3.5 \times 10^{-5}\ cm^2/sec\ e^{-\frac{0.038\ ev}{kT}}$
F	$D = 1.52 \times 10^{-5}\ e^{-0.222\ ev/kT}$
G	Exhibited laminar and turbulent flow
H	$D = 1.34 \times 10^{-8}\ e^{-0.413\ ev/kT}$
J	$D = 1.26 \times 10^{-5}\ e^{-0.830\ ev/kT}$
$X_{(Before\ Inflection)}$	$D = 5.2 \times 10^{-6}\ cm^2/sec\ e^{-\frac{0.310\ ev}{kT}}$
$X_{(After\ Inflection)}$	$D = 2.5 \times 10^{-9}\ cm^2/sec\ e^{-\frac{0.132\ ev}{kT}}$
$Z_{(Before\ Inflection)}$	$D = 7.3 \times 10^{-6}\ cm^2/sec\ e^{-\frac{0.326\ ev}{kT}}$
$Z_{(After\ Inflection)}$	$D = 9.8 \times 10^{-6}\ cm^2/sec\ e^{-\frac{0.774\ ev}{kT}}$

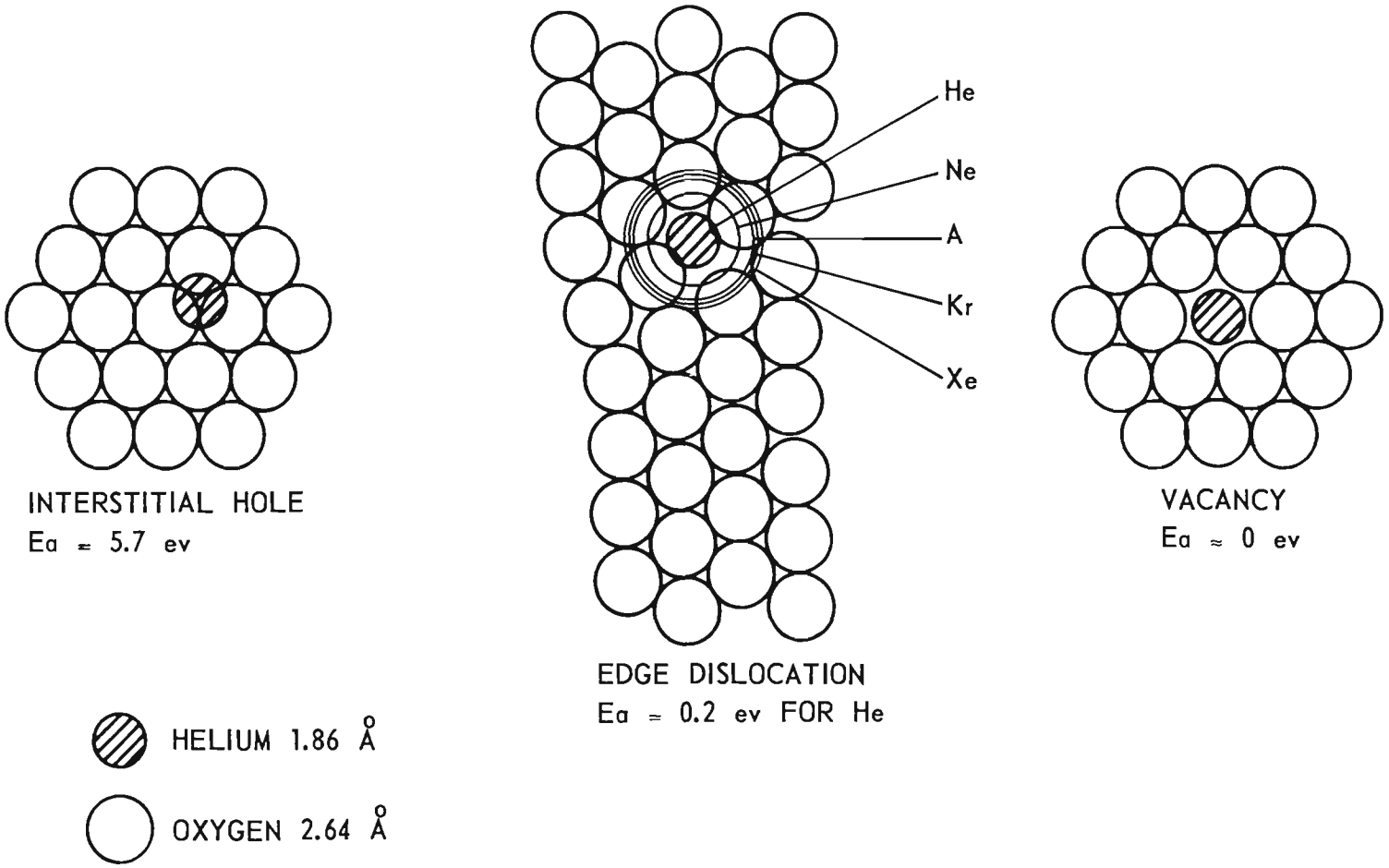

Figure 20. Schematic Diagram for Calculated Activation Energies for Helium Diffusion through Basal Plane of Al_2O_3.

diffusion and diffusion constant. The values of 10^{-5} to 10^{-9} cm^2/sec, Table X, for the diffusion constant, D_o, are quite low in comparison to values[16] of 10^{-2} which are considered ideal for perfect crystals. Since D_o is a function of many variables such as grain boundaries, dislocations, experimental accuracy, etc., it is beyond the scope of this investigation to elaborate extensively on the numerical value of the diffusion constant other than to state that the specimens could not be exact duplicates of each other in terms of imperfections.

B. Single Crystal Al_2O_3

For the case of the single crystal Al_2O_3, an inflection or discontinuity for diffusion, Fig. 17, was noted in the region of 725° C. A decrease in the diffusion coefficient on the order of one magnitude occurred in the temperature region noted, 725° C. This feature was consistent in Series X and Series Z, whose thickness differed by one-third. Following the sudden decrease, the diffusion coefficient value increased until the limiting temperature of the furnace was reached. The activation energy values determined for Series X and Series Z were in close agreement below the discontinuity temperature. Above the discontinuity temperature the activation energy values differed greatly.

The relative size of the helium atom would prohibit interstitial diffusion and would require a high activation energy value of approximately 5.7 ev. The calculated value of 0.2 ev for an edge dislocation mechanism agrees with the experimental results for the single crystal at temperatures up to the inflection temperature. Above the inflection temperature there is a wide variance of 0.6 ev in the determined activation energy values as shown in Fig. 17. At the inflection temperature, there appears to be an annealing of

imperfections in Series Z and a generation of additional types of imperfections in Series X. The annealing effect is in agreement with the theory of the annealing of edge dislocations on the basal plane at approximately 900° C.

Lattice parameter measurements made on single crystal Al_2O_3 barrier fragments indicate that an expanded lattice may occur in the diffusion barrier. Although the evidence was inconclusive, the presence of a typical diffusion concentration gradient is suggested by the comparative measurements made on fragments from different parts of the barrier.

There were two attempts to fabricate tubes with single crystal barriers cut parallel to the c-axis. On the first attempt, the barriers developed many parting and cleavage cracks during the fast seal firing. The second specimen was sealed satisfactorily but received a thermal shock from a power failure in the diffusion cell system and developed similar cracks.

C. Polycrystalline Al_2O_3

Figs. 18 and 19 show the results of helium diffusion through polycrystalline Al_2O_3. The coefficient of diffusion equations for each specimen are given in Table X. Series B and J exhibit inflection points at 525° and 625° C with a decrease and increase in activation energy respectively. In each case, there was a marked increase in the helium flow rate. The single crystal specimen exhibited an opposite effect in that the flow rate decreased at a higher temperature. The effect from the inflection point for the polycrystalline specimen can be attributed to changes in the grain boundary. Below the discontinuity temperature, grain boundary defects and edge dislocations appear to constitute the diffusion mechanism. Above the inflection point, grain boundary defects may control the diffusion rate as the number of vacancies

increases due to higher temperatures. However, there is no satisfactory explanation for the occurrence of an inflection point. The activation energy value increase observed with second cycle heating Series B may be attributed to the annihilation of some grain boundary defects and edge dislocations. In general, the activation energy values were indicative of the atom-vacancy interchange mechanism along grain boundaries.

Series C appeared to have a laminar rather than a diffusion type of mass transport.

Certain points must be kept in mind when considering the experimental values of the activation energy. The steady-state leak rate readings at low temperatures, below 500° C, during the early portions of an experiment were subject to doubt. The thickness of the barrier plays an important role. If the barrier length is quite small, it is possible that only one grain occupies the entire length of the barrier. The grain boundary would be an extremely easy diffusion path and a low activation energy would be expected. If the path were longer, the diffusing gas atoms would have to follow several grain boundaries; and, where one boundary stopped, it would have to search for another path to reach the next grain boundary. A mechanism of this type would be much more "activated." The longer path length would also require a longer time to reach the equilibrium state. This would be especially true at lower temperatures. Experimental values of the steady-state readings would be uniformly low if insufficient time were spent at the temperature levels. Barriers were formed by ultrasonic impact grinding. If a barrier were formed of a thickness such that only one or two grains occupied the path length, it is possible that the entire barrier could be mechanically shocked by the method of formation, opening up new diffusion paths. The thickness of the barriers

used in this experimental work was such that there should be many grains in the diffusion path. No correlation could be determined between the thickness of the barriers and any experimental results in this investigation except for the very thin barriers that exhibited laminar type mass transport.

The helium flow rates through the two Lucalox alumina specimens, up to 700° C, were too low for any steady-state analysis. It may be possible to obtain more reliable data by the early-time or late-time approximation technique. As the Lucalox alumina had been treated with small amounts of MgO to aid in sintering and densification, 3.97 gm gm/cc, which is almost theoretical density, it is quite possible that the Mg^{++} ions occupy the vacant sites in grain boundaries and dislocations to give a structure with few if any readily available diffusion paths.

For several reasons, Series G gave indications of mass transport phenomenon other than diffusion. The specimen leak rates recorded were 500 to 1000 times greater than any obtained for the other specimens studied. The time necessary to reach equilibrium was never in excess of 10 to 15 minutes. During the heating cycle, the specimen leak rate was temperature dependent and highly pressure dependent. The specimen leak rate after cycling from 400° C to room temperature was higher than at 400° C. Specimen leak rate was still pressure dependent. The higher leak rate after the heating cycle indicated more structural damage to the material. The types of molecular flow processes were considered in order to determine, if possible, the type of flow present in this specimen.

A plot was made of $\frac{du}{dt}$, the equilibrium flow rate in atoms/sec, as a function of the pressure on the high pressure side of the barrier at constant temperature, Fig. 21. The equations for laminar flow all state that the flow

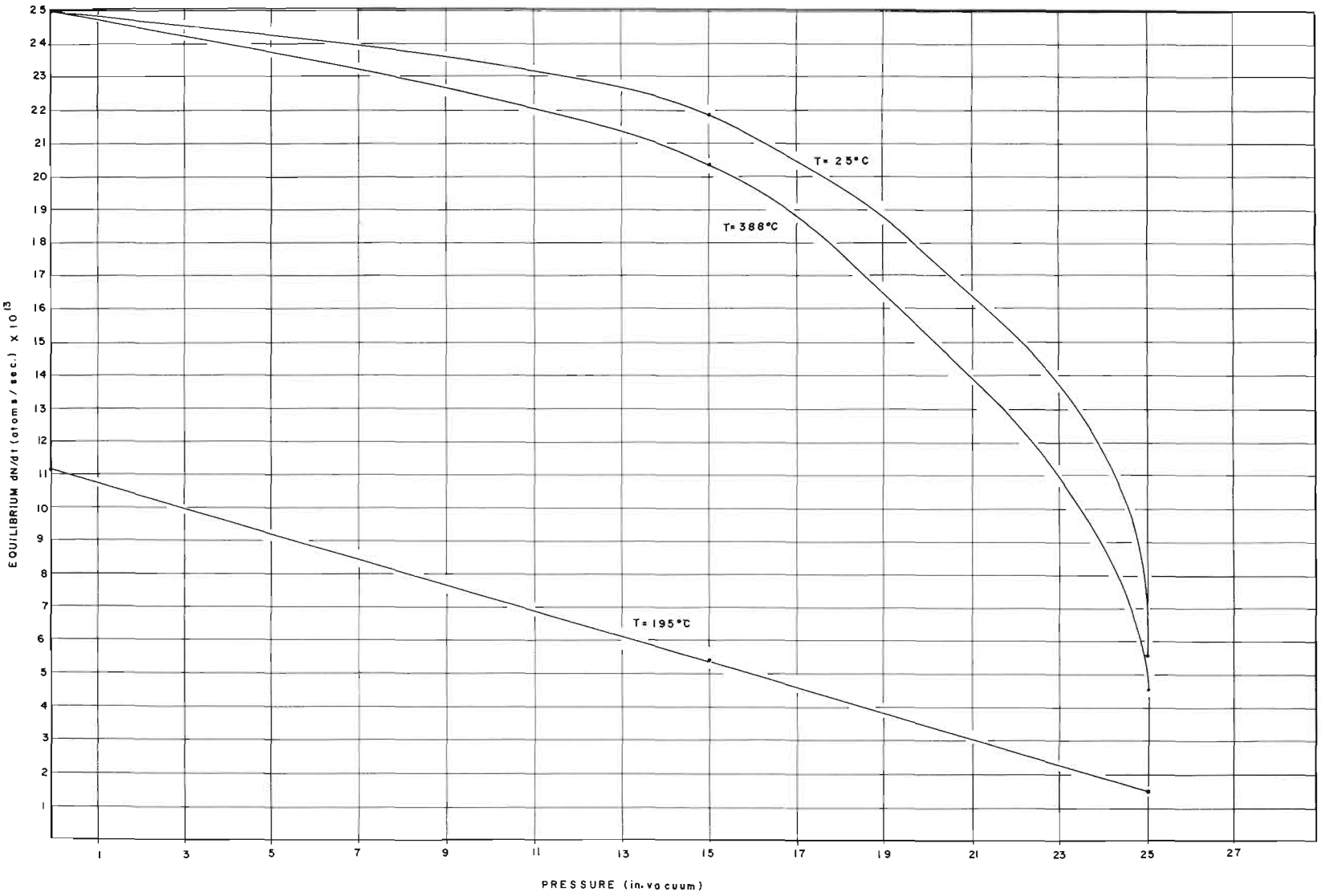

Figure 21. Equilibrium Helium Flow Rate versus Pressure for Series G.

rate at a constant temperature is linearly proportional to the pressure differential. The pressure on the high vacuum side of the barrier was $< 10^{-5}$ mm Hg and may be neglected. Any deviation from a linear function at a constant temperature would indicate a divergence from laminar flow.

Figure 21 shows that during the heating cycle at 195° C, the measured values approximate a straight line very closely. The flow is apparently laminar. At 383° C, the next temperature level, the same plot deviates from a straight line, and the flow rates increased, to indicate that it is turbulent flow. The system was then cooled to room temperature and helium again admitted to the system. The room temperature leak rates recorded were higher than at 382° C, indicating that still further damage had been done to the specimen. Again the plot deviated from a straight line, indicating a turbulent flow as the helium passed down the path.

The type of laminar flow experienced at 195° C can be predicted to some extent. The flow could not have been molecular effusion through a thin plate since the gas did have a finite distance to travel. This leaves molecular streaming or Poisueille types of flow. Since there is undoubtedly some friction as the gas collides with the walls of the flow path, the friction factor found in the Knudsen equation would have to be employed. When the Poisueille equation is corrected for friction on the walls, it assumes the form of the Knudsen equation. The type of flow experienced at 195° C was quite probably Knudsen flow on the basis of these facts.

One further point should be noted. The time necessary to reach equilibrium conditions of flow rate on Series G was approximately 10 minutes. Series F, H, and J all required a minimum of 8 hours to come to equilibrium. Series J, the thickest specimen studied, did not reach equilibrium conditions in less

than 3 days at the temperature levels studied (see Fig. 15). Since the barrier thickness of Series G and Series H are practically the same and the barrier thickness of Series F is even thinner, the length of time to reach a steady state flow rate is a strong argument for the diffusion mechanism of atom transport.

V. CONCLUSIONS

1. The coefficients of diffusion of helium mass transport in single crystal and polycrystalline Al_2O_3 can be experimentally determined by means of a mass spectrometer.
2. The equation for the coefficient of diffusion of helium through single crystal Al_2O_3 in the temperature range 200° to 700° C was determined to be:

$$D = 6.2 \times 10^{-6} e^{-\frac{0.32 \text{ ev}}{kT}} \qquad (27)$$

3. The activation energy calculated from the experimental data on helium diffusion through single crystal Al_2O_3 was 0.32 ev in the temperature range 200° to 700° C.
4. The most probable basic mechanism for diffusion of helium through single crystal Al_2O_3 is an atom-vacancy interchange type occurring along edge dislocations.
5. In the region around 725° C annealing of internal strains and annihilation of dislocations probably occurs in the single crystal Al_2O_3.
6. The mass transport rate of helium through polycrystalline Al_2O_3 may be affected by density and thickness and tends to decrease with repeated heatings to elevated temperatures.
7. Densities above 3.70 gm/cm^3 may be sufficiently high to give diffusion rather than laminar flow type mass transport.
8. Activation energies for diffusion of helium through polycrystalline Al_2O_3 varied from 0.10 to 0.80 ev and D_o values varied from approximately 10^{-8} to 10^{-5} cm^2/sec.

9. The most probable basic mechanism for diffusion of helium through polycrystalline Al_2O_3 is an atom-vacancy interchange type occurring mainly along grain boundaries.

VI. PERSONNEL

Project Director

W. E. Moody

Graduate Student Assistant

W. B. Campbell

J. J. Hurst, Jr.

Technician

Tom Mackrovitch

Respectfully submitted:

Willis E. Moody
Project Director

Approved:

Frederick Bellinger, Chief
Material Sciences Division

VII. APPENDIX

Reprint of an Article from The Journal of the American Ceramic Society 42, No. 5 (May 1959) entitled "Thorium Oxide and Uranium Oxide Cleavage," by William B. Campbell, Vernon J. Hurst, and Willis E. Moody.

[Reprinted from The Journal of The American Ceramic Society, Vol. 42, No. 5. May, 1959.]

Thorium Oxide and Uranium Oxide Cleavage

by WILLIAM B. CAMPBELL, VERNON J. HURST, and WILLIS E. MOODY

THE crystallographic properties of most natural crystals have been determined. However, some of the crystals in use today do not occur in nature. These synthetic crystals are in limited distribution and have not been studied extensively. Apparatus involving these synthesized crystals necessitates a knowledge of specific crystal properties such as cleavage planes and their associated imperfections. A search of the literature disclosed no information pertaining to the cleavage of ThO_2 or UO_2.

A thorium oxide crystal obtained from the electric furnace process by Norton Company, Worcester, Massachusetts, was examined by the writers with a two-circle optical goniometer, and the cleavage poles were plotted on a stereographic net. An oriented fragment of the same crystal was mounted on a Buerger precession camera and a plot of the axes was obtained. This plot was superimposed on the stereographic net. Although the uncertainty in translating the crystallographic orientation of the X-rayed fragment back to the parent crystal might easily be as much as 5°, the correspondence of the axes and cleavage poles clearly shows that the cleavage is cubic, i.e., parallel to the (100), (010), and (001) planes.

The cleavage of the specimen was good but not perfect. All three cleavage surfaces gave streaky and multiple reflections on the optical goniometer. On a stereographic plot the cleavage poles were grouped about the crystallographic axes as shown in Fig. 1. One cleavage reflection was offset 6° to 10° from *a;* another 12° from *b;* and the third cleavage gave a streaky reflection which ranged from $\bar{c}$ to 24° away from $\bar{c}$. This was attributed to internal strain in the synthesized crystal.

A synthesized urania (UO_2) crystal obtained from the same source was subjected to a similar investigation and was found to have no cleavage. Its fracture was conchoidal but in a few cases it was planar.

The single-crystal test specimens are shown in Fig. 2.

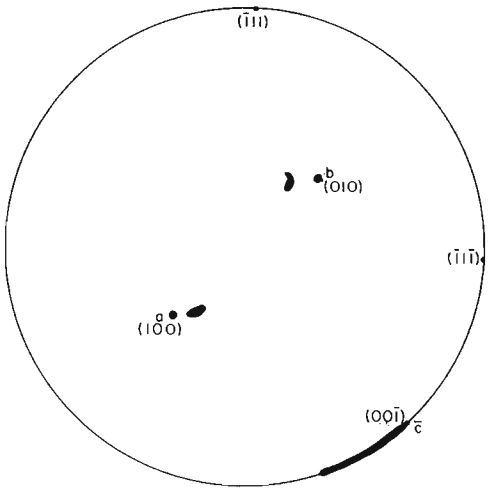

Fig. 1. Stereogram showing reflections from cleavages (*black areas*) as measured on the two-circle optical goniometer in relation to the crystallographic axes as determined by X-ray diffraction.

Fig. 2. Test specimens.

This investigation was conducted under a Georgia Institute of Technology Engineering Experiment Station project sponsored by the Atomic Energy Commission.

The writers are, respectively, research assistant, Engineering Experiment Station, Georgia Institute of Technology, Atlanta, Georgia; geologist, State of Georgia Department of Mines, Mining, and Geology, Atlanta, Georgia; and associate professor, School of Ceramic Engineering, Georgia Institute of Technology.